ÉCOLE DE TECHNOLOGIE SUPÉRIEURE
UNIVERSITÉ DU QUÉBEC

MASTER'S THESIS PRESENTED TO
ÉCOLE DE TECHNOLOGIE SUPÉRIEURE

IN PARTIAL FULFILLEMENT OF THE REQUIREMENTS FOR
MASTER'S DEGREE IN MECHANICAL ENGINEERING
M. Eng.

BY
Saeed MOJARAD FARIMANI

EXPERIMENTAL PROCESS DEVELOPMENT AND AEROSPACE ALLOY FORMABILITY STUDIES FOR HYDROFORMING

MONTREAL, DECEMBER 18 2013

BOARD OF EXAMINERS

THIS THESIS HAS BEEN EVALUATED

BY THE FOLLOWING BOARD OF EXAMINERS

Mr. Henri Champliaud, Thesis Supervisor
Mechanical engineering department at École de technologie supérieure

Mr. Javad Gholipour Baradari, Thesis Co-supervisor
National Research Council, Institute for Aerospace Research, Aerospace Manufacturing Technologies Center

Mr. Van Ngan Lê, President of the Board of Examiners
Mechanical engineering department at École de technologie supérieure

Mr. Mohammad Jahazi, External Evaluator
Mechanical engineering department at École de technologie supérieure

Mr. Jean Savoie, External Evaluator
Pratt & Whitney Canada

THIS THESIS WAS PRENSENTED AND DEFENDED

IN THE PRESENCE OF A BOARD OF EXAMINERS AND PUBLIC

DECEMBER 02 2013

AT ÉCOLE DE TECHNOLOGIE SUPÉRIEURE

To

The love of my life

Vida

ACKNOWLEDGMENT

I would like to thank my supervisor, Professor Henri Champliaud for his support and invaluable trust throughout this master program. I want to thank him for the opportunity that he gave to me and for all his supports. Those two and a half years have been great and full of knowledge.

I would like to extend my special thanks to my co-supervisor Dr. Javad Gholipour Baradari from National Research Council of Canada (NRC)-Aerospace for his helpful and insightful advice as well as his constant availability. Our many discussions helped me improve my critical thinking abilities, build my profile as a researcher and a whole lot more.

I would like to thank Dr. Van Ngan Lê and Dr. Mohammad Jahazi, professors at ETS, for accepting to be part of my board of examiners.

I also sincerely thank to Dr. Jean Savoie from Pratt & Whitney Canada for his enthusiastic support and pertinent suggestions all along the Project. This work was made possible by the financial support provided by Pratt & Whitney Canada, NRC-Aerospace, Natural Sciences and Engineering Research Council of Canada (NSERC) and Consortium de recherche et d'innovation en aérospatiale au Québec (CRIAQ).

I am particularly grateful to my friends and colleagues who put up with me during the hard and the joyful times.

My special thanks go to my parents; you supported me throughout my studies and helped me achieve what I have accomplished so far. It would not be possible for me to accomplish all these without your help and encouragement.

Last but not least, I would like to send my special thanks to Vida for always being there for me; I will always be grateful for your patience, love and support.

EXPERIMENTAL PROCESS DEVELOPMENT AND AEROSPACE ALLOY FORMABILITY STUDIES FOR HYDROFORMING

Saeed MOJARAD FARIMANI

RÉSUMÉ

Dans le procédé d'hydroformage, la pression d'un fluide est utilisée pour déformer plastiquement un tube paroi mince à l'intérieur d'une matrice fermée afin de remplir la cavité de la matrice. L'hydroformage des tubes possède de nombreux avantages qui rendent ce procédé très intéressant pour plusieurs industries telles que l'automobile et l'aérospatiale. Mais, à cause de différents facteurs tels que la formabilité des matériaux, l'ordre et les séquences du chargement (force de compression axiale et pression interne pendant le procédé), la géométrie de l'outil et la friction, c'est un procédé de mise en forme assez complexe. Ainsi, la simulation par éléments finis combinée à des méthodes d'optimisation peuvent réduire significativement le coût de l'approche "Essai – Erreur" utilisée dans les méthodes conventionnelles de mise en forme. Dans ce mémoire, pour étudier les effets de différent paramètres tels que les conditions de friction, l'épaisseur du tube et la compression axiale sur la pièce finale, des essais d'hydroformage de tube ont été menés en utilisant une matrice de forme ronde à carrée. Les expériences ont été effectuées sur des tubes d'acier inoxydable 321 de 50.8 mm (2 in) de diamètre et deux différentes épaisseurs ; 0.9 mm et 1.2 mm. L'historique du chargement a été enregistré avec le système d'acquisition de la presse. Un système de mesure de déformation automatique, Argus, a été utilisé pour mesurer les déformations sur les tubes hydroformés. Les données collectées à partir des essais initiaux ont été utilisées pour comparer avec les simulations. Le procédé a été simulé et optimisé à partir des logiciels Ls-Dyna et Ls-Opt, respectivement. Les variations de déformations et d'épaisseurs mesurées à partir des expériences ont été comparées aux résultats de la simulation par éléments finis dans les zones critiques. La comparaison des résultats de la simulation et des expériences sont en bon accord indiquant que l'approche peut être utilisée pour prédire la forme finale et les variations d'épaisseurs de pièces hydroformées pour des applications aérospatiales.

Mots-clés: Hydroformage de tube; analyse par éléments finis, optimisation, alliages aéronautiques

EXPERIMENTAL PROCESS DEVELOPMENT AND AEROSPACE ALLOY FORMABILITY STUDIES FOR HYDROFORMING

Saeed MOJARAD FARIMANI

ABSTRACT

In tube hydroforming process, a pressurized liquid is used to expand a thin walled tube inside a closed die in order to fill the die cavity. Tube hydroforming has many advantages that make it interesting for different industries such as automotive and aerospace, but due to the effects of different factors, such as formability of the material, load path (end feeding force and internal pressure during the process), tool geometry and friction, it is a quite complex manufacturing process. Therefore, finite element simulation along with optimization methods can significantly reduce the cost of trial and error approach used in conventional manufacturing methods. In this work, to investigate the effects of different process parameters such as friction condition, tube thickness and end feeding on the final product, tube hydroforming experiments were performed using a round to square-shape die. Experiments were performed on stainless steel 321 tubes with 50.8 mm (2 in) diameter and two different thicknesses; 0.9 mm and 1.2 mm. Experimental load paths were obtained via the data acquisition system of the hydroforming press, which is fully instrumented. An automated deformation measurement system, Argus, was used to measure the strains on the hydroformed tubes. Data collected from the initial experiments were used to simulate and then optimize the process. The process was simulated and optimized using Ls-Dyna and Ls-Opt software, respectively. Strains and thickness variations measured from experiments were compared to FE simulation results at critical sections. The comparison of the results from FE simulations and experiments were in good agreement, indicating that the approach can be used for predicting the final shape and thickness variations of the hydroformed parts for aerospace applications.

Keywords: Tube hydroforming; Finite element analysis; Optimization, Aerospace Alloys

TABLE OF CONTENTS

Page

INTRODUCTION 1

CHAPTER 1 LITERATURE REVIEW 5

1.1 EFFECTIVE PARAMETERS IN THF PROCESS 5

1.1.1 Effect of material properties 5

1.1.2 Effect of geometrical factors 11

1.1.3 Effect of loading path 12

1.1.4 Effect of friction and lubrication 15

1.2 INSTABILITIES AND FAILURES 18

1.3 FINITE ELEMENT MODELING 21

1.4 PROCESS OPTIMIZATION 23

CHAPTER 2 METHODOLOGY 27

2.1 FINITE ELEMENT MODEL (FEM) 27

2.1.1 Contact condition 29

2.1.2 Load path simulation 30

2.1.3 Material model 31

2.1.4 Time scaling 32

2.1.5 Spring back 32

2.2 EXPERIMENTAL SETUP 33

2.2.1 Die 34

2.2.2 Plungers 35

2.2.3 Expansion measurement unit 35

2.2.4 Tube preparation 37

2.2.5 Hydroforming 40

2.2.6 Strain and thickness measurement 43

2.3 OPTIMIZATION 45

CHAPTER 3 RESULTS AND DISCUSSION 49

3.1 EXPERIMENTAL RESULTS 49
3.2 FEM VERIFICATION 53
3.2.1 Material properties 53
3.2.2 Different element types 57
3.2.3 Strain distribution 62
3.3 EFFECT OF LUBRICATION 66
3.4 OPTIMIZATION 72
CONCLUSION 77
RECOMMENDATIONS 79
APPENDIX A 81
APPENDIX B 85
APPENDIX C 89
APPENDIX D 91
APPENDIX E 95
APPENDIX F 99
APPENDIX G 101
APPENDIX H 103
APPENDIX I 105
LIST OF BIBLIOGRAPHICAL REFERENCES 107

LIST OF TABLES

Page

Table 2.1 Material properties of the SS321 tubes 31

Table 2.2 Optimization settings in LS-OPT 48

Table 3.1 Optimization results for 0.9 mm tube thickness 73

Table 3.2 Optimization results for 1.2 mm tube thickness 74

LIST OF FIGURES

Page

Figure 0.1 Typical tube hydroforming process 2

Figure 1.1 Tensile test specimens cut from the tube 6

Figure 1.2 The schematic of free expansion test 7

Figure 1.3 Wall thickness distribution for different n-values 9

Figure 1.4 The effect of n-value and K-value on bursting pressure 9

Figure 1.5 The effect of r-value on bursting pressure in THF process 10

Figure 1.6 The effect geometrical parameters on bulge height in T-shape THF 11

Figure 1.7 Schematic of single and multiple strokes axial feed paths in THF 14

Figure 1.8 (A) Pressure advanced, (B) Linear, and (C) Feed advanced loading paths 14

Figure 1.9 Friction zones in THF 16

Figure 1.10 (a) Corner fill and (b) Pear-shaped expansion test for evaluate the lubricants in expansion zone 17

Figure 1.11 Different failure mode in THF process 19

Figure 1.12 Process windows for THF process 19

Figure 1.13 A typical FLD 20

Figure 1.14 (a) Direct and (b) approximate optimisation 25

Figure 2.1 Symmetry planes 28

Figure 2.2 (a) shell and (b) solid FEM 29

Figure 2.3 A typical end feed and internal pressure versus time curve 30

Figure 2.4 True stress-strain curves for tubes with (a) 0.9 mm and (b) 1.2 mm thicknesses 32

Figure 2.5 Hydroforming press at NRC 33

Figure 2.6 Round-to-square die Set....34

Figure 2.7 Plungers setup....35

Figure 2.8 Expansion measurement unit (a) initial stage (b) final stage....36

Figure 2.9 Setup of the expansion measurement units....37

Figure 2.10 The ultrasonic thickness measurement device (38DL Plus)....38

Figure 2.11 Circumferential thickness variation for tubes with (a) 0.9 mm (b) 1.2 mm thickness (dimensions in mm)....38

Figure 2.12 Pattern produced on the tube surface....39

Figure 2.13 Free end load path for tube with 0.9 mm thickness....42

Figure 2.14 Loading paths for tubes with (a) 0.9 mm and (b) 1.2 mm thickness....42

Figure 2.15 Camera movement around measuring object....43

Figure 2.16 Pictures from different views of the deformed tube....44

Figure 2.17 Thickness measurement regions....45

Figure 2.18 Design variables (P and F) in optimum loading path....46

Figure 2.19 FLD for SS321tubes with 0.9 mm and 1.2 mm thicknesses....47

Figure 3.1 Expansion in tubes with (a) 0.9 mm and (b) 1.2 mm thickness....50

Figure 3.2 Thickness variation of tubes with (a) 0.9 mm and (b) 1.2 mm thickness....51

Figure 3.3 Tube position after hydroforming....52

Figure 3.4 Tube expansion in 0.9 mm thick tube (a) free end (b) load path 1 (c) load path 2 and (d) load path 3....54

Figure 3.5 Expansion of the tubes with 1.2 mm thickness (a) free end (b) loading path 1 (c) loading path 2 and (d) loading path 3....55

Figure 3.6 Thickness variation in tubes with 0.9 mm thickness (a) free end (b) loading path 1 (c) loading path 2 and (d) loading path 3....56

Figure 3.7 Thickness variation in tubes with 1.2 mm thickness (a) free end (b) loading path 1 (c) loading path 2 and (d) loading path 3....57

Figure 3.8 Expansion of the tubes with different element types for 0.9 mm thick tube (a) free end (b) loading path 1 (c) loading path 2 and (d) loading path 3 58

Figure 3.9 Expansion of the tubes with different element types for 1.2 mm thick tube (a) free end (b) loading path 1 (c) loading path 2 and (d) loading path 3 59

Figure 3.10 Thickness variation in tubes with 0.9 mm thickness (a) free end (b) loading path 1 (c) loading path 2 and (d) loading path 3 60

Figure 3.11 Thickness variation in tubes with 1.2 mm thickness (a) free end (b) loading path 1 (c) loading path 2 and (d) loading path 3 61

Figure 3.12 Major strain distribution on the surface of the tube for loading path 1 (0.9 mm) (a) simulation (b) experiment....63

Figure 3.13 Minor strain distribution on the surface of the tube for loading path 1 (0.9 mm) (a) simulation (b) experiment....63

Figure 3.14 Major strain distribution on the surface of the tube for loading path 3 (0.9 mm) (a) simulation (b) experiment....64

Figure 3.15 Minor strain distribution on the surface of the tube for loading path 3 (0.9 mm) (a) simulation (b) experiment....65

Figure 3.16 Strain distribution for mid length cross section of 0.9 mm tubes hydroformed with (a) loading path 1 (b) loading path 3....66

Figure 3.17 Expansion for tubes with different lubricants (a) 0.9 mm and (b) 1.2 mm thick tubes 68

Figure 3.18 Thickness variation of tubes with different lubricants (a) 0.9 mm and (b) 1.2 mm thick tubes 69

Figure 3.19 Tube expansion curves for different COFs (a) 0.9 mm (b) 1.2 mm thick tubes 70

Figure 3.20 Tube thickness variation for different COFs (a) 0.9 mm (b) 1.2 mm thick tubes 71

Figure 3.21 Loading paths for tubes with (a) 0.9 mm (b) 1.2 mm thicknesses....73

Figure 3.22 Tube expansion curves for optimum loading paths (a) 0.9 mm and (b) 1.2 mm thicknesses....75

Figure 3.23 Tube thickness variations for optimum loading paths (a) 0.9 mm and (b) 1.2 mm thicknesses.....76

LIST OF ABREVIATIONS

THF	Tube Hydroforming
FEA	Finite Element Analysis
FEM	Finite Element Model
SS321	Stainless Steel 321
COF	Coefficient of Friction
n-value	Strain Hardening Exponent
r-value	Material Anisotropy
HPTH	High Pressure Tube Hydroforming
LPTH	Low Pressure Tube Hydroforming
FLD	Failure Limit Diagram
FLC	Failure Limit Curve
ESD	Effective Strain Diagram
FLSD	Forming Limit Stress Diagram
FLSC	Forming Limit Stress Curve
XSFLD	Extended Stress Based Forming Limit Diagram
XSFLC	Extended Stress Based Forming Limit Curve
GA	Genetic Algorithms
NRC	National Research Council of Canada
Tshell element	Thick shell element

INTRODUCTION

By increasing demand from different transportation industries for producing low weight and safe structures, manufacturers have to use cutting edge materials and manufacturing techniques to make lightweight, reliable and, cost-efficient structures with consistent quality. During last decade, Tube hydroforming (THF) process has emerged as a suitable manufacturing process to produce complex shapes with minimum dimensional variations and fewer secondary operations. Hence, having a good insight into this relatively new metal forming process is quite important. This chapter will put forward a brief introduction about THF process and its pros and cons. Then the objectives of the present study will be presented followed by the thesis outline.

Hydroforming concept

The fundamentals of hydroforming were established in 1940s when Grey et al. used internal pressure and axial load to investigate the production of seamless copper fittings with T protrusions (Alaswad, Benyounis et Olabi, 2012). The first use of the hydroforming process in mass production dates back to about 40 years ago when it was used to manufacture copper tubes for sanitary industry. By growing demand for more efficient manufacturing methods, hydroforming has widely opened its way in various industries such as automotive and aerospace as an advanced manufacturing technology and as an alternative for conventional production processes such as stamping and welding. Exhaust manifolds, exhaust pipes, radiator enclosures, frame rail, chassis and engine cradles are some of the most well-known hydroformed parts in automotive industries (Dohmann et Hartl, 1997). Although different classifications have been made by different researchers (Siegert et al., 2000; Zhang, 1999), hydroforming can be classified into two main categories, sheet hydroforming and tube hydroforming (Koç et Altan, 2001). Despite some differences between these two processes, the basic principle remains the same: using an internal fluid pressure to form a blank material. The focus of the present study is on the tube hydroforming process.

Tube hydroforming

Tube hydroforming is a metal forming process in which a tube is formed into complex shapes inside a closed die using simultaneously an internal pressure and axial loads at the tube ends. Figure 0.1 shows the sequence of a typical THF process. The process begins with placing the blank tube, which has been cut to the appropriate length, inside the die cavity (Figure 0.1a). Then the die closes and the plungers move towards the tube ends to press against the ends of the tube and seal it (Figure 0.1b). In the next step, the liquid is pressurized inside the tube and axial force is applied to the tube ends to form the tube into the die shape (Figure 0.1c).

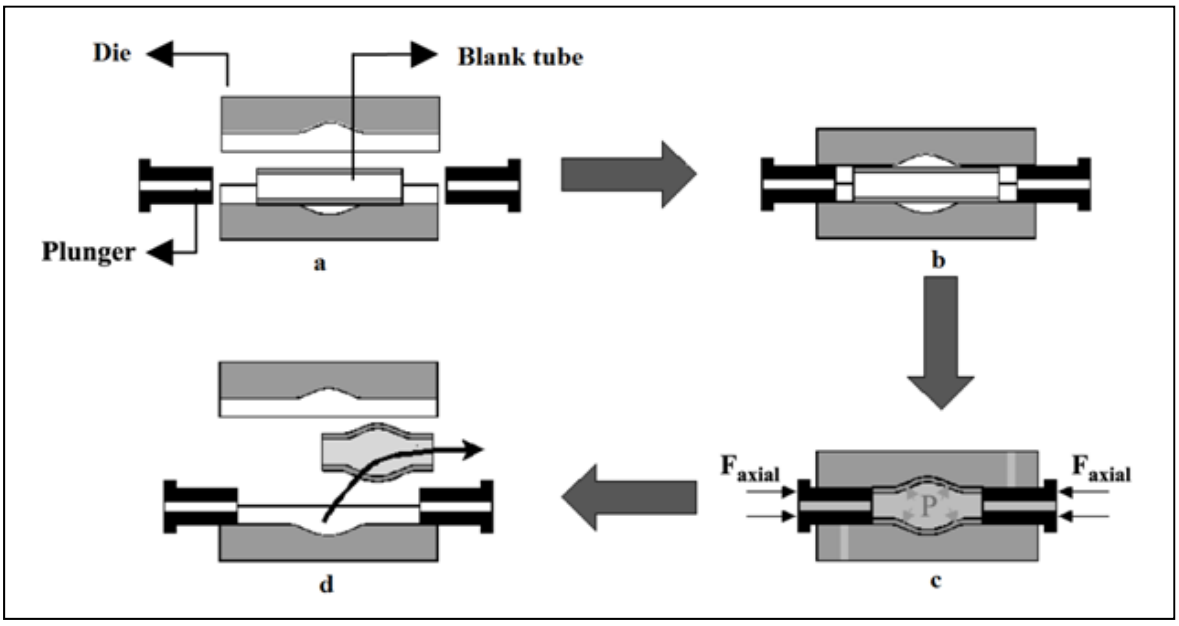

Figure 0.1: Typical tube hydroforming process
(Guan, Pourboghrat et Yu, 2006)

Thanks to the recent technological improvements, especially in control systems, tube hydroforming of massive parts has become a viable technique during the last two decades. Tube hydroforming offers many advantages in comparison with traditional manufacturing methods (Ahmetoglu et Altan, 2000; Dohmann et Hartl, 1996; 1997) such as:

1) weight reduction of the final part through tailoring of the section design and tube geometry.
2) decreasing the production costs by eliminating the secondary operations, such as welding/trimming, and reduction in material waste.
3) reducing the labor costs through part consolidation, tighter tolerances and reduced spring back that increases production repeatability.
4) increasing structural strength through optimized section design.

With its unique advantages, THF have some drawbacks (Ahmetoglu et Altan, 2000; Ahmetoglu et al., 2000; Koç, 2008; Koç et al., 2000; Zhang, 1999) such as:

1) slow cycle time;
2) expensive equipments;
3) insufficient existing knowledge base for process and tool design.

To fill this lack of knowledge and to improve and optimise THF process, many studies have been carried out up to now. In the next chapter a thorough review of the past research will be presented.

Research objectives and methodology

In this thesis, we will follow two main goals. The first one is to study the effect of different parameters like material properties, tube thickness, load path and friction condition on THF process. To study these parameters, a finite element model (FEM) was developed using 3D non linear LS-DYNA as the solver. For validating the FEM, a series of experiments have been performed using stainless steel 321 (SS321) with two different thicknesses; 0.9 mm and 1.2 mm. A fully instrumented hydroforming press was used to apply different loading paths during the experiments. A laser measurement system was mounted on the press to measure tube expansion during the hydroforming process. Furthermore, the strains on the surface of the deformed tubes were measured using an automated deformation measurement system

(ARGUS®). In the end, the results from finite element analysis (FEA) and the experiments were compared to check the reliability of the FEM.

The second objective of this project was to predict the optimum loading path for the tube hydroforming process using LS-Opt software. The objectives of the optimization procedure were to maximise the expansion of the tubes with minimum wall thickness variation.

Thesis outline

This thesis will be presented in the following chapters:

In chapter 1 a thorough literature review on FEA, parameters that affect the THF process and optimisation procedures will be presented. In chapter 2 the FEM, the experimental and the optimization approach used for this study will be explained. In Chapter 3 the results that have been obtained from the FEA and experiments will be presented and discussed. And finally, chapter 4 summarizes the conclusions of this research and offers some recommendations for future works.

CHAPTER 1

LITERATURE REVIEW

This chapter presents an overview of available published results concerning various aspects of THF. First, the design parameters and process condition that affect the forming process is presented. After that, the failure modes that usually occur during the process and the technique to predict and avoid these failure modes are discussed. Finally, an overview on the optimisation techniques used to improve the quality of final part is presented.

1.1 Effective parameters in THF process

The end result of a THF process is highly relied on different parameters like the tube material properties, the geometrical parameters of the tube and die such as corner radius of the die, tube length, tube diameter and tube thickness and the process parameters such as load path and friction condition. The effect of each parameter should be taken into consideration to produce a sound product. Many researchers have studied the effects of these parameters in THF process up to now. In this section a review on these researches is presented

1.1.1 Effect of material properties

Material property plays an important role in THF process. It can affect the magnitude of the process parameters such as the internal pressure and the axial load as well as the tube expansion and the thickness variation (Ahmetoglu et Altan, 2000). On the other hand, as mentioned before, FEA has become a common tool in investigating the THF process and it demands reliable material parameters such as elastic module, yield strength, ultimate tensile strength and anisotropy to simulate the forming process of the tube accurately. However, there is not a standard procedure for extracting the material properties of the tubular materials and different researchers proposed different approaches.

Uni-axial tensile test is the most common way to extract the material property and stress-strain relationship in the sheet metal forming process. In this test, samples with a dog bone shape and with a standard size are cut out of the metallic sheet. Due to the tube manufacturing process that can include rolling or extrusion, welding and sizing operations, the characteristics of the tube can be different than those of blank sheet from which the tube is made. So the material properties of the blank sheet is not similar to the tube and it is not very useful for FEM of the THF, even if they have the same grade and composition (Fuchizawa et Narazaki, 1993). To eliminate this error, the samples that are cut directly from the tube are used in tensile testing (Figure 1.1).

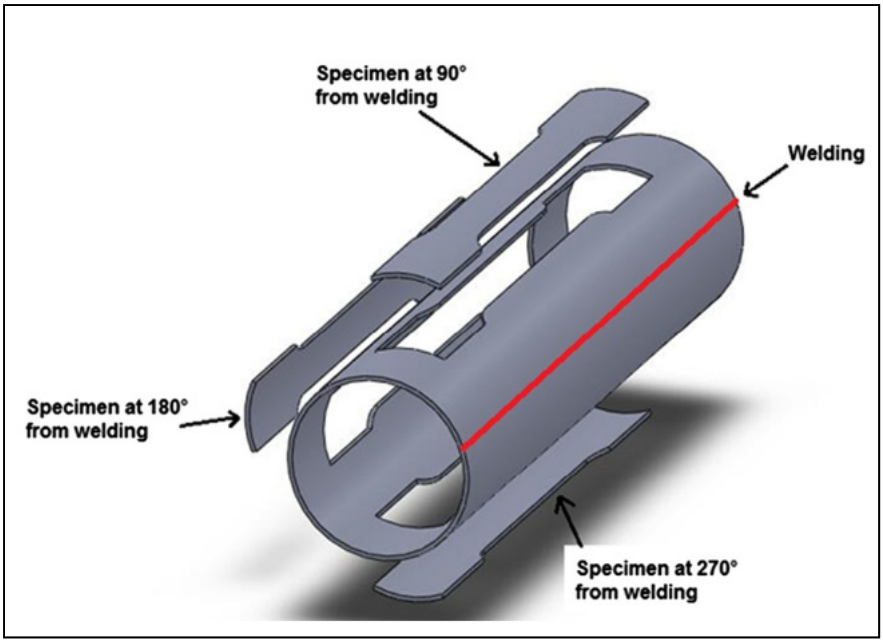

Figure 1.1: Tensile test specimens cut from the tube
(Zribi, Khalfallah et BelHadjSalah, 2013)

Even in this case, using the material properties extracted from tensile testing for the THF process is questionable as (a) the force that is used to straighten the specimens curvature may alter the material property of the samples, (b) the stress state in tensile test is uni-axial whereas bi-axial stress state is governing in THF and (c) the friction conditions in THF and tensile test are not similar (Koç, Aue-u-lan et Altan, 2001). Therefore, using a test that

represent the bi-axial condition can provide more reliable material properties and stress-strain relationship. Free expansion or bulge test is a suitable approach for this purpose as it has the most similarity to the THF process (Jansson, Nilsson et Simonsson, 2005; Strano et al., 2004). In this test a tube is sealed from its both ends. Then the tube is filled with a fluid that is used to increase the internal pressure of the tube up to the bursting. So far, several procedures have been proposed for obtaining the tube material properties in a bulge test (Fuchizawa et Narazaki, 1993). The main problem in this approach is the measurement of the longitudinal curvature (r_φ) of the deforming tube (Figure 1.2), which is used for stress components calculation. Basically two main methods for obtaining r_φ have been proposed: analytical calculation and experimental measurement.

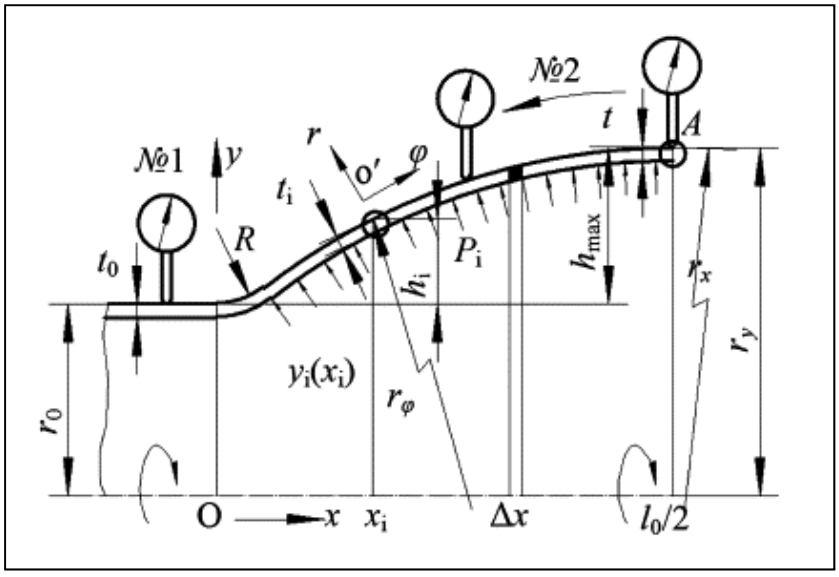

Figure 1.2: The schematic of free expansion test
(Lianfa et Cheng, 2008)

As experimental measurement of the r_φ is difficult and needs special equipment, many researchers have tried to evaluate the r_φ based on the assumptions of specific geometrical profiles encountered during the tube deformation in bulge test (i.e. circular and elliptical profiles) (Hwang et Lin, 2002; Hwang, Lin et Altan, 2007; Velasco, Boudeau et Michel, 2008). However, these profiles may be different from what happens in real bulge forming

and because of that the accuracy of the results might be questionable. Despite the difficulties in experimental measurement, some researchers tried to measure the r_φ by experimental means (Bortot, Ceretti et Giardini, 2008). But up to the recent years, an accurate experimentally measurement of the r_φ in bulge forming was not possible. In the recent years, thanks to the improvements in optical measurement systems, the online and accurate measurement of the strain distribution and bulge shape of the deformed tubes becomes possible.

Study on the effect of material characteristics on final part dates back to 1966 when Fuchs (Fuchs, 1966) conducted some experiments on expansion and flanging of copper tubes to explore the effect of material tensile strength. He concluded that a small increase in tensile strength would increase the formability severely. The effect of strain hardening exponent (n-value) was investigated by Fuchizawa (Fuchizawa, 1984). He concluded that by increasing the amount of n-value, more uniform thickness is achievable and besides greater expansion becomes possible. In addition the required internal pressure to form a certain bulge height decreases by higher n-value. Manabe et al. (Manabe et Nishimura, 1983) reached to the same results in a separate study. Kridli (Kridli et al., 2003) developed a 2D FEM of hydroforming process in a square-shape die using commercial finite element code ABAQUS/Standard. He showed that tubes with higher n-value can be formed to smaller die corner radius. In other words, by increasing the n-value the formability of the tube increases as well. Also, wall thickness variation decreases by increasing the n-value (Figure 1.3). In another study, an analytical model was developed by Orban (Orban et Hu, 2007) for the same problem and the same conclusions were made. Carleer et al. (Carleer et al., 2000) investigated the effect of material properties by means of an analytical model along with FEA and experiments in free expansion process. He reached to the same conclusion for the effect of n-value.

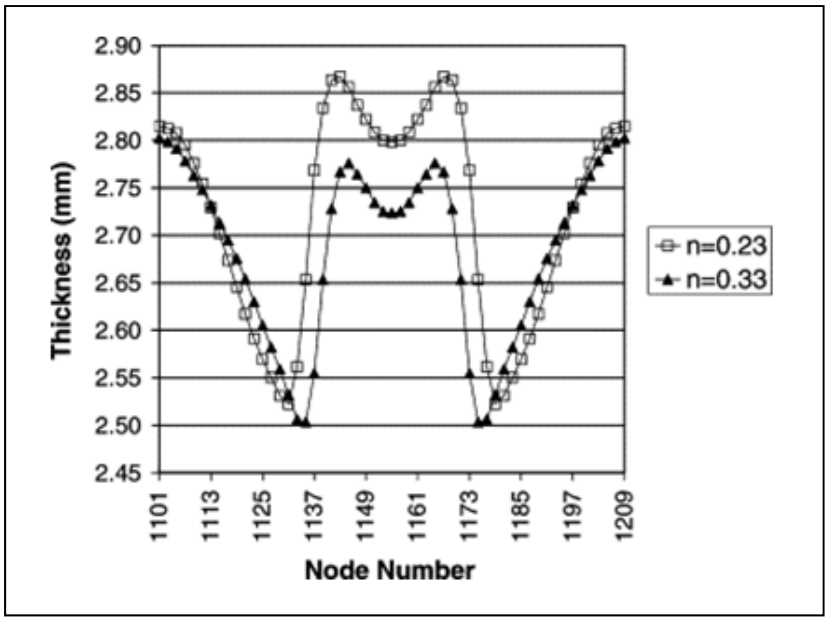

Figure 1.3: Wall thickness distribution for different n-values
(Kridli et al., 2003)

Kim et al. (Kim et al., 2006) investigated the influence of material parameters, n-value and strength coefficient (K-value), on bursting pressure. Their results showed that the bursting pressure increases by increasing the K-value or by decreasing the n-value as presented in Figure 1.4.

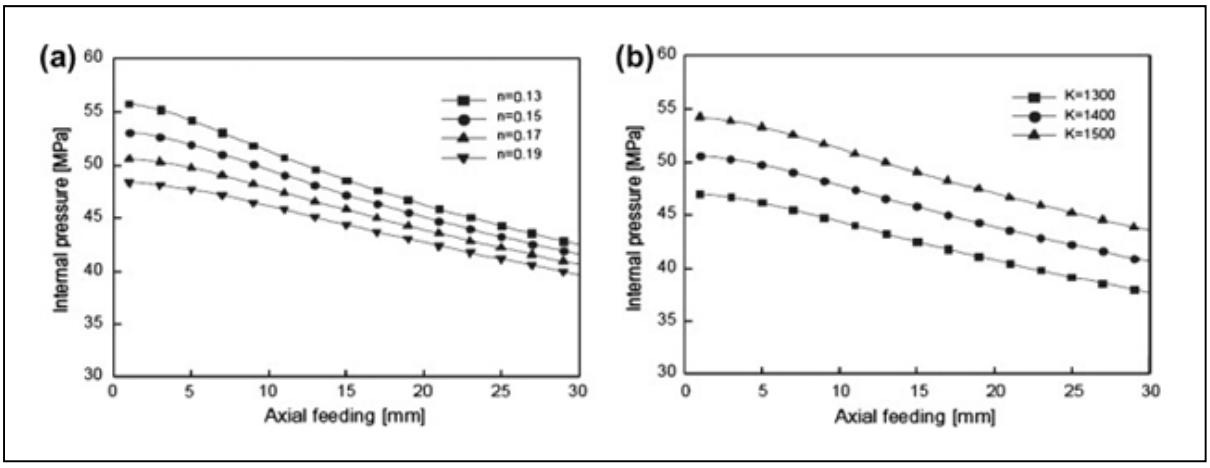

Figure 1.4: The effect of n-value and K-value on bursting pressure
(Kim et al., 2006)

The other important material parameter in THF is anisotropy (r-value). Fuchizawa (Fuchizawa, 1987) explored the effect of r-value on deformation of thin-wall tubes in hydroforming process. His study showed the critical role of the r-value in THF process. Based on his results, anisotropy in longitudinal direction has considerable influence on expansion limit and thinning ratio while anisotropy in hoop direction affects the required internal pressure. Xia (Xia, 2001) studied the effect of r-value on bursting pressure through a mathematical analysis (Figure 1.5). He presented the results of his research as hydroforming failure diagram in the end feed—internal pressure space. Other researchers reached to the same results for the effect of r-value in THF process (Carleer et al., 2000; Kim et Kim, 2002; Manabe et Nishimura, 1983).

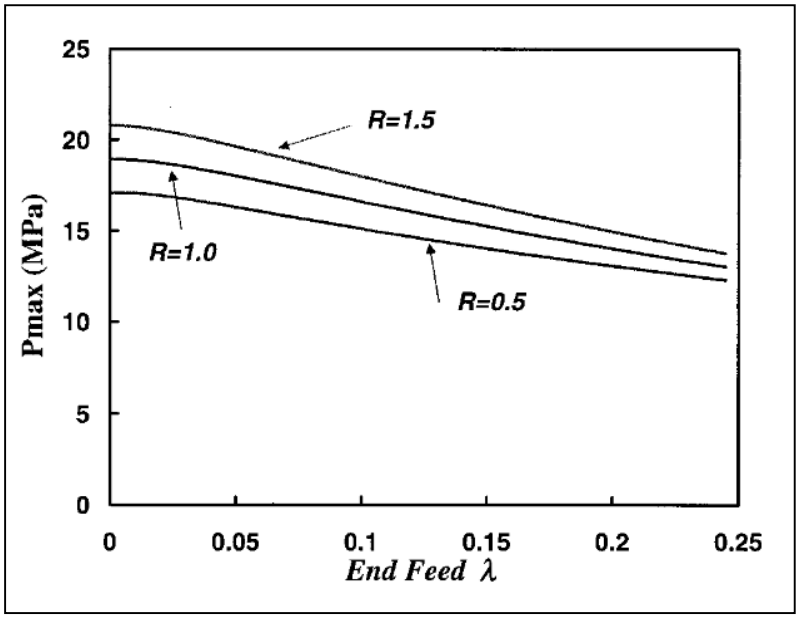

Figure 1.5: The effect of r-value on bursting pressure in THF process
(Xia, 2001)

1.1.2 Effect of geometrical factors

Geometrical factors have an important influence on the THF process. The effect of the tube diameter on formability and thickness variation in THF of a vehicle bumper rail with complex cross section was investigated by Kang et .al (Kang, Kim et Kang, 2005). They found that increasing the tube thickness by 10% will decrease the thinning rate by one-third and will result in more uniform thickness distribution. Also, for the tubes with outer diameter more than 100 mm the influence of the pre-pressure is more distinct. Koc et al (Koç et al., 2000) used Low Cost Response Surface Method (LCRSM) which is a design of experiments technique along with FE simulations to study the effect of geometrical parameters on T-shape THF process as plotted in Figure 1.6. With this study, they concluded that the most affecting parameters on bulge height (H_p) are the distances between protrusion and edges (Lpe1 and Lpe2).

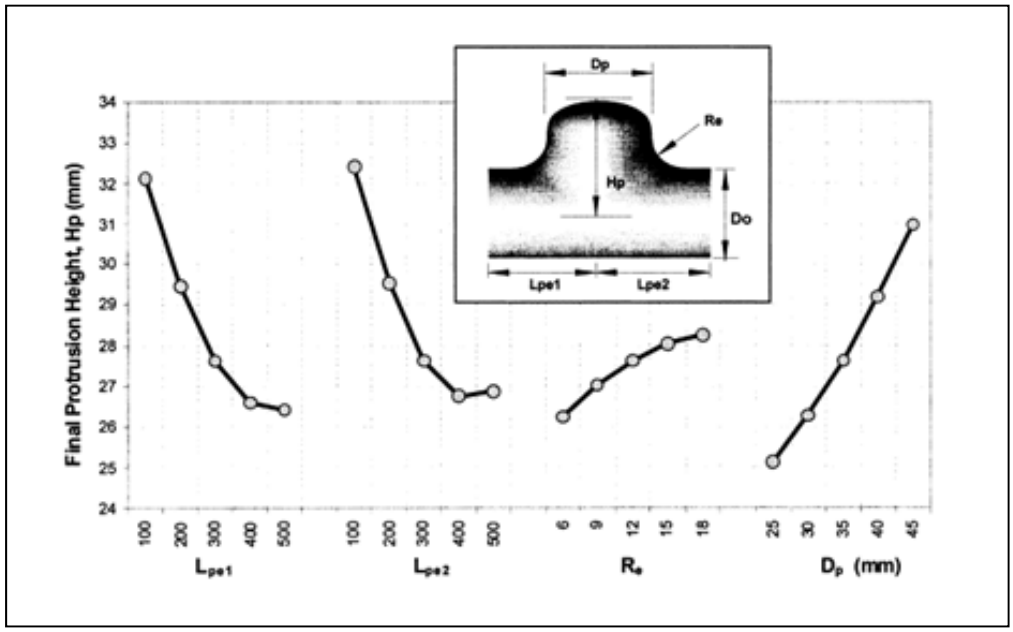

Figure 1.6: The effect geometrical parameters on
bulge height in T-shape THF
(Koç et al., 2000)

Kridli et al. (Kridli et al., 2003) investigated the effect of the die corner radius and initial tube thickness on corner filling and thickness distribution in a square cross section THF process. They concluded that with a larger corner radius, more uniform thickness distribution is attainable. Also, they reported that the initial thickness mostly affects the required internal pressure and the thinning pattern remains the same for all the thicknesses. In another research, the effects of tube outer diameter on hydroforming with a square cross section die performed by Kömmelt (Kömmelt, 2004). He concluded that by increasing the tube diameter, the thickness distribution of the hydroformed part will be more uniform.

1.1.3 Effect of loading path

The effect of loading path (internal pressure and axial loading) during the THF process is a key factor for production of a sound hydroformed part. Therefore, considerable researches have been carried out by various researchers on this matter. In 1968, Ogura and Ueda (Ogura et Ueda, 1968) investigated the effect of internal pressure and axial loading in T-branch hydroforming of low and medium carbon steel tubes. A variety of combinations of internal pressure and end feed were tested and finally a proper forming zone was defined for the T-branch hydroforming. In 1973, Limb et al. (Limb et al., 1973) presented their results on bulge forming of different materials with different thicknesses. They found that applying internal pressure and axial feeding simultaneously leads to better thickness distribution and tube expansion. In the same year, Woo (Woo, 1973) studied the effect of internal pressure and axial-feeding in bulge forming of copper tubes experimentally and numerically. The stress-strain relationship in his FE simulation was obtained from bi-axial test and the results were in good agreement with experimental results. In 1976, a study was carried out by Kandil (Kandil, 1976) on THF of tubes with different materials such as Brass, Aluminum and Copper using only internal pressure. Manabe et al. (Manabe et al., 1984) used an analytical approach to predict the required internal pressure and axial load for hydroforming of aluminum tubes. Then a computer control press was used to implement predefined loading paths to investigate the deformation behavior and forming limits of the aluminum tubes. In a later research, two different loading paths: pressure predominant and feed predominant

loading path were compared to each other by Ahmed and Hashmi (Ahmed et Hashmi, 1998). They concluded that using pressure predominant loading path leads to better deformation as feed predominant loading path may result in buckling or wrinkling. Ahmetoglu et al. (Ahmetoglu et al., 2000) in their study declared that it is better to increase the axial feed to obtain better wall thickness uniformity. However, by increasing the end feed the required internal pressure increased too. Effect of axial load on wall thickness distribution was studied by Manabe and Amino (Manabe et Amino, 2002) analytically and numerically. They observed that axial feeding and lubrication condition have a great influence on tube thickness distribution in THF process. Koc (Koç, 2003) studied the effects of loading path and material properties of blank tubes in hydroforming process of a production scale automotive structural frame part. The results showed the significant effect of loading path on the final part. The effect of three different end conditions: free end, fixed or pinched end and forced end on forming limit diagram (FLD) of aluminum alloy AA6082-T4 were examined by Imaninejad et al. (Imaninejad, Subhash et Loukus, 2004). It was noticed that free end condition has the lowest forming limit followed by fix end and forced end conditions. They also found that weld material anisotropy and end-condition are the two major parameters that affect the failure location in hydroforming of the tubes. In a subsequent work Imaninejad et al. (Imaninejad, Subhash et Loukus, 2005) suggested multiple strokes for axial and vertical actuators to improve the formability of the process (Figure 1.7). Also they found that the majority of the axial feed should be provided after tube material yielding under internal pressure.

Hama et al. (Hama et al., 2006) developed FE simulation to study the effect of three different loading paths: pressure advanced, linear and feed advanced (Figure 1.8) on THF process with a rectangular cross section die. The results showed that the pressure advanced loading path in which the internal pressure increases to a certain amount prior to starting the axial feeding leads to better formability as the initial internal pressure prevents the local wrinkling in the early stage of the process and thus the compressive longitudinal stress will be attained in the whole process.

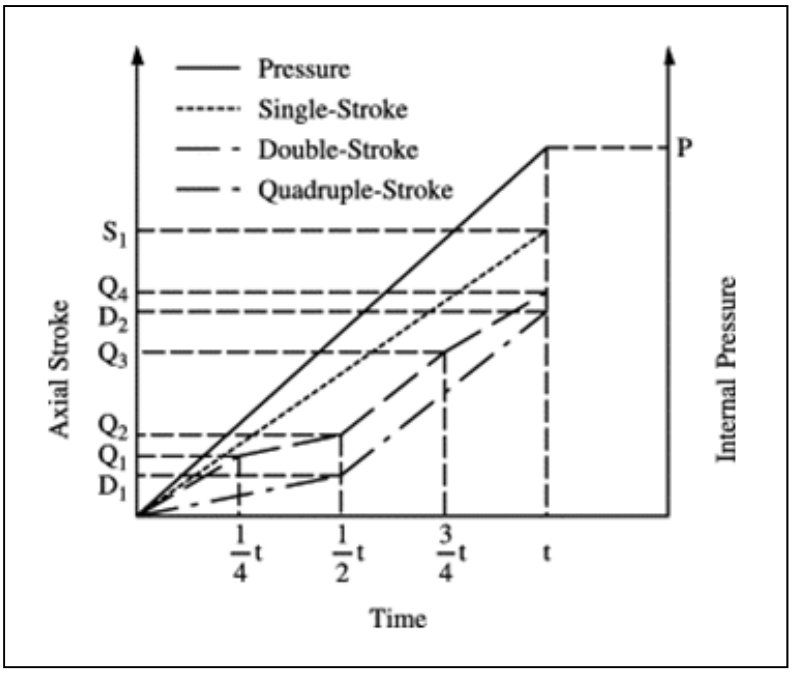

Figure 1.7: Schematic of single and multiple strokes axial feed paths in THF
(Imaninejad, Subhash et Loukus, 2005)

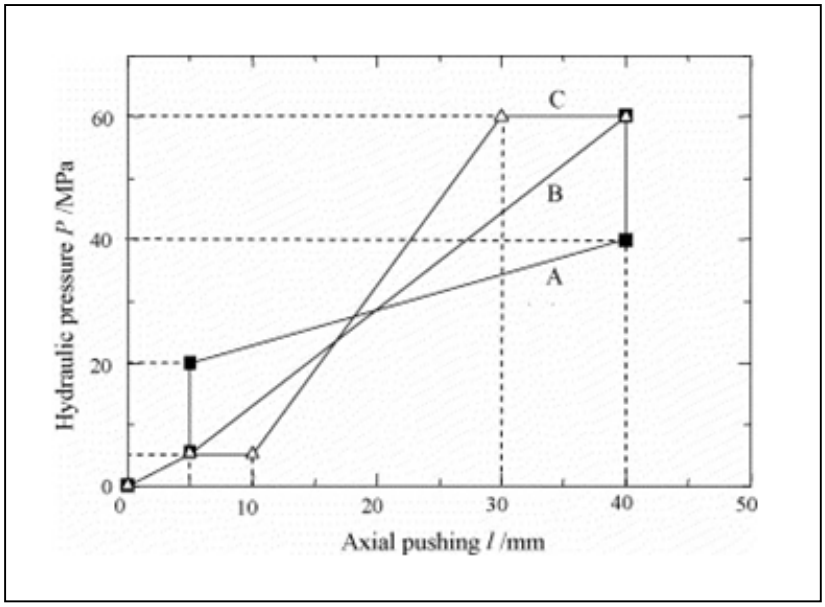

Figure 1.8: (A) Pressure advanced, (B) Linear, and (C) Feed advanced loading paths
(Hama et al., 2006)

However, in another study performed by Ray (Ray et Mac Donald, 2005) on X-shape tube hydroforming, it was recommended to use feed advanced loading path as pressure advanced loading path may causes bursting due to excessive wall thinning at certain weak points or sensitive zones. Kang et al. (Kang et al., 2007) conducted hydroforming experiments with different die shapes such as rectangular, circular and triangular for production of metallic elbows. It was concluded that proper axial feed avoids occurrence of cracks in all the cases. In a later study by Varma et al. (Varma et Narasimhan, 2008), the effects of two different pressurizing methods: prescribing fluid pressure and specified volume flow rate were investigated. They found that using specified volume flow rate method leads to proportional strain path while using prescribing fluid pressure will results in non-proportional strain path.

1.1.4 Effect of friction and lubrication

High contact pressures and large contact surfaces between the die and the tube in THF process lead to high frictional forces between the tube and the die. Furthermore, as mentioned before, in most cases in the THF process, axial feeding is required to feed the material into the deforming zone. In addition, hydroforming from a circular cross section to the die cross section requires minimum material movement resistance to fill the die completely. Therefore, careful consideration should be taken to decrease the friction between the tube and the die to avoid failures such as bad surface quality due to sticking and galling or bursting due to excessive thinning. Schmoeckel et al. (Schmoeckel et al., 1997) classified three different friction zones: guiding zone, transition zone and expansion zone in a typical THF process as presented in Figure 1.9. Base on their study, the friction condition, sliding velocity and stress state identified to be different in each of the mentioned zones. In the guiding zone, compressive state of the stress, high sliding velocity and low surface strains are governing. In the transition zone the expansion or reduction of the tube is notable. The stress state consisted of compressive stresses due to the axial load and tensile hoop stresses due to expansion of the tube and the sliding velocity is less than the guiding zone, but still appreciable. In the expansion zone, sliding velocity is negligible and tube expansion is large and tensile stresses in hoop direction are dominant.

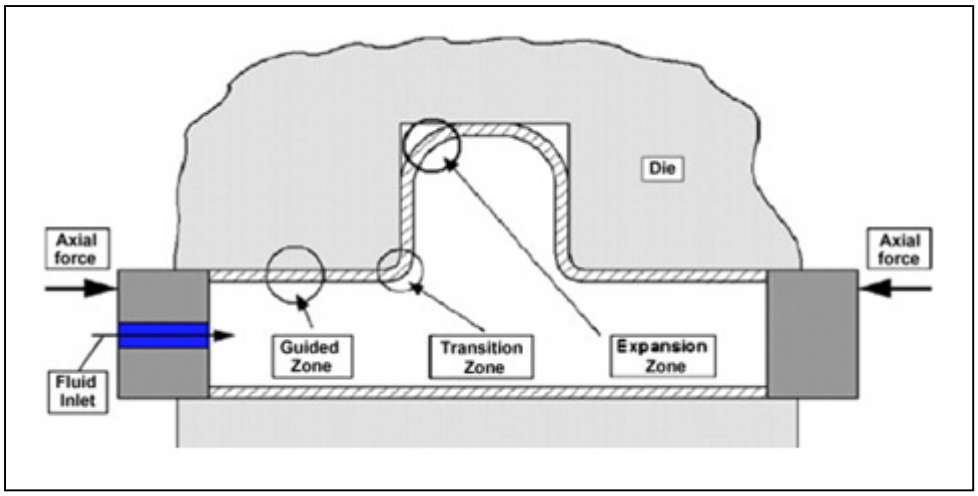

Figure 1.9: Friction zones in THF
(Plancak, Vollertsen et Woitschig, 2005)

The parameters that affect the friction condition are categorised to four groups: (I) process parameters, such as internal pressure, (II) tool parameters like die surface finish and die hardness, (III) workpiece parameters, such as tube surface condition and tube material properties and (IV) lubricant (Ahmetoglu et Altan, 2000).

Lubrication in THF process is very important; as a good lubrication allows the tube to expand much more than a bad lubrication, which causes excessive friction stress and will result in wrinkling, bursting or bad surface quality. To evaluate lubricants for hydroforming applications, different tests have been proposed (Koç, 2008). Corner fill test and Pear-shaped expansion test are two main experimental methods to evaluate the lubricants for hydroforming applications. In the corner fill test (Figure 1.10a), the tube corner radius along with wall thickness distribution are two references for evaluating the lubricant performance. In pear-shaped expansion test (Figure 1.10b), the performance evaluation of the lubricants can be achieved based on wall thinning distribution, protrusion height (δ) and bursting pressure.

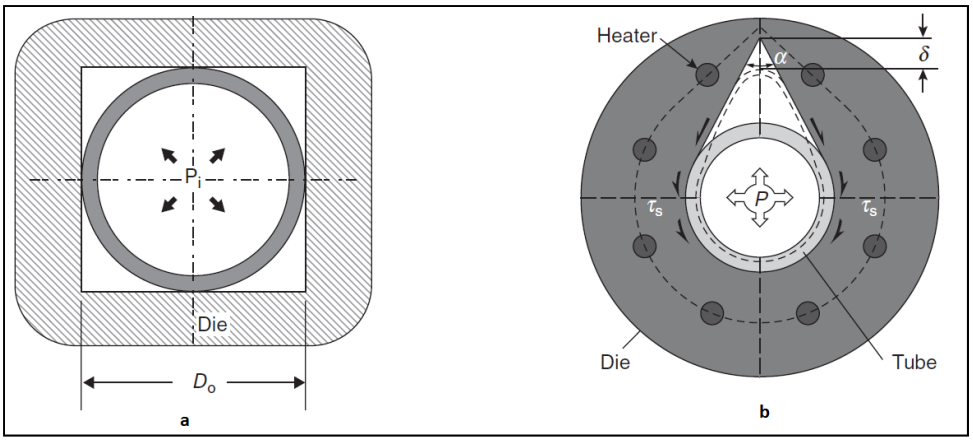

Figure 1.10: (a) Corner fill and (b) Pear-shaped expansion test
for evaluate the lubricants in expansion zone
(Koç, 2008)

Studying the effects of friction and lubrication in THF process date back to 1973 when Limb et al. (Limb et al., 1973) presented their results on the effect of friction and different lubrications on protrusion height in T-branch hydroforming process. It was reported that a lower protrusion height was obtained and the bulged dome of the T branch became more pronounced due to improper lubrication condition while proper lubrication condition resulted in higher protrusion height as well as a flat bulge protrusion area. Lee et al. (Lee, Keum et Wagoner, 2002) designed a sheet metal friction tester to investigate the effect of lubricant viscosity on friction. The results showed that the lubricant viscosity has an inverse relation with coefficient of friction (COF). In the same paper the effect of surface roughness on COF was investigated. They concluded that for all lubricants in an extremely high (< 1 μm) or low (> 0.5 μm) surface roughness, the COF is higher. The COF in guiding zone for different materials and different lubricants was studied by Vollertsen and Plancak (Vollertsen et Plancak, 2002) using an experimental procedure that is called upsetting test. Tube upsetting test was recognised a good mean for evaluating COF for the processes with plastic deformation. Ngaile et al. (Ngaile, Jaeger et Altan, 2004a; 2004b) studied lubrication mechanisms and the appropriate tests for measuring the COF in transition and expansion zones. They concluded that the limiting dome height (LDH) and pear-shaped expansion tests are appropriate for evaluating the COF in transition and expansion zones, respectively. Yeong-Maw et al. (Yeong-Maw et Li-Shan, 2005) investigated the effect of axial feeding

velocity and internal pressure on COF. They found that by increasing the internal pressure, the contact surface increases resulting in the tube surface roughness decreases, which leads to a decrease in the COF. Also, they found that axial feeding velocity has not significant effect on COF value. Plancak et al. (Plancak, Vollertsen et Woitschig, 2005) proposed an analytical model based on the tube-material properties and the tube geometry before and after deformation in the tube-upsetting test for calculating the COF. They also concluded that higher amount of internal pressure will results in lower COF values and by decreasing the friction, the thickness variation decreases too. An analytical model was proposed by Orban and Hu (Orban et Hu, 2007) to study the effect of the COF and material properties on wall thickness distribution in THF process. They explained how a sticking friction develops and restricts the material from further stretching. In a recent study, Yi et al. (Yi et al., 2011) investigated the COF in three different die shapes. They found that an increase in lubricants viscosity, tube diameter and tube material strength, the COF decreases. It was reported that the COF in guiding zone is lower than that in expansion zone and the die shape does not have any effect on the COF.

1.2 Instabilities and failures

THF is a highly nonlinear process in which loads in different directions and ratio acts during forming process. So, it is important to delimit affecting parameters to avoid instability and defects throughout the process. The loading limits in the THF process are imposed by three main failure modes namely: buckling, wrinkling and bursting (Figure 1.11). The danger of buckling prevails especially at the initial stages of hydroforming process when excessively high axial load is applied on long tubes. Wrinkling is most probable at initial and intermediate stages of hydroforming. Depending the severity of the wrinkle, it may be eliminated by increasing the internal pressure. During the final stage of the forming process, high internal pressure along with insufficient material flow may cause local necking and finally bursting of the tube. These failure modes can be postponed or avoided through the adjustment of tube material properties, friction condition, process control parameters and tool design.

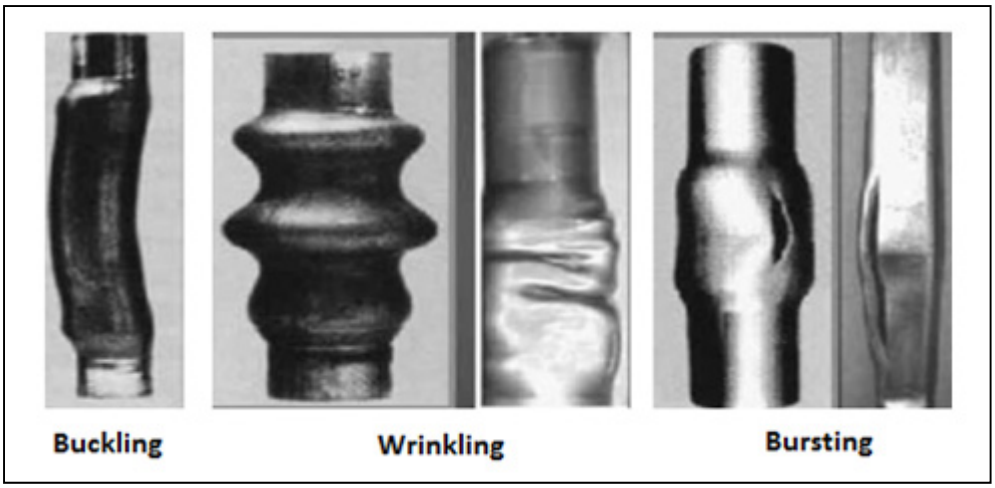

Figure 1.11: Different failure mode in THF process
(Abrantes, Szabo-Ponce et Batalha, 2005)

In order to achieve a defect free workpiece in THF process, a proper load path should be considered. A proper load path for a THF process resides within the operating window (Figure 1.12) which varies for different material and different tube dimensions.

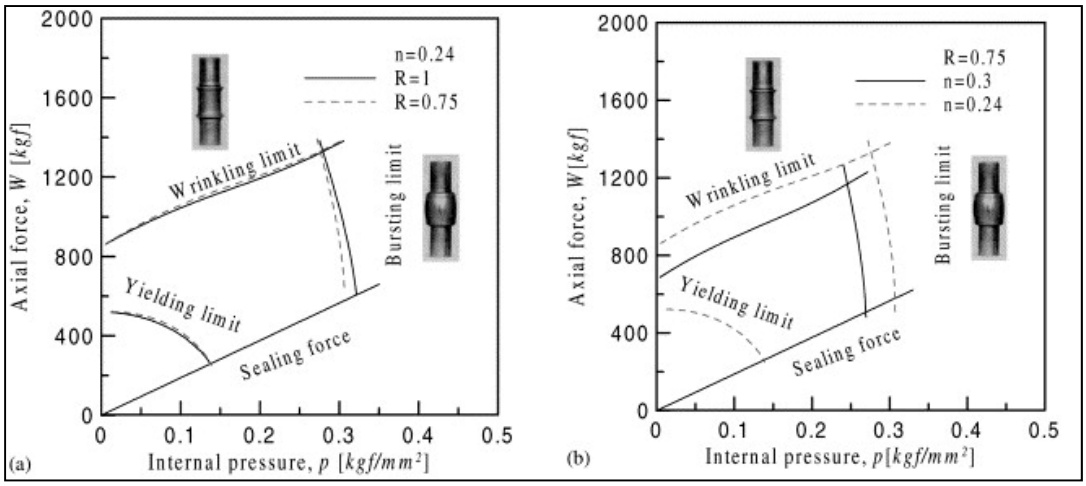

Figure 1.12: Process windows for THF process
(Kim et Kim, 2002)

Bursting as one of the failure modes in THF process is an irrecoverable defect in contrast with buckling and wrinkling. Therefore, predicting the bursting is from a high degree of

importance. Failure limit diagram (FLD) is a standard approach for measuring the formability in sheet metal forming and burst prediction. For generating the FLD, a series of material failure tests have to be done. By plotting major strain versus minor strain for different linear strain paths, the FLD can be generated. The formability limit on a FLD is presented as a line at which failure is onset and is called failure limit curve (FLC). The area below the FLC shows the safe region while the area above the FLC represents the failed region. Figure 1.13 shows a typical FLD and different linear strain paths.

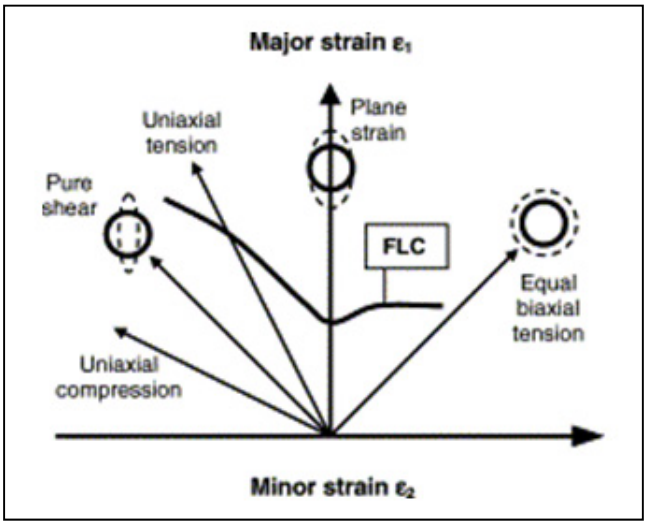

Figure 1.13: A typical FLD
(Holmberg, Enquist et Thilderkvist, 2004)

Koc and Altan (Koç et Altan, 2002) developed an analytical model based on membrane and thin-thick walled tube theories to predict the process limits and parameters in THF process. Although their model was not designed for complex parts, it could give an initial guess for further investigation with the use of FEA. An analytical model for analysing the tube material properties effect on different failure mode was determined by Chu et al. (Chu et Xu, 2004). Their study showed that the geometrical parameters such as the ratio between the initial tube thickness to the initial tube radius (t_0/r_0), the ratio between the initial tube radius to the initial tube length ($r_0/l_{0)}$ and work hardening coefficient have great effect on the occurrence of buckling and axisymmetric wrinkling. It also revealed that wrinkling is the

dominant failure in short tubes while buckling occurs in longer tubes. In a different investigation, the bursting of seamed tube in bulge tube hydroforming was studied by Kim et al. (Kim et al., 2004) through FEA. They found that the initial fracture takes place on heat affected zone near the weld line. Yuan et al. (Yuan et al., 2007; Yuan, Yuan et Wang, 2006) divided the wrinkling effect in THF into three groups including dead wrinkles, that are not removed by the end of THF, bursting wrinkles, that result to bursting of the tube and useful wrinkles, that can be removed by the end of THF. They mentioned that while the dead and bursting wrinkles considered as defects, useful wrinkles can improves the expansion ratio in THF. But the drawback of useful wrinkles is the ununiform thickness distribution along the axial direction. The minimum wall thickness is found at top of wrinkle wave whereas the maximum wall thickness can be found in the bottom of wrinkle wave.

1.3 Finite element modeling

As discussed before, THF has many advantages, though it is quite a complex process due to many parameters involve in it, such as formability of the material, loading path (end feeding force and internal pressure), tool geometry and friction. Hence having a good understanding of these parameters helps to improve the quality of the final part. Hydroforming try-outs to investigate the effect of these parameters is expensive and highly time consuming. Therefore, the application of numerical simulation for investigating and optimizing the hydroforming process has become a standard practice for engineers. The FEA can be used at designing stage to verify the feasibility of the process and to predict failure location. In this stage the FEA helps to improve the part design. In the next stage, the computer simulation along with optimization algorithms can be used to optimize the process parameters.

The history of using FEA for metal forming processes dated back to 1960s when the first commercial FEA codes were developed. At that stage due to the technological limitations, the application of the FEA was restricted to deformations with less than 1% strain. By the end of 1970s, a few nonlinear FE solvers was introduced to the world. But only by the beginning of 1990s the use of FEA became a standard tool for researchers to investigate the

metal forming processes (Alaswad, Benyounis et Olabi, 2012; Koç et Altan, 2001). Nowadays, many commercial FE modeling softwares such as LS-DYNA, ABAQUS, ANSYS, AUTOFORM are used to predict the output of the metal forming processes.

Depending on the complexity of the analysis and the required degree of accuracy, the FE model can be constructed with a wide range of options; from a simple implicit two-dimensional (2D) model to a very complex explicit three-dimensional (3D) model. Because of the severe non linearity due to large deformations, plastic behavior of the material and contact conditions in THF process, usually a 3D model is required to present the real forming condition and make it possible to detect forming defects during the process, such as wrinkling and buckling. From the formulation point of view, there are two types of approaches to develop FEM; implicit and explicit formulations. The implicit approach is mainly used for analyzing the static models while the explicit approach is used for dynamic ones. There are also a few processes that can be analysed either by implicit or explicit formulation. These processes are called quasi-static problems. THF can be considered as a quasi-static problem due to the low strain rates during the process. Modeling the THF process with either of the formulations has its own pros and cons. An implicit formulation is less time consuming and is effective especially for simplified problems. Many researchers have used this technique to reduce the processing time (Ahmed et Hashmi, 1998; Koç et al., 2000; Mac Donald et Hashmi, 2000; Ray, 2005). But implicit approach is not as effective as explicit technique when dealing with more complex problems. Explicit formulation has better capabilities for modeling nonlinear problems with high degree of deformations and gives a better insight into the forming process (Rebelo et al., 1992). There are many parameters to take in consideration for developing an accurate and efficient FE model; assumptions and simplifications, elements type, mesh density, boundary conditions and material formulation.

In 1991, Lange et al. (Lange et al., 1991) developed a finite element code for modeling metal forming processes like bending and bulge forming base on elasto-plastic material model. Ahmed and Hashmi (Ahmed et Hashmi, 2001) used LS-DYNA software to simulate the T-

branch bulge forming under two different loading conditions. Because of the symmetry, only a quarter of the problem was modeled using solid elements to describe both the die and the tube. A piecewise linear plastic material model was used to describe the tube while the die was considered as rigid. They showed that with the same axial load rate, using the lower internal pressure rate will results in more uniform stress strain distribution and will enable the internal pressure to reach to the higher values. The comparison between implicit and explicit method in FEA for predicting the wrinkling in THF process was investigated by Kim et al. (Jeong, Sung-Jong et Beom-Soo, 2003). They also studied the effects of time scaling and mass scaling in explicit method. It was explained that implicit method requires more attention especially for friction force calculation while the dynamic explicit method leads to more reasonable results that are in good agreement with experimental results. Also they concluded that for a suitable scaling factor, the kinetic energy must be less than 0.1 of the internal strain energy. The effect of internal pressure in THF process was investigated using FE simulations by Nikhare et al. (Nikhare, Weiss et Hodgson, 2009). The results showed that in high pressure tube hydroforming (HPTH) the stress variation and thinning are more pronounced that low pressure tube hydroforming (LPTH). Also it was showed that HPTH is more sensitive to friction than LPTH.

1.4 Process optimization

Finding the optimum combination of the process parameters in THF in order to produce the desired part have been always the main challenge for manufacturer. The traditional method of trial and error is time consuming and non-systematic and usually does not lead to optimum combination of input parameters. Though, optimization methods along with FE simulations can help to overcome this problem. These methods can be classified in two major groups: adaptive simulation methods and optimisation procedures (Jansson, Nilsson et Simonsson, 2007).

In the adaptive method, the FE simulation is continuously monitored for defects and input parameters are adjusted in each subsequent time increment. This procedure was used by

many researchers to optimise the loading path in THF process (Aydemir et al., 2005; Johnson et al., 2004; Labergere et Gelin, 2004; Ray et Mac Donald, 2004; Sillekens et Werkhoven, 2001a). The advantage of this method is the optimum parameters can be obtained in only one FE simulation.

The optimisation procedures try to find the optimum solution in an iterative way and by using the constraints of the process. The optimisation methods divided in three sub groups including (I) iterative algorithms, (II) evolutionary and genetic algorithms (GA) and (III) approximate optimization algorithms (Meinders et al., 2008). Classical iterative optimisation algorithms like conjugate gradient, BFGS, etc try to find the optimum solution based on minimisation of an objective function and with repeating FE simulations. As illustrated in Figure 1.14a, there is a direct interface between the FE simulation and optimisation algorithm in iterative optimisation methods which means for each function evaluation of the algorithm a FE calculation needs to be run. Despite these algorithms are well known and widely spread which is their advantages, they may trap in local optimum solutions instead of the global ones which is disadvantageous of these techniques. However, these methods have been used by many researchers to optimise the THF input parameters. (Endelt et Nielsen, 2001; Fann et Hsiao, 2003; Jirathearanat et Altan, 2004; Sillekens et Werkhoven, 2001b; Yang, Jeon et Oh, 2001).

To overcome the disadvantages of iterative algorithms, GA can be used to find the global optimum solution. The GA is an optimising method that mimics the process of natural evolution. However, the large number of required FE simulations in this method makes it very time consuming and is considered as a serious drawback. Abedrabbo et al. (Abedrabbo et al., 2011) used this method and LS-DYNA finite element code to optimise the load path in THF process.

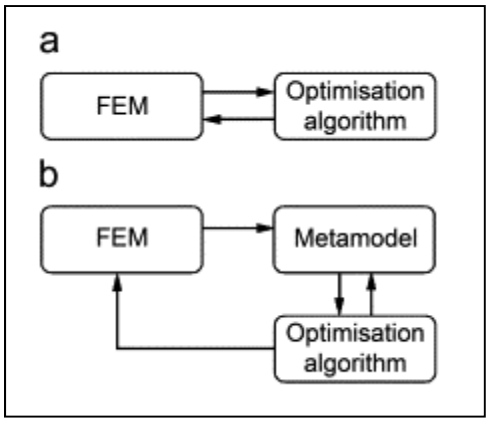

Figure 1.14: (a) Direct and
(b) approximate optimisation
(Meinders et al., 2008)

The last group of optimisation method is the approximate optimization algorithms. Response surface methodology (RSM) is a well known method among this group. In this method a set of input parameters are chosen and through FE simulations, the response to each of these sets are calculated. Then a low order polynomial is used to fit through response points and the best combinations are used for the next step, by repeating this process the optimized combination could be found. In this approach there is not a direct link between FE simulation and optimization algorithm as it was in two previous methods and a metamodel is placed in between as a buffer (Figure 1.14b). Kriging and neural networks are two other metamodeling techniques. Compared to iterative algorithms, approximate optimization algorithms have the ability to find the global optimum solution and at the same time they are less time consuming compared to evolutionary algorithms. These advantages make it appealing for researchers in metal forming process (Alaswad, Olabi et Benyounis, 2010; 2011; Koç et al., 2000).

CHAPTER 2

Methodology

THF is an advanced metal forming process that requires special attention in designing the part/tool and developing the process parameters due to hard tooling involved in it. The process development stage is an expensive and time consuming part of the THF process in complex shapes. Thus, using a trial and error procedure for developing a THF process is not an option and using FEA as a predictive tool seems inevitable. FEA increases the efficiency by reducing the lead time and the total cost of manufacturing through eliminating the trial and error procedure. To conduct FEA, a FEM with appropriate geometrical contacts, boundary conditions and material model has to be developed. Once the results of the FEA are verified by the experimental results it can be used to study the affecting parameters and to predict the failure/defects and critical regions in the THF process of components with similar complexity.

The first goal of the present work is to study the effects of different process parameters such as geometrical characteristics, load path and friction condition in the THF process. Therefore, a FEM, that will be described, was developed and validated by comparing the numerical and experimental results.

2.1 Finite element model (FEM)

The FEM that was used in this study consisted of two parts; (i) tube and (ii) rigid die. The process is called round-to-square hydroforming as it starts with a tubular shape material and the final product has a square shape. Due to symmetry planes over the tube length and the cross section, the model was simplified by applying the symmetry boundary conditions to the boundary nodes along the symmetry planes. Only half of the length and one quarter of the cross section of the tube and the die were used in the simulation (Figure 2.1). The initial tube

length and the outer diameter were 220 mm and 50.8 mm (2”) respectively. The tube material was stainless steel 321 (SS321) with two different wall thicknesses; 0.9 mm and 1.2 mm.

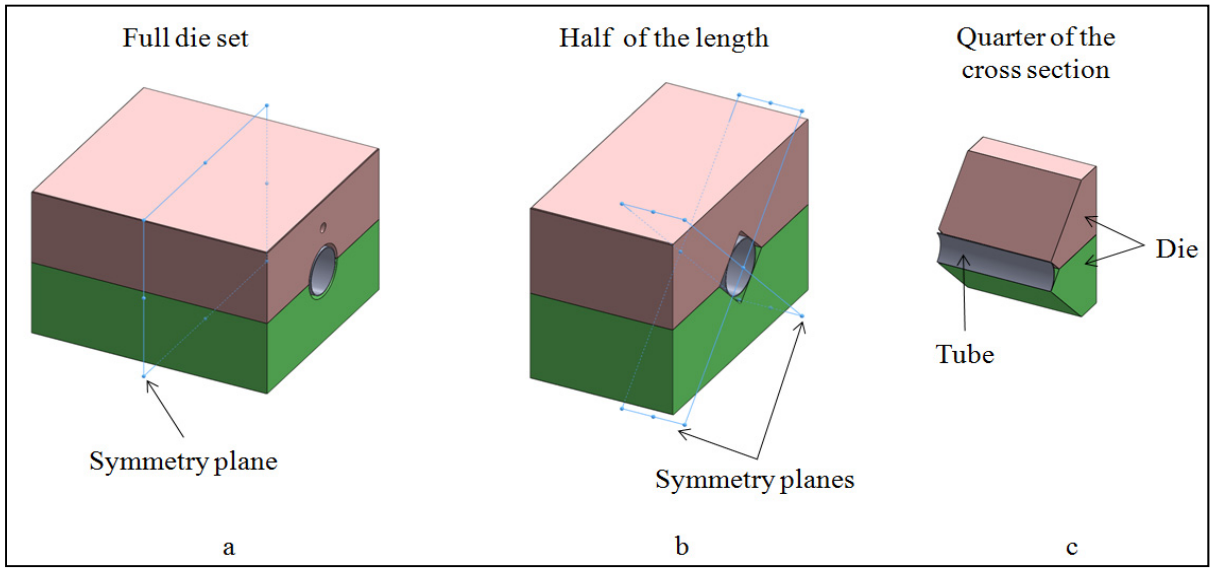

Figure 2.1: Symmetry planes

The tube thickness was varied in the circumferential direction for both tube thicknesses, so the average values of the thicknesses (0.94 mm and 1.22 mm) were used for modeling the tubes. Ansys v13.0 was used to mesh the model and Ls-Dyna v970 was used as the FEM solver. 4619 four nodes Belytschko-Tsay shell elements with aspect ratio of 1 and with five integration points through the thickness were used to generate the tube model. As shell elements are not able to capture the through thickness stress, two other models were generated using solid elements and thick-shell (Tshell) elements to compare the results. Tshell element is a special element in LS-DYNA which is developed to have both advantages of solid and shell elements. It can capture 3D stresses like solid element, but it needs less computation time. The solid model was generated using 13279 constant stress solid elements with three elements through wall thickness. The aspect ratio of the solid elements for the FEM of both tubes thicknesses was equal to one. The Tshell model consisted of 8839 elements with 2 elements through thickness, as recommended by LS-DYNA (LS-Dyna

Keyword User's Manual, 2013). The aspect ratio of the TShell elements for the FEM of both tube thicknesses was equal to one. The die was modeled as rigid body using 6669 four nodes shell elements. Figure 2.2 illustrates the FEMs with different element types.

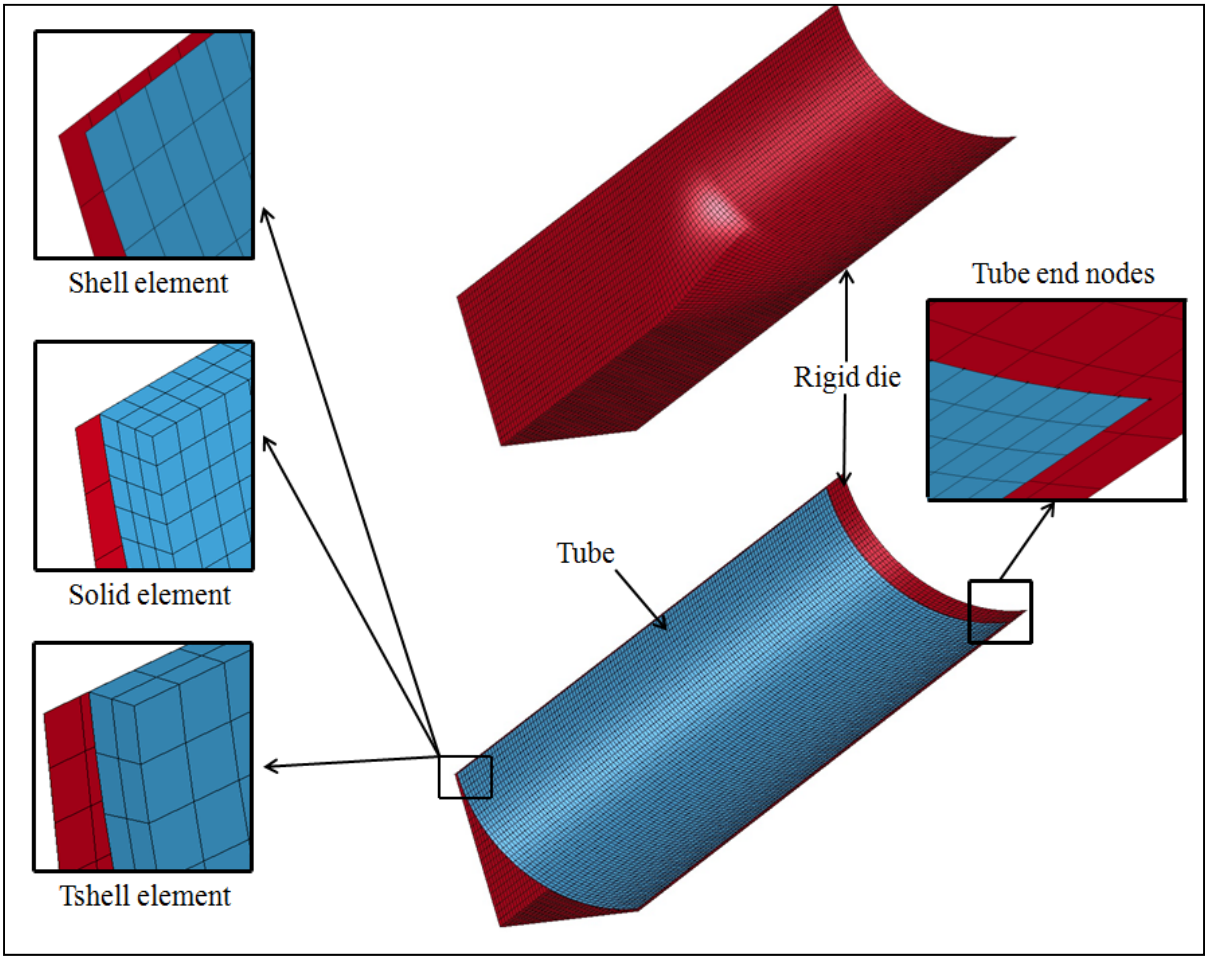

Figure 2.2: (a) shell and (b) solid FEM

2.1.1 Contact condition

To simulate the contact condition between the tube and the die, a surface to surface contact (CONTACT_SURFACE_TO_SURFACE) with Coulomb friction law was applied and different COF values from 0.01 to 0.2 were applied to study the effect of COF on thickness variation and the expansion of the tube. In the shell element model, to avoid tube self

penetration in case of wrinkling or buckling, a contact with single surface entity (CONTACT_AUTOMATIC_GENERAL) was defined for the tube.

2.1.2 Load path simulation

For simulating the load path during the process, different displacement curves were assigned to the tube end nodes to simulate the end feed condition. A linear path was defined for increasing the internal pressure during the process. As shown in Figure 2.3, the forming process consisted of three stages: (a) sealing, (b) forming and (c) calibration stages. At the beginning of the process a displacement was applied to the end of the tube to mimic the sealing operation. During the experiments it was noticed that in order to seal the tube end we need 35 kN load which was obtained at 1.2 mm end feed displacement. During the sealing period the internal pressure is equal to zero. At the second stage of the process, while the internal pressure starts to increase linearly, the end feed increases with a high slope. In the last part of the process or the calibration stage the internal pressure continues to increase while there is no noticeable end feeding. This load path was obtained from the experiment, which will be described later in the THF experiments section.

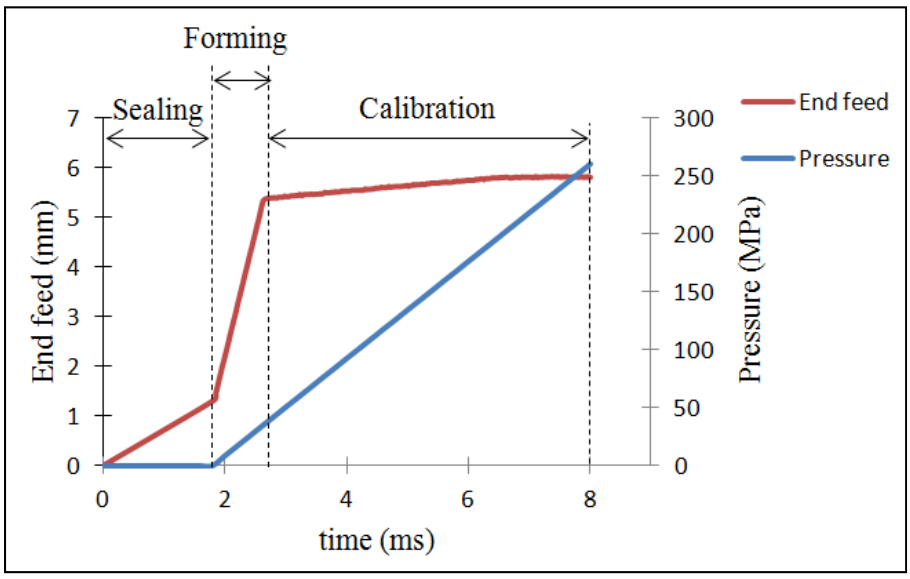

Figure 2.3: A typical end feed and internal pressure versus time curve

2.1.3 Material model

In order to simulate the tube material behavior, the Swift work hardening law (Equation 2.1) was used.

$$\sigma = K(\varepsilon_0+\varepsilon)^n \tag{2.1}$$

where σ is the true stress, ε_0 is the initial true strain, ε is the true strain, K is the strength coefficient and n is the strain hardening exponent. The material properties were used from an ongoing study in the THF process. The material was considered isotropic and the material properties of the tubes (0.9 mm and 1.2 mm) were extracted by performing free expansion test and tensile test. The samples for tensile test were cut from the tubes based on ASTM E8. Using the data obtained from the free expansion test and tensile test the values for ε_0, K and n were obtained. Table 2.1 summarizes the experimental material parameters used for the SS321 tubes. Figure 2.4 illustrates the related true stress-strain curves for both tube thicknesses, which are extrapolated up to 100% strain.

Table 2.1: Material properties of the SS321 tubes

Stainless Steel (SS321) Material	Thickness = 0.9 mm		Thickness = 1.2 mm	
	Free Expansion	Tensile	Free Expansion	Tensile
K (MPa)	1427.4	1458.29	1397.8	1461.54
n	0.53	0.49	0.62	0.62
ε_0	0.03	0.026	0.05	0.048
Yielding Stress (MPa)	250		260	
Density (g/mm³)	8.0E-03		8.0E-03	
Elastic Modulus (MPa)	193.00E+03		193.00E+03	
Poisson Ratio	0.29		0.29	

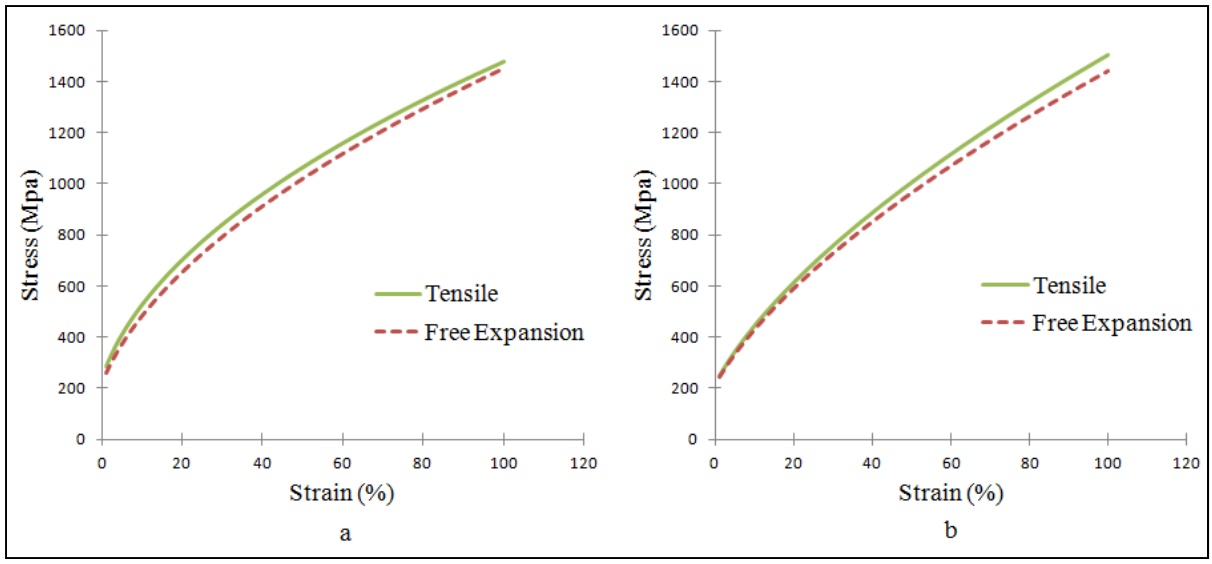

Figure 2.4: True stress-strain curves for tubes with (a) 0.9 mm and (b) 1.2 mm thicknesses

2.1.4 Time scaling

According to Jeong et al. (Jeong, Sung-Jong et Beom-Soo, 2003) for time scaling in quasi static processes like hydroforming, the kinetic energy should be maintained less than 10% of the internal strain energy during the simulation. In this case the dynamic effect in explicit method, which may affect the results accuracy in FEA, will be minimized. Therefore, different simulation durations were tested and their ratio of the kinetic energy to the internal strain energy was checked to find an appropriate time scaling for the simulations. After a few trials, 8 ms was selected as termination time. In other words, to minimize the dynamic effect in the simulation and to avoid high computational costs, the total hydroforming process was modeled in 8 ms compared to 150 s in the experiments. The hydroforming codes for shell, solid and Tshell FEMs are shown in Appendix A.

2.1.5 Spring back

After the hydroforming simulation, a file was generated (Dynain file) by LS-DYNA which contained the deformed mesh, stress, and strain state of the tube. This file was used as an

input for the spring back simulation, using a static implicit solver in LS-DYNA. The material information used in the spring back simulation was the same as the hydroforming simulation. The spring back code is presented in Appendix B.

2.2 Experimental setup

In order to verify the FEA results, the experimental data is required. The THF experiments were conducted at NRC using a fully equipped hydroforming press manufactured by Interlaken Technology Corporation (Figure 2.5).

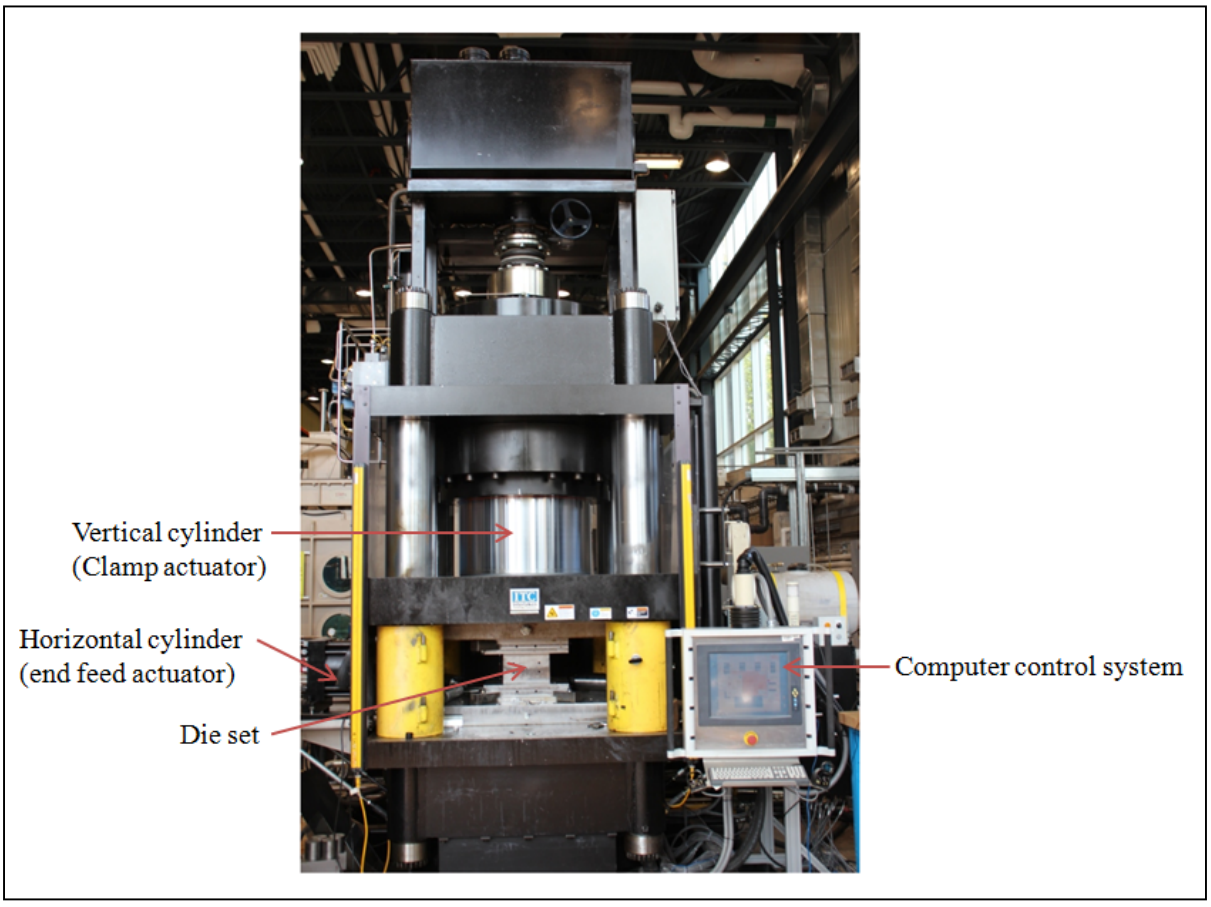

Figure 2.5: Hydroforming press at NRC

The vertical cylinders of the press delivers a 1000 ton clamping force and the two horizontal cylinders provide maximum capacity of 1000 kN axial load at each end of the tube. The

pressure intensifier unit of the press was designed to apply a maximum internal pressure of 413 MPa (60000 Psi). To perform the THF experiments, a tooling system consisted of the die, end plungers and expansion measurement units was designed and manufactured at NRC.

2.2.1 Die

A round-to-square die set was designed and manufactured at NRC. The die was made of hardened tool steel and had a square cross section with corner radii of 2.4 mm. In Figure 2.6, the die and its guiding zone, transition zone and expansion zone are illustrated.

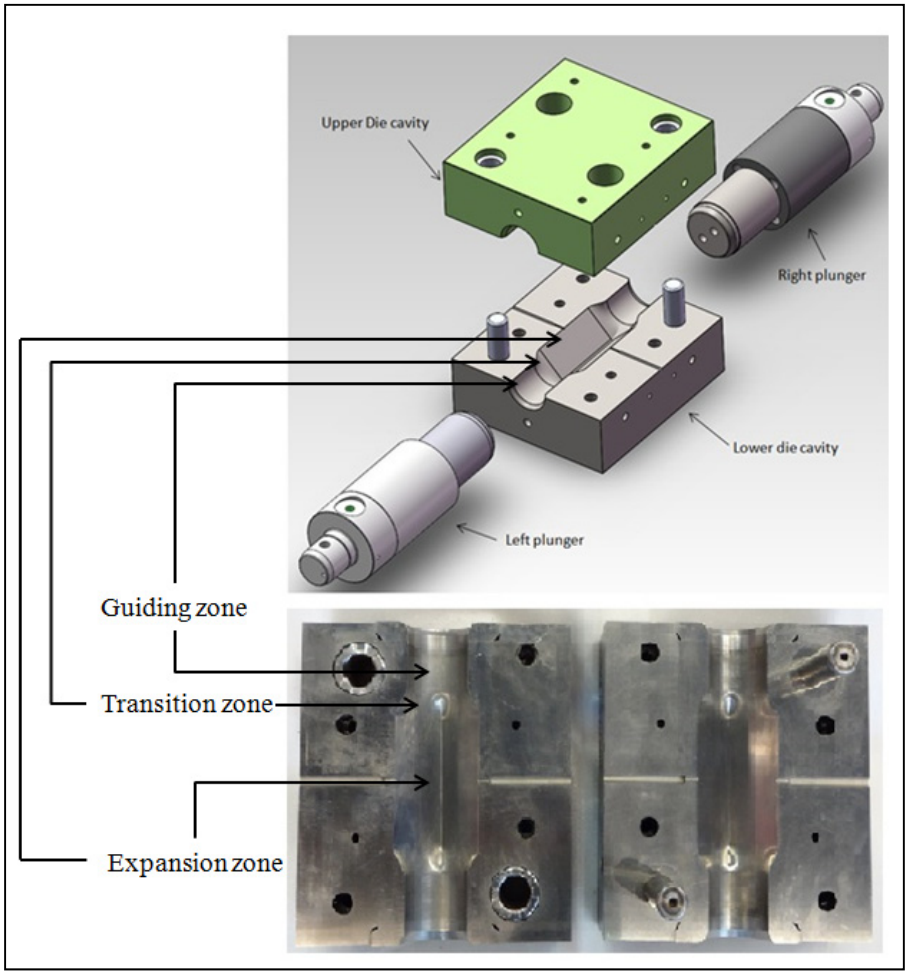

Figure 2.6: Round-to-square die Set

2.2.2 Plungers

The plungers (Figure 2.7) were designed and mounted on the left and right horizontal cylinders of the press. The plungers slide in the guiding zone of the die and apply the axial load on both ends of the tube. The sealing shoulder of the plungers provides the sealing required during the hydroforming process.

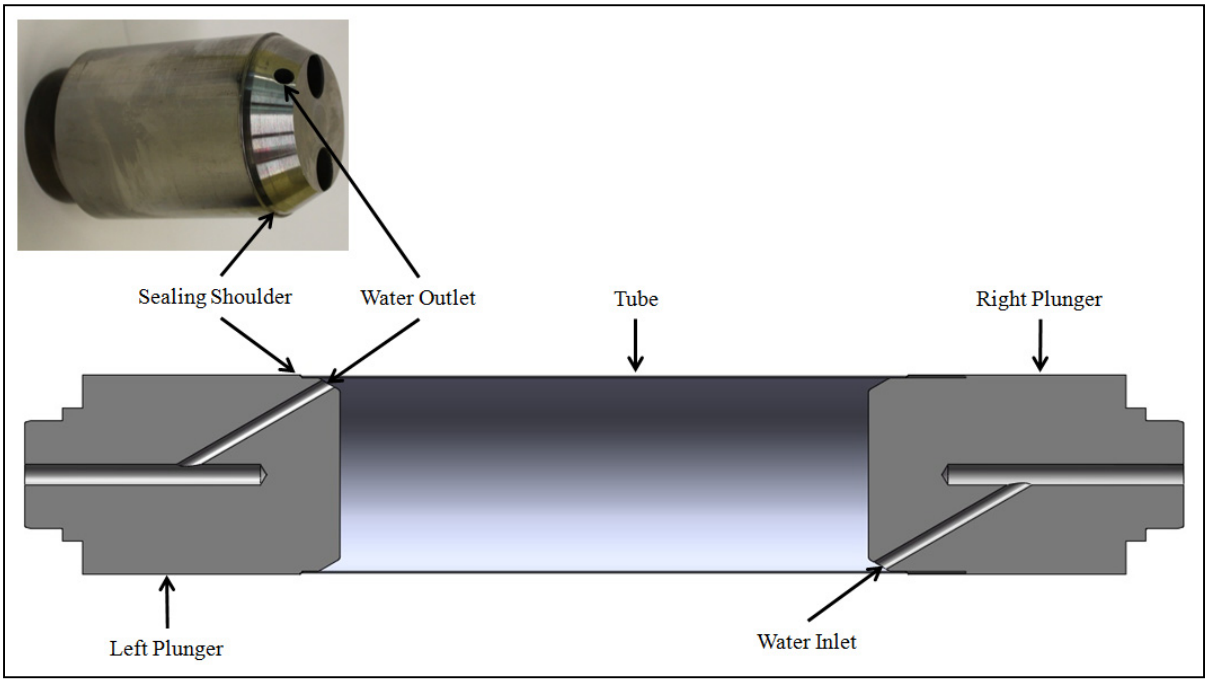

Figure 2.7: Plungers setup

2.2.3 Expansion measurement unit

The distance that the tube expands at the corners of the square was considered as the expansion of the tube (Figure 2.8). To monitor the expansion of the tubes during the THF process, two laser measurement systems in conjunction with two expansion measurement devices, implemented inside the die, were used during the experiments. As illustrated in Figure 2.8a, at the beginning of the process the distance between the laser measurement unit

and the expansion measurement device is equal to L_0. As the hydroforming process starts, the tube pushes the pins outward and as the result, the value that is read by laser measurement unit at each time increment (L_n) decreases (Figure 2.8b). The laser measurement units were connected to the data acquisition system of the press and record the expansion of the tube during the THF process. The difference between the L_n and L_0 was considered as the expansion of the tube at each time increment. In Figure 2.9 the expansion measurement unit setup on the hydroforming press is presented.

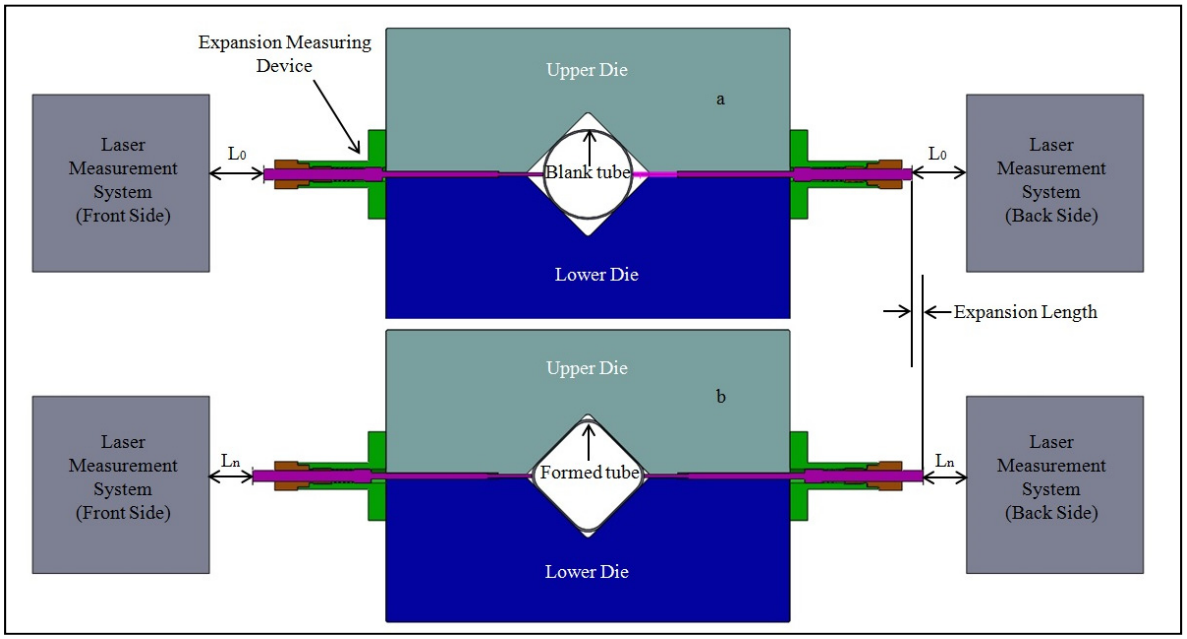

Figure 2.8: Expansion measurement unit (a) initial stage (b) final stage

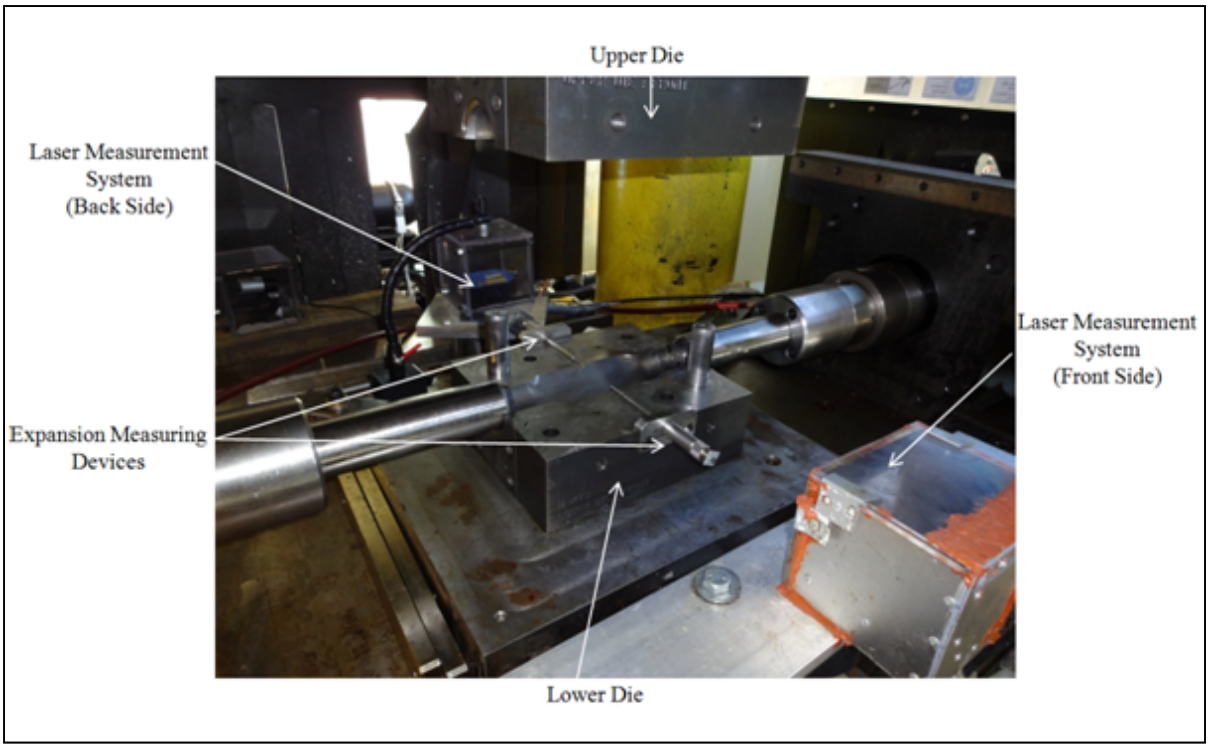

Figure 2.9: Setup of the expansion measurement units

2.2.4 Tube preparation

Before the THF experiments, the tubes were cut with a band saw and the two ends of the tube were straight cut, using a turning machine, to the final length of 220 mm. Then, the outer surface of the tube was polished by a sandpaper (CAMI Grit designation = 100) to prepare the surface for electrochemical etching. To check the thickness uniformity in the blank tubes, the thicknesses were measured in longitudinal and circumferential directions using an ultrasonic thickness measurement device (38DL Plus) manufactured by Olympus Corporation company (Figure 2.10).

It was noticed that the thickness along longitudinal direction was uniform while in circumferential direction the thickness variation was about 0.05 mm and 0.07 mm for the 0.9 mm and 1.2 mm thick tubes, respectively (Figure 2.11).

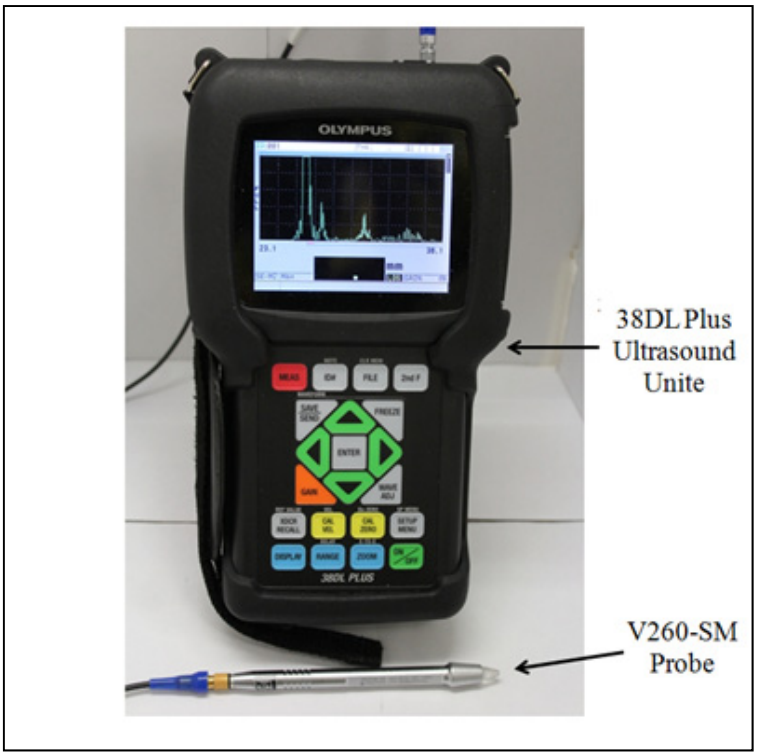

Figure 2.10: The ultrasonic thickness measurement device (38DL Plus)

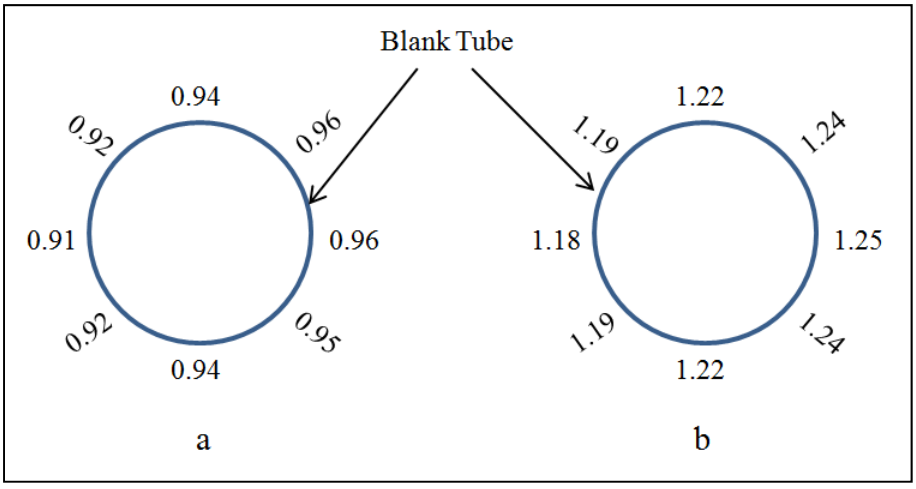

Figure 2.11: Circumferential thickness variation for tubes with (a) 0.9 mm (b) 1.2 mm thickness (dimensions in mm)

In order to be able to measure the strains after the hydroforming process, a pattern of black circle dots was etched on the outer surface of the tubes. Since the tubes are in contact with

the die during the hydroforming process, electrochemical etching process was required to get more stable dots on the tubes, so the dots will be more visible at the contact zone between the tube and the die after deformation. The electrochemical etching system consisted of an anode (positive pole), a cathode (negative pole), power unit, electrolyte solution and a stencil sheet. The stencil is used to produce the dot pattern on the surface of the tube. In our case, the dot pattern was 1mm in diameter with 2 mm distance between the centers of the dots (Figure 2.12).

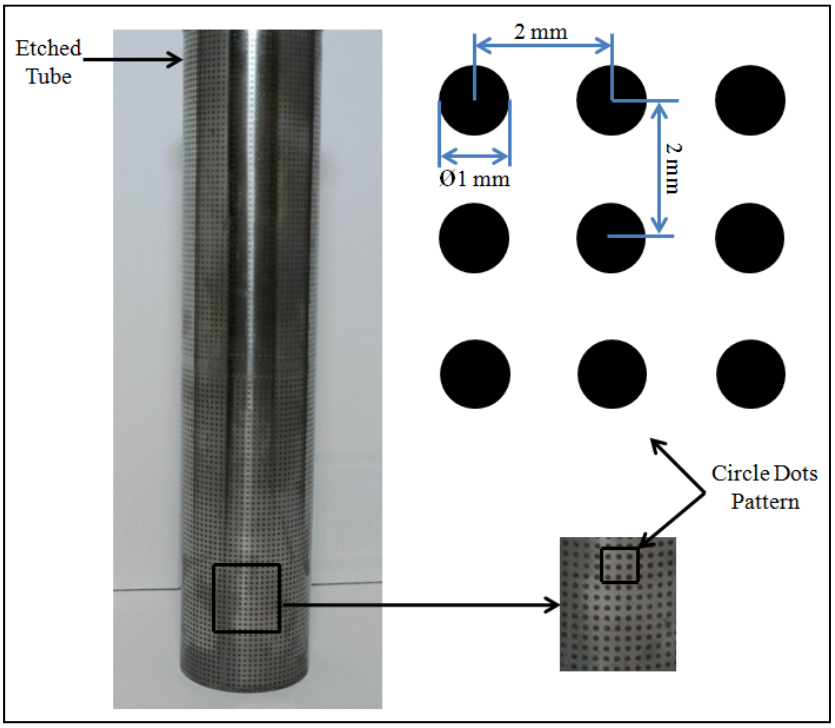

Figure 2.12: Pattern produced on the tube surface

In order to investigate the effect of lubrication in the THF process, two different lubricants were applied on the surface of the tubes using an air spray device. To obtain the best lubrication condition, the lubricant thickness should be between 0.04 to 0.06 mm according to the manufacturer. After the lubricants dried, the thickness of the lubricants on the surface of the tubes was measured for uniformity, using an ultrasound device to check that a uniform lubrication was applied on the surface of the tubes.

2.2.5 Hydroforming

After the tube preparation, the tubes were placed inside the die for the hydroforming process. As mentioned before, the pressure intensifier of the press was capable of delivering 413 MPa (60000psi) internal pressure, but during the experiments it was noticed that 260 MPa pressure is enough to fill the die completely in all cases. For this reason 260 MPa was selected as the maximum internal pressure for the experiments. During the experiments, the pressure started from zero at the end of the sealing stage at the beginning of the forming stage and increased linearly up to the maximum value of 260 MPa.

The control system of the press has the ability to end feed material into the die cavity in two different methods: (i) force control and (ii) position control. In the first method, the amount of axial load at the tube ends is specified while in the second method the position of the plungers during the hydroforming process is controlled by the control system of the press. A typical THF process is divided into three stages including sealing, forming and calibration stages (Figure 2.13). At the beginning of the experiments (sealing stage), a 35 kN sealing force was applied at tube ends, using the force control method. For the forming and calibration stages two different approaches were used. In the first approach, the force control method was used in the forming and calibration stages to conduct a free end hydroforming process. During the free end hydroforming, the end feeding forces that are applied to the tube are enough to only hold the sealing during the process and no material is fed into the die cavity. To calculate the required end feeding force at any specific time, the following equation was used:

$$F = P \cdot A/1000 + 35 \tag{2.2}$$

Where F is the end feeding force in kN, P is the internal pressure in MPa at any given time and A is the plunger's cross section area in mm^2. 35 kN in this equation is the initial sealing force before applying the internal pressure. According to the equation 2.2, by increasing the internal pressure the end feeding force increases, compensating the opposing force on the

plunger due to the internal pressure. Therefore, the plungers will apply a constant 35 kN end feeding force at the tube ends during the THF process. Using the equation 2.2 and a few tests, the final end feeding force curve was obtained for the free end hydroforming for both tube thicknesses. These tests showed the plungers' axial movement data and the minimum required end feed for a successful THF process. Values lower than the minimum end feed will lead to loosing the seal. As is shown in Figure 2.14a and b, the minimum end feed for tubes with 0.9 mm and 1.2 mm thickness is 5.5 mm and 4.5 mm, respectively. Also, the curves show that most of the plungers' movement occur up to the 40 MPa of internal pressure, which is the transition from the forming to the calibration stage. In the second approach, based on the free end experiments, three loading paths were considered and tested for each tube thickness using the position control approach. Load path 1 was representing the minimum end feed condition. Load path 2 and load path 3 were obtained by doubling and tripling the load path 1. Figure 2.14 illustrates the three load paths applied during the THF experiments. The advantage of the position control end feeding over the force control end feeding is that in the position control method, the end feeding is more uniform on the tube ends.

To investigate the effect of lubrication on the thickness variation and the tube expansion, two more contact conditions were tested using the lubricated tubes. Free end feed experiment using force control method was not appropriate due to severe non-uniform end feeding on left and right sides of the tube. Also, loading path 1 was not applicable as the sealing could not be maintained during the THF process. Hence, loading path 2 was chosen for the THF experiments with lubricated tubes.

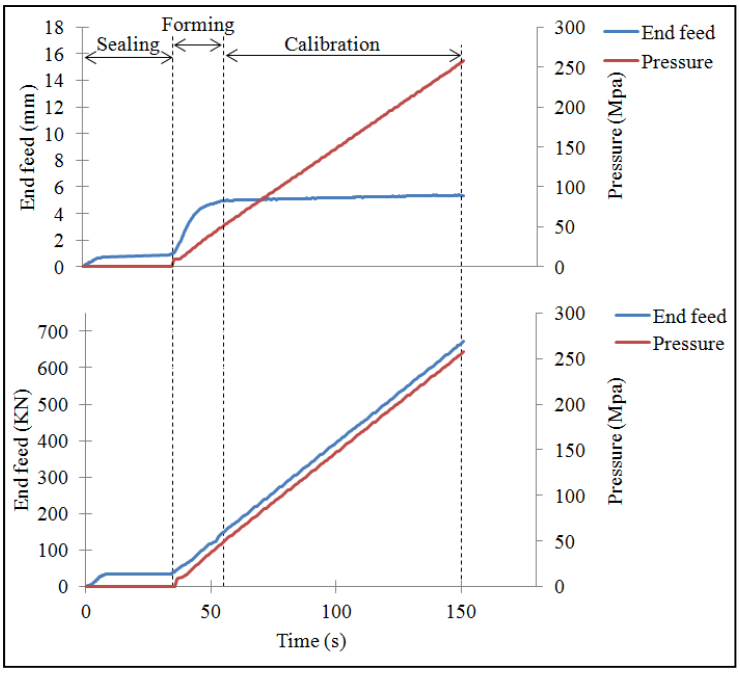

Figure 2.13: Free end load path for tube with 0.9 mm thickness

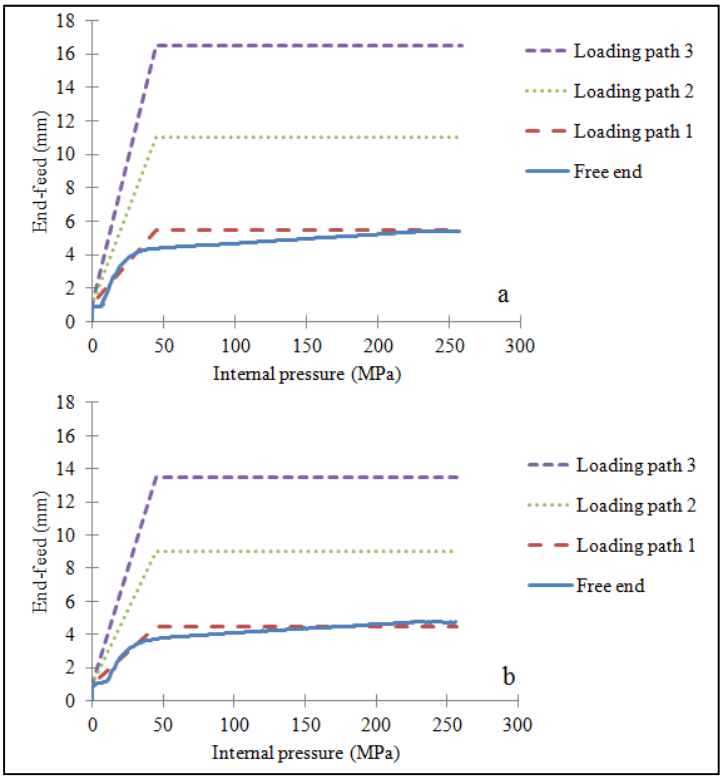

Figure 2.14: Loading paths for tubes with
(a) 0.9 mm and (b) 1.2 mm thickness

2.2.6 Strain and thickness measurement

To capture the strain state of the deformed tubes after the hydroforming process, ARGUS® measurement system was used. ARGUS® is a non-contact optical 3D deformation measurement system that can automatically analyze, calculate and document the deformation that occurred in the deformed part. Prior to the deformation, as mentioned in section 2.2.1, a dot pattern was applied to the outer surface of the tubes. After the hydroforming process, a camera records the measuring points through several images that are captured from different views (Figure 2.15 and Figure 2.16). These pictures are then transferred to the ARGUS® software. The ARGUS® software correlates the images and the center position of each point in the space will be calculated using the reference points. Finally, The ARGUS® software generates the 3D measuring data by comparing the 3D positions of the deformed points with undeformed points.

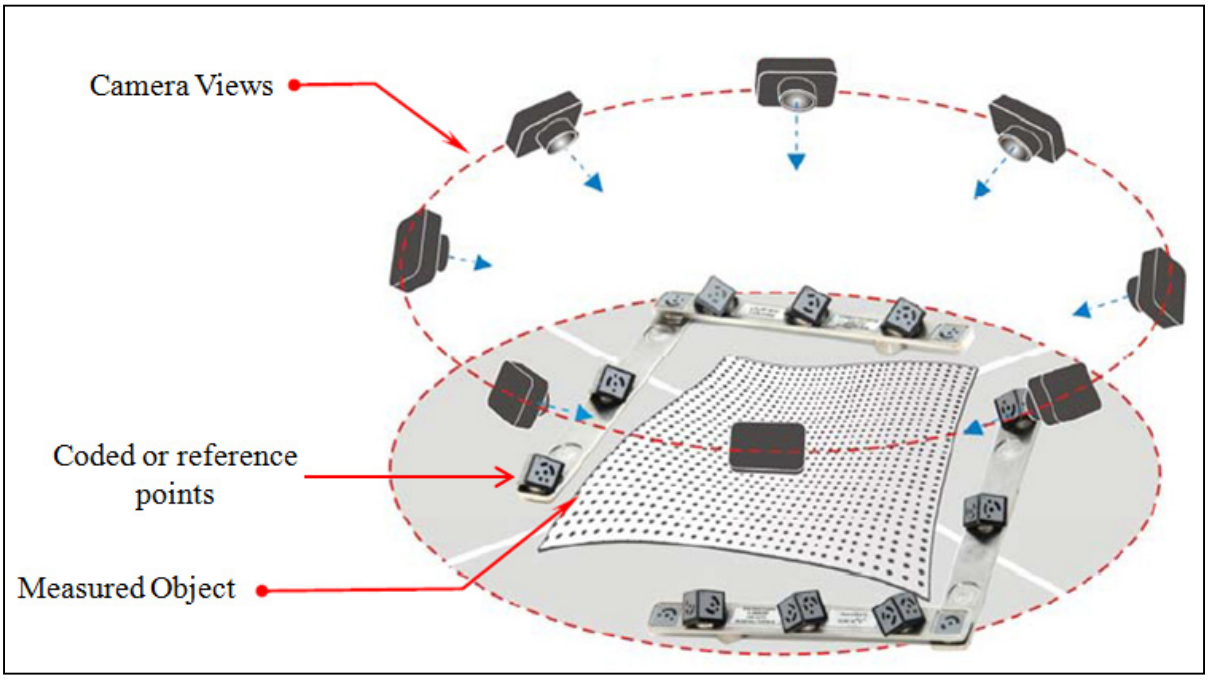

Figure 2.15: Camera movement around measuring object
(ARGUS User's Manual, 2012)

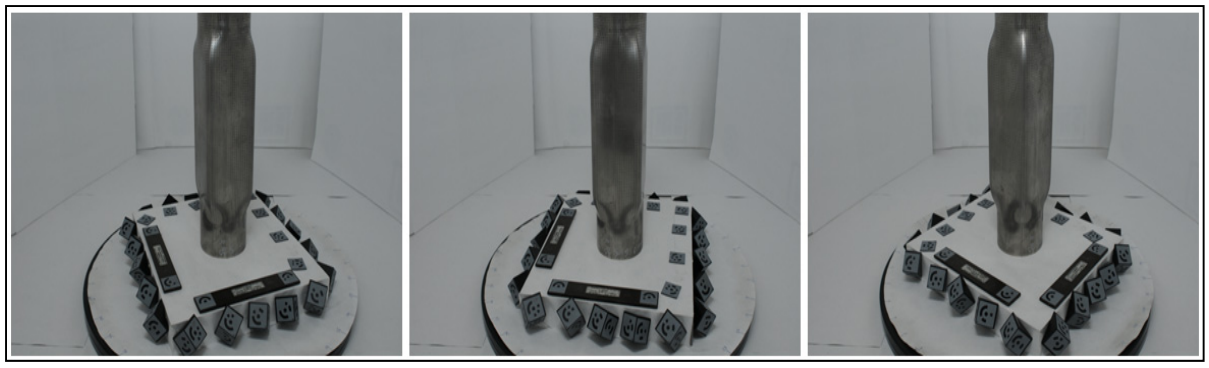

Figure 2.16: Pictures from different views of the deformed tube

The other parameter that was measured after the hydroforming process was the tube thickness. The thickness of the deformed tubes was measured using the same ultrasonic thickness measurement device which was presented in Figure 2.10. A cross section at the mid length of the tubes was used for the thickness measurements. As mentioned before, a quarter of the tube cross section was used for the simulations, which represents 90° of the cross section. In addition, as mentioned before, tube thickness at the cross section was not uniform (Figure 2.11). In order to track this un-uniformity, always the tubes were placed in the die in a way that the minimum thickness was in the front quarter and the maximum thickness was in the back quarter. Therefore, as illustrated in Figure 2.17, the front and back quarters of the tube cross section were measured to compare the thickness variations with the FEA results.

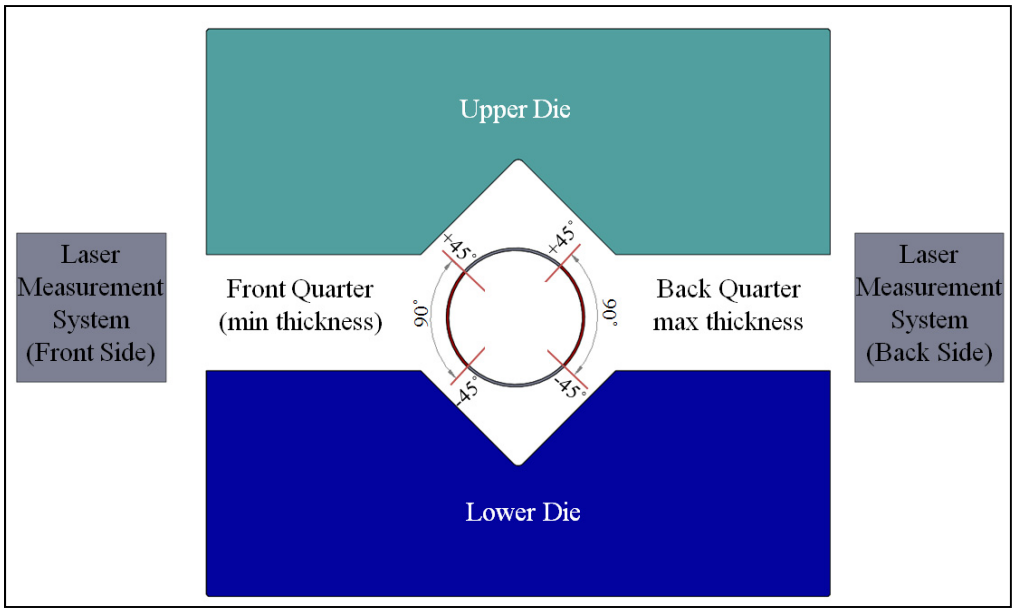

Figure 2.17: Thickness measurement regions

2.3 Optimization

As mentioned before, finding the best load path in the THF process is highly desired for production purposes. Therefore, a commercial optimization software, LS_OPT v4.2, was used to find the optimum loading path for the hydroforming process. The objective was to minimize the thickness variation in the hydroformed tubes. Therefore, two objective functions were defined as follow:

$$Obj_1 = \left(\frac{MinThickness - NomThickness}{NomThickness}\right)^2 \quad (2.3)$$

$$Obj_2 = \left(\frac{MaxThickness - NomThickness}{NomThickness}\right)^2 \quad (2.4)$$

Where the MinThickness and the MaxThickness are the minimum and the maximum tube thickness after hydroforming, and the NomThickness is the nominal tube thickness (before

hydroforming), which was equal to 0.94 and 1.22 for the two different tube thicknesses used in this study.

As most of the end feeding was applied during the forming stage, finding the optimum internal pressure (P) and end feeding (F) at the end of the forming process is critical. So, these two parameters were chosen as the two design variables. The free end load path gave a good estimation of the internal pressure at the end of the forming stage in the THF process (Figure 2.18). Based on the experimental free end load path, 20 MPa and 60 MPa were considered as the lower and upper band values for the internal pressure at the end of the forming stage. By performing a few FEAs, 20 mm was selected as the upper band for end feeding. The lower band value for the end feeding was set to zero.

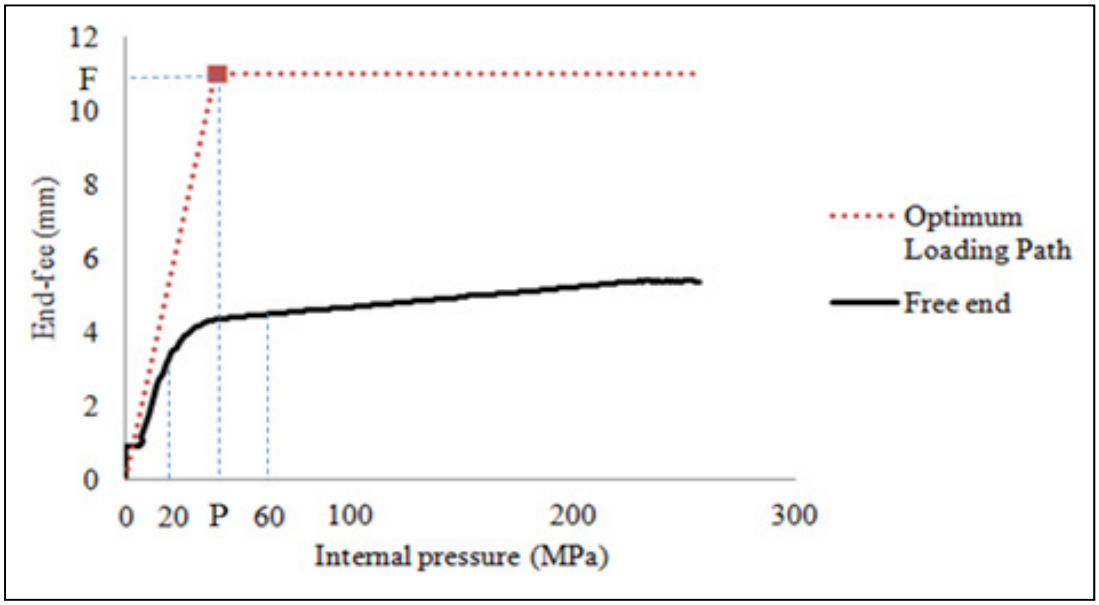

Figure 2.18: Design variables (P and F) in optimum loading path

To prevent the occurrence of the failure modes such as bursting and severe wrinkling, FLD of the materials was selected as the constraint for the optimization process. Like the material parameters, the FLCs were generated separately in an ongoing study. Figure 2.19 shows the FLCs used for both tube thicknesses.

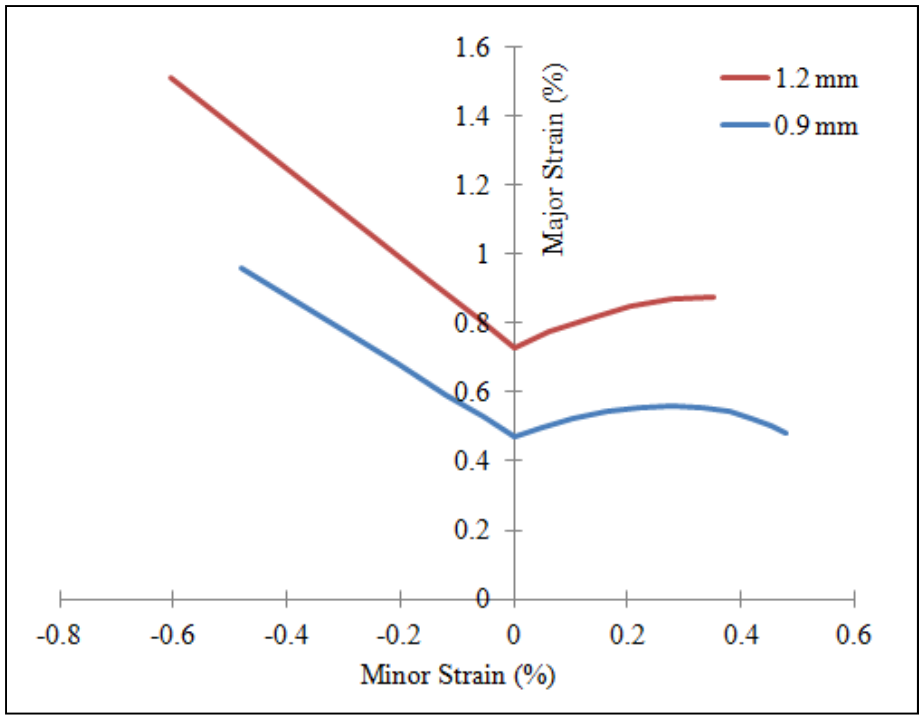

Figure 2.19: FLD for SS321tubes with
0.9 mm and 1.2 mm thicknesses

Optimization strategy, sampling method and algorithm are the other required settings that were set in the LS-OPT software using the graphic user interface (GUI). These settings, which are based on the previous study done by An (An, 2010), are listed in Table 2.2 and the optimization codes are presented in Appendix C. in Table 2.2, The first column is the strategy for choosing the sampling points in the experimental design. By selecting the strategy, the sampling parameters will be set automatically. By the settings mentioned in this table, 10 points are selected at each iteration base on the Doptimal design. Using the selected points as the input parameters, the simulations are done and the results obtained (responses). In the next step a quadratic polynomial surface (response surface) will be passed through the responses. Then a hybrid genetic algorithm (hybrid GA) is used to find the optimum point in the response surface. The hybrid GA algorithms start with the GA to find an approximate global optimum after which the gradient-base algorithm is used to sharpen the solution. With this method, the computational time is reduced compared to the GA method.

Table 2.2: Optimization settings in LS-OPT

Strategy	Sampling	Algorithms
sequential with domain reduction (SRSM)	1) metamodel: polynomial; 2) order: quadratic; 3) point-selection: Doptimal; 4) number of simulation points: 10	hybrid GA with population size: 100 and number of generations: 250

CHAPTER 3

RESULTS AND DISCUSSION

In this chapter the results obtained from the experimental and numerical analysis will be presented and discussed. In each section the results for the tube expansion and the tube thickness as the measuring parameters will be presented. In the first section, the experimental data from the THF experiments for both tube thicknesses will be discussed. To verify the developed FEMs, the FEA results obtained from the two different material properties and three element types (shell, solid and Tshell) will be compared with the experimental results. After finding the best material property and element type, the strain distribution of tubes, measured by ARGUS® measurement system, will be compared with this FEA results. Then, the effect of COF on the tube expansion and tube thickness will be discussed and finally the last section will present the optimized load-path and its results.

3.1 Experimental results

Four different loading paths, one with force control and three with position control method, were applied to the tubes ends for both tube thicknesses. Each Loading path was repeated three times (Appendix D) and the mean value was used to plot the tube expansion versus the internal pressure (Figure 3.1). As illustrated in Figure 3.1a and b, by increasing the internal pressure, the tube starts to expand rapidly up to about 40 MPa which is the end of forming stage. By the beginning of the calibration stage, the tube expansion rate decreases. This stage continues till the internal pressure reaches to 260 MPa. The tube expansion during the first 40 MPa internal pressure is almost equal to the amount of tube expansion during the rest of the process. In other words, for both tube thicknesses half of the tube expansion occured up to the 40 MPa internal pressure; during the forming stage.

Figure 3.1 also reveals the effect of end feeding on the tube expansion. The maximum tube expansion for free end loading path is 8.8 mm and 8.5 mm for the 0.9 mm and 1.2 mm tubes, respectively. By tripling the end feed (loading path 3), the maximum tube expansion was

decreased to 8.65 mm and 8.2 mm for the 0.9 mm and 1.2 mm tubes, respectively, and the expansion trend remains the same. This phenomenon can be explained as the higher end feeding results in less thickness reduction and so the tube is thicker/tougher to deform at the corners. As the differences in total expansion are small, it can be concluded that the end feeding does not have a noticeable effect on the total tube expansion for both tube thicknesses.

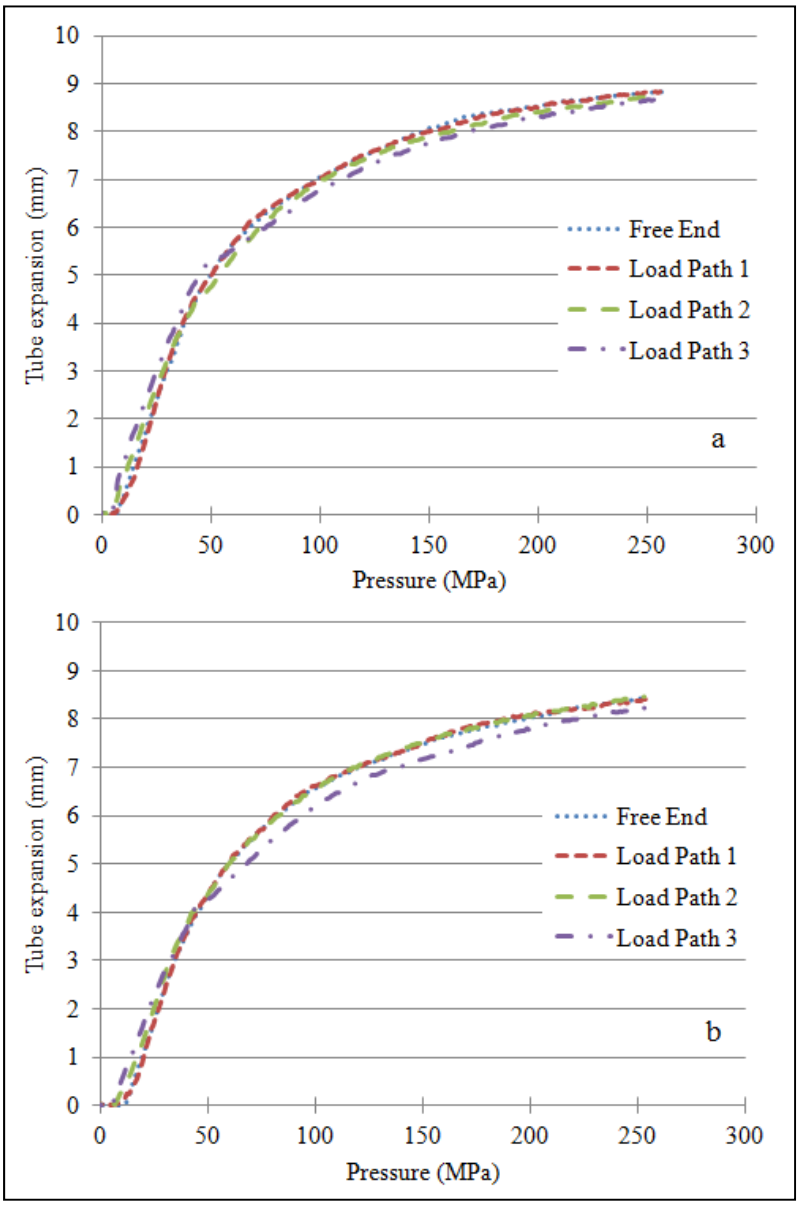

Figure 3.1: Expansion in tubes with
(a) 0.9 mm and (b) 1.2 mm thickness

Tube thickness was the other parameter that was measured after the hydroforming process. As illustrated in Figure 2.17, the tube thickness in two quarters of the tube mid cross section was measured using the ultrasound thickness measurement device. The thickness measurement results for all cases are presented in Appendix E. Figure 3.2 illustrates the average thickness value of the front and back sides of the tubes for both tube thicknesses.

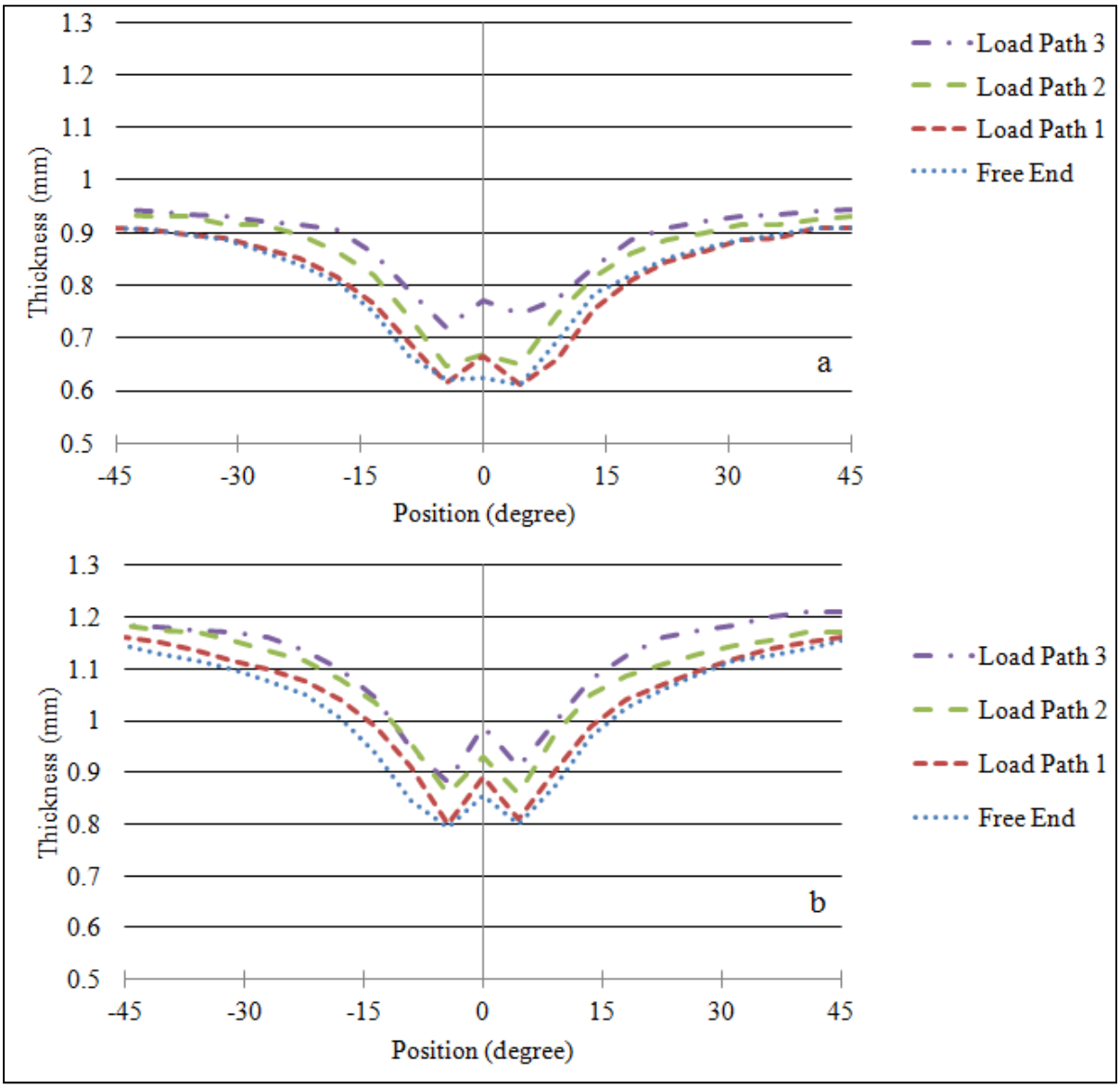

Figure 3.2: Thickness variation of tubes with
(a) 0.9 mm and (b) 1.2 mm thickness

In this figure, 0˚ corresponds to the tube corner and +45˚ and -45˚ correspond to the end points on one quarter of the tube, as shown in Figure 3.3. Twenty one points were selected in each quarter and thickness was measured 3 times at each point. At each point the average value from the front and back quarters was considered to draw the experimental curves in Figure 3.2. It can be seen that the maximum thinning occurs at the end of the contact region between the tube and the die. This region of the tube is subjected to a tensile stress in circumferential direction, but the tube is stuck to the die at this region due to high friction forces, which limits the material flow. It was observed that the thinning pattern is similar for both tube thicknesses. Also, by tripling the end feeding, the minimum thickness increased by 18% and 10% for tubes with 0.9 mm and 1.2 mm thickness, respectively. These results suggest that end feeding results in more uniform thickness distribution since the end feeding assists the material flow into the deformation zone.

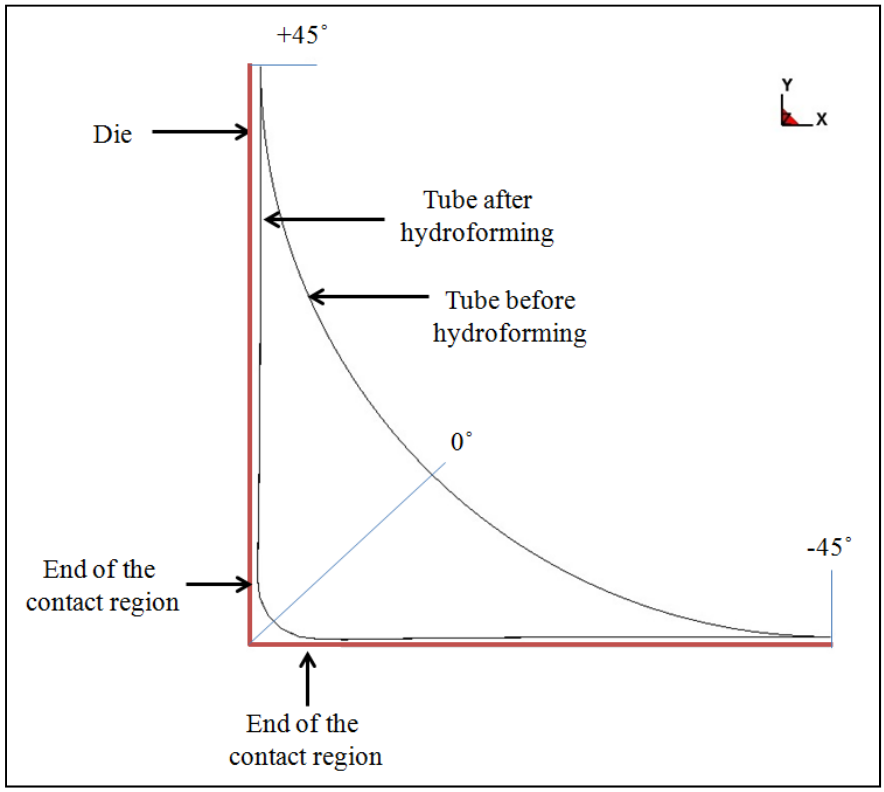

Figure 3.3: Tube position after hydroforming

3.2 FEM verification

To find the best FEM that can represent the real THF process, the FEA results were verified by comparing them with the results obtained from experiments. As mentioned before, several FEMs with two different material properties and three element types were developed. The tube expansion and tube thickness results from these FEMs were extracted for comparison purpose.

3.2.1 Material properties

As mentioned in the previous chapter, free expansion test and tensile test were used to extract the material properties. Using the shell FEM, the tube expansion and the tube thickness variation predicted by these two material properties were compared with the experimental results. Figure 3.4 illustrates the tube expansion versus internal pressure for 0.9 mm tube with different load paths. Here, Figure 3.4a and b, which represent the tube expansion with minimum end feedings, the tube expansion curve is smooth during the process. For load paths with higher end feedings (Figure 3.4c and d) there is a sudden slope in the curve at the end of the forming stage. The slope change is amplified with the increase of the end feeding. This jump is due to pushing extra material into the die cavity, which results in the formation of good wrinkles during the forming stage. They are called good wrinkles because they will disappear later by increasing the internal pressure. Also, Figure 3.4 shows that the FEA results for both material properties show the same trend and they are relatively in good agreement with the experimental results.The maximum deviation between the simulation and experimental results for expansion of the 0.9 mm tubes is about 5% at the end of the THF process.

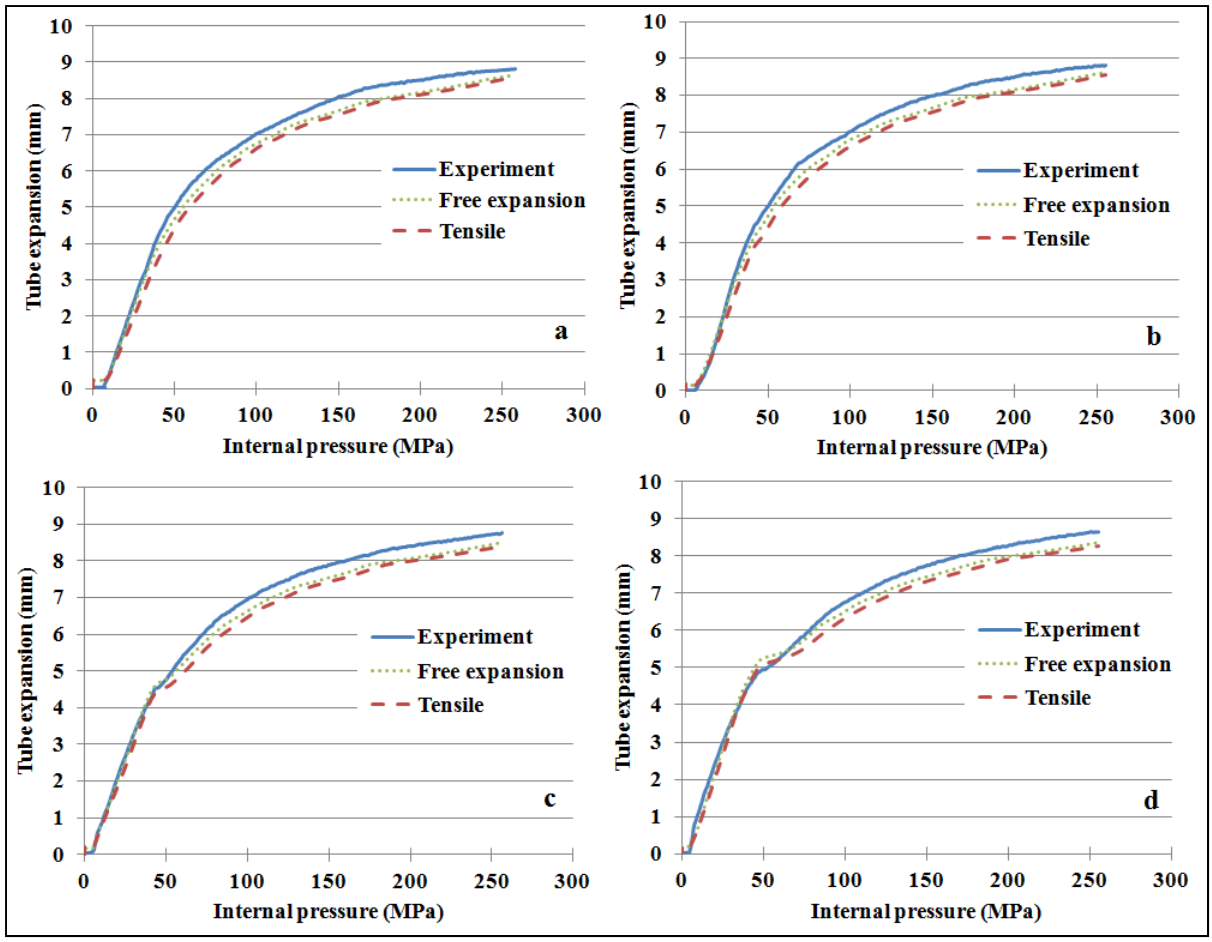

Figure 3.4: Tube expansion in 0.9 mm thick tube
(a) free end (b) load path 1 (c) load path 2 and (d) load path 3

Figure 3.5 illustrates the expansion results for the 1.2 mm thick tubes with different end loading conditions. Here, like the 0.9 mm tubes, the predicted expansion results for both material properties follow the same trend as the experimental data, but the expansion curves resulted from the tensile testing show higher deviation from the experimental curves. On the other hand, the results from the free expansion show a good agreement with the experimental data.

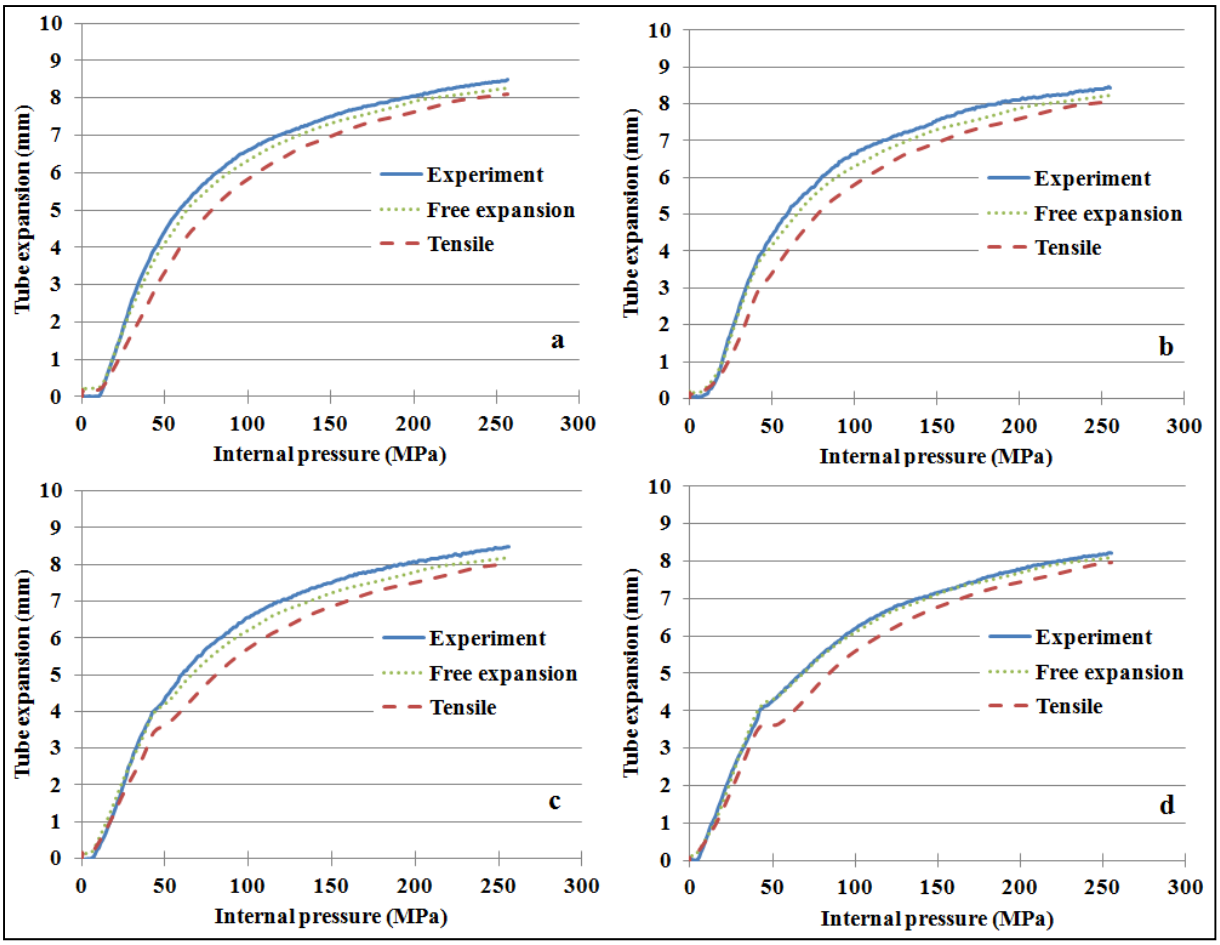

Figure 3.5: Expansion of the tubes with 1.2 mm thickness
(a) free end (b) loading path 1 (c) loading path 2 and (d) loading path 3

Figure 3.6 and Figure 3.7 represent the tube thickness variation for 0.9 mm and 1.2 mm tubes, respectively. As mentioned before, the thickness of the blank tubes varies along the circumferential direction. So, the thickness measurement results in both figures represent the front and back quarters of the tubes. These results are average results of three measurements.

In addition to the experimental results, the FEA results obtained from both material properties (free expansion and tensile tests) are presented in both figures. As it can be seen from these figures, the FEA results could predict the tube thickness variation of both tube thicknesses with a good accuracy. At the end of the contact regions the experimental results show a higher variation compared to the FEA results. The experimental thickness curves have a W-shape at the corners, while the simulation results are almost flat and cannot capture

extra thinning at the contact regions. This can be due to the inefficiency of the shell element that cannot capture through thickness stresses. Therefore, at the tube corners where the through thickness stresses are high, it is probable that the FEM cannot predict the material behaviour and as a result the difference between the FEA and experimental results starts to increase in these regions.

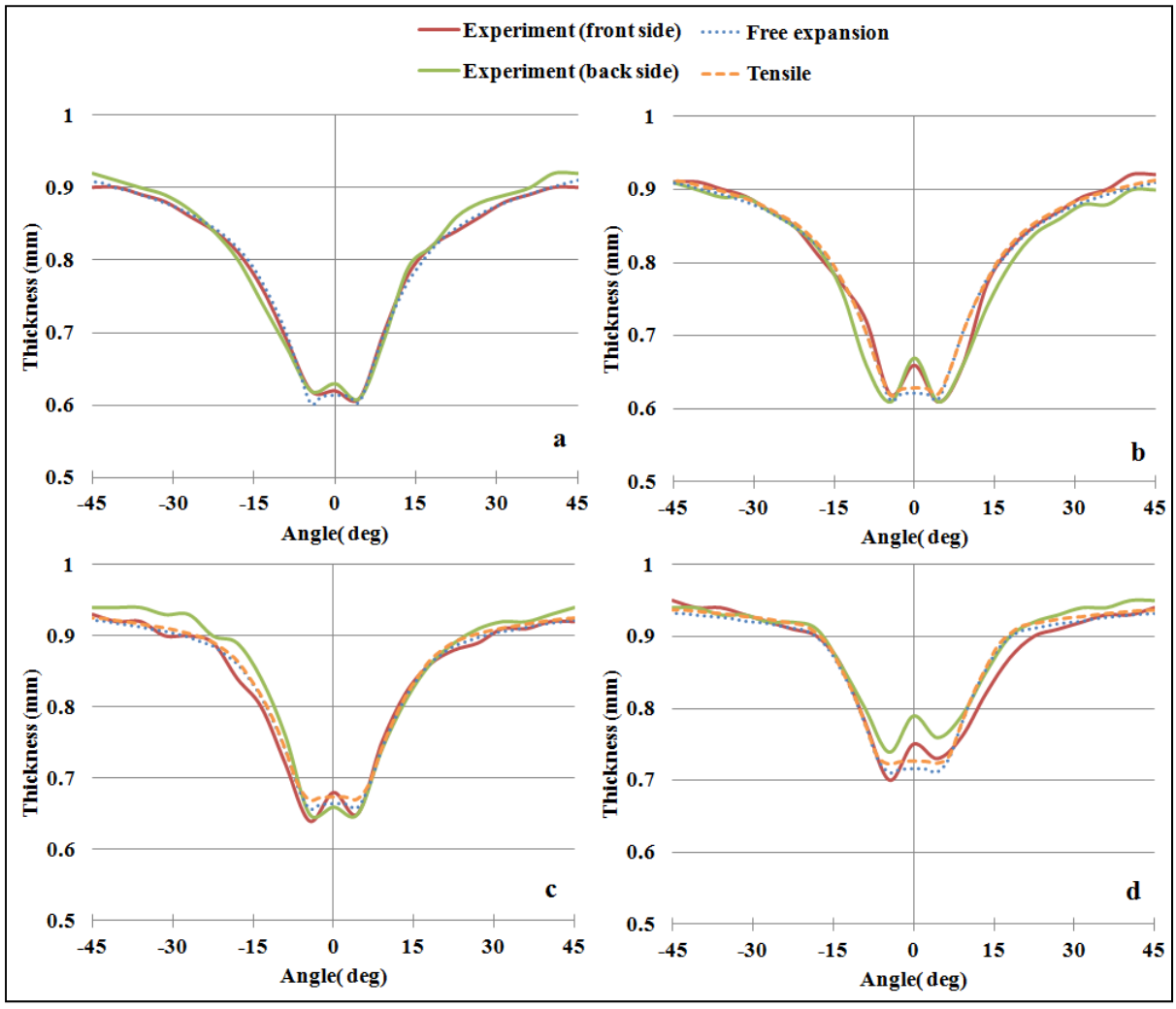

Figure 3.6: Thickness variation in tubes with 0.9 mm thickness
(a) free end (b) loading path 1 (c) loading path 2 and (d) loading path 3

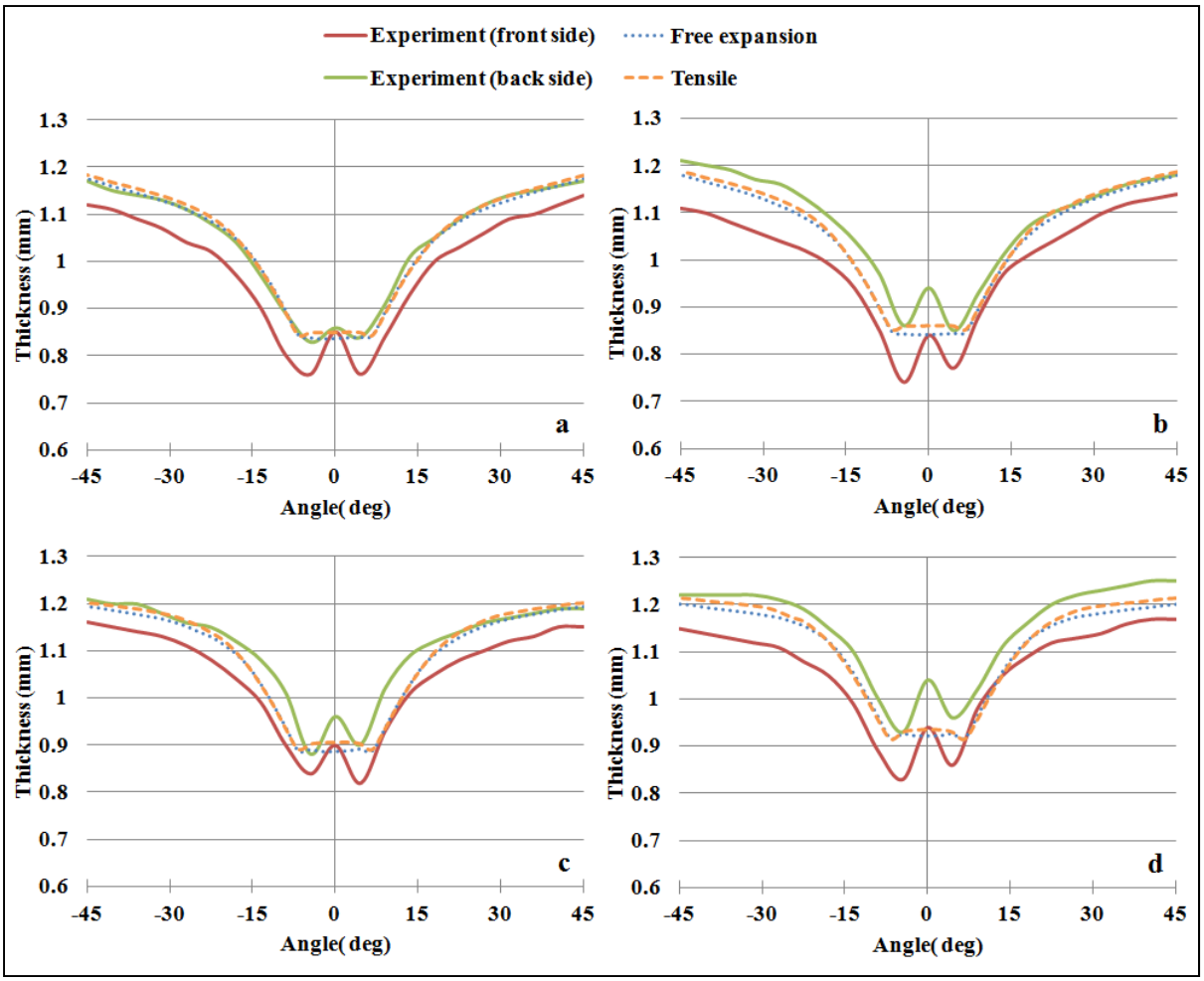

Figure 3.7: Thickness variation in tubes with 1.2 mm thickness
(a) free end (b) loading path 1 (c) loading path 2 and (d) loading path 3

By comparing the results of both material properties, it is concluded that the material properties that are obtained from the free expansion test leads to better results and can simulate the real THF process better than the material properties that are based on tensile test.

3.2.2 Different element types

To compare the effect of element type on the simulation results, FEMs with three different element types; shell, solid and Tshell, were developed. Then, the FEA results for the tube expansion and thickness variations were plotted to compare with each other.

Figure 3.8 and Figure 3.9 illustrate the expansion of 0.9 mm and 1.2 mm thick tubes with different element types, respectively. As it can be seen from the figures, the trends and magnitudes of all the results obtained from different elements are very similar and there is no noticeable difference between the results obtained from the three types of elements.

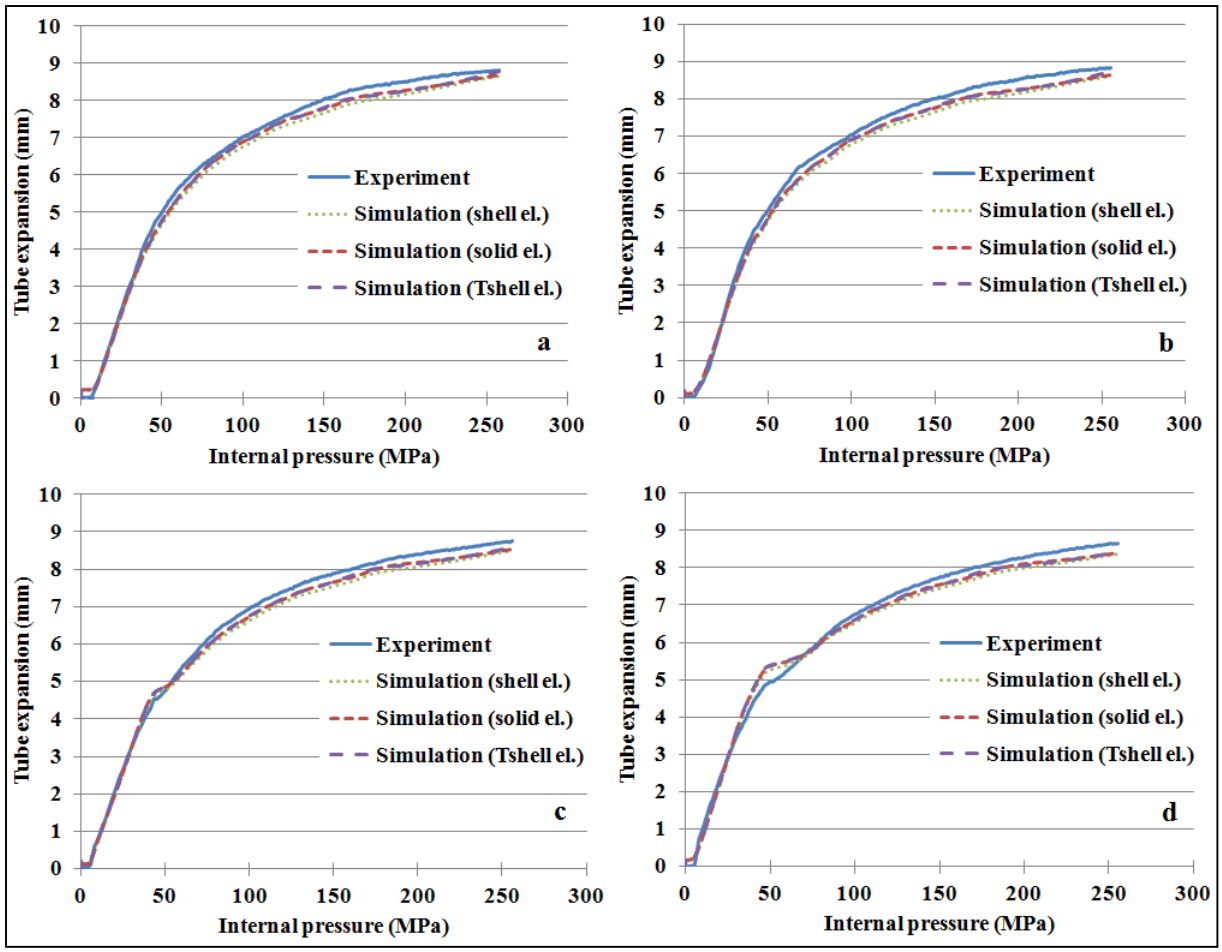

Figure 3.8: Expansion of the tubes with different element types for 0.9 mm thick tube (a) free end (b) loading path 1 (c) loading path 2 and (d) loading path 3

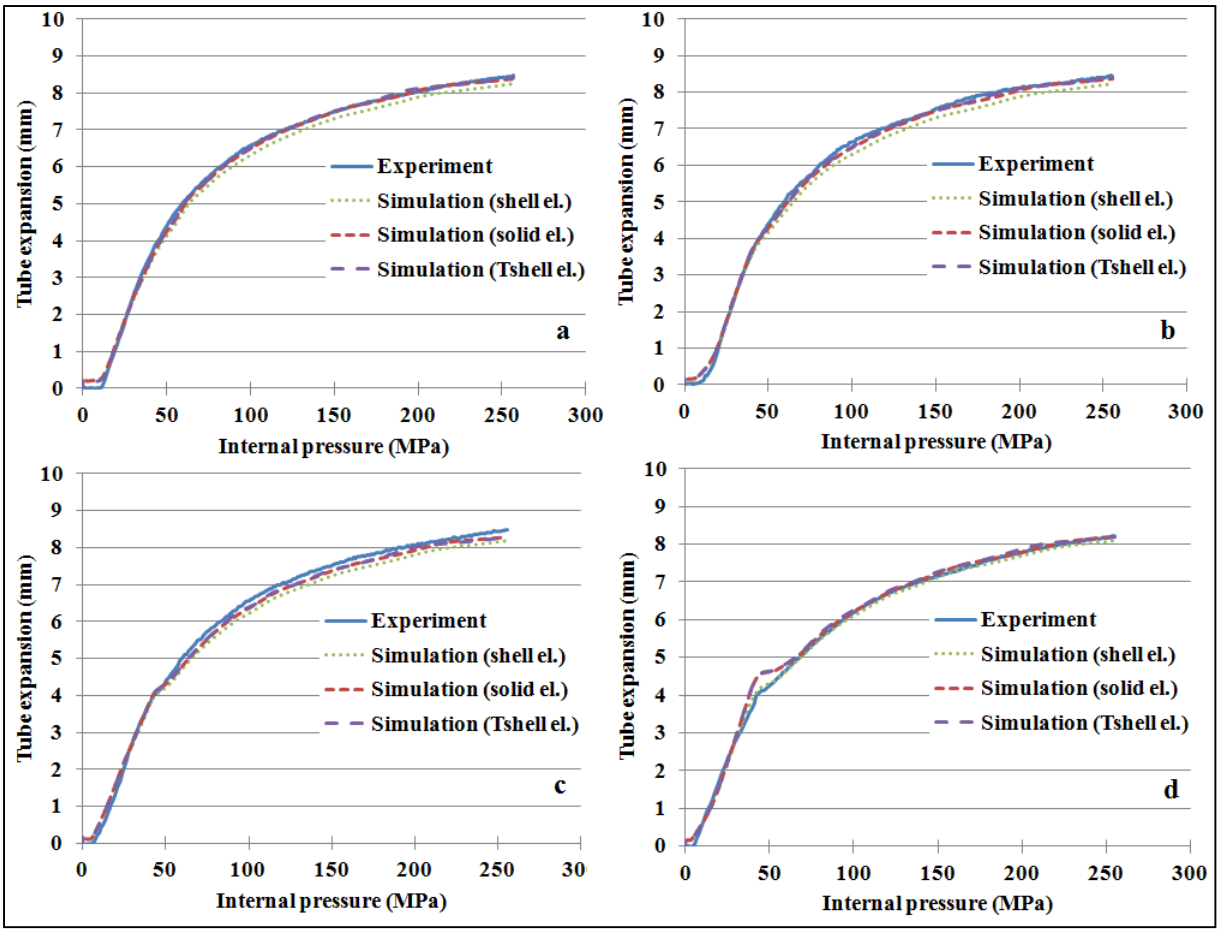

Figure 3.9: Expansion of the tubes with different element types for 1.2 mm thick tube (a) free end (b) loading path 1 (c) loading path 2 and (d) loading path 3

In Figure 3.10 and Figure 3.11 the tubes thicknesses at the mid length of the tubes after hydroforming are presented for 0.9 mm and 1.2 mm thick tubes, respectively. As the thickness parameter is not calculated for solid and Tshell elements by LS-DYNA, the thickness of the deformed tubes was measured by comparing the distance between the inner and outer nodes at different locations throughout the cross section. All three element types predicted the tube thickness with good accuracy at the regions far from the tube corner, but, at the tube corner (-15° to 15°) the results are different from experiment. At this region, the shell element resulted in the lowest values. The results obtained from the solid element have the same trend as the shell element, but with slightly higher values. Although a small W-shape was observed in the results that were obtained from the shell and solid elements, neither the shell nor the solid element could capture the W-shape, which was observed in the

experimental data. On the other hand, the Tshell element could capture the W-shape at the tube corner, but with deviation from the experimental data. From the Figure 3.10 and Figure 3.11, it can be seen that the tube thickness results obtained from the shell and solid elements were relatively closer to the experimental results compared to the Tshell element.

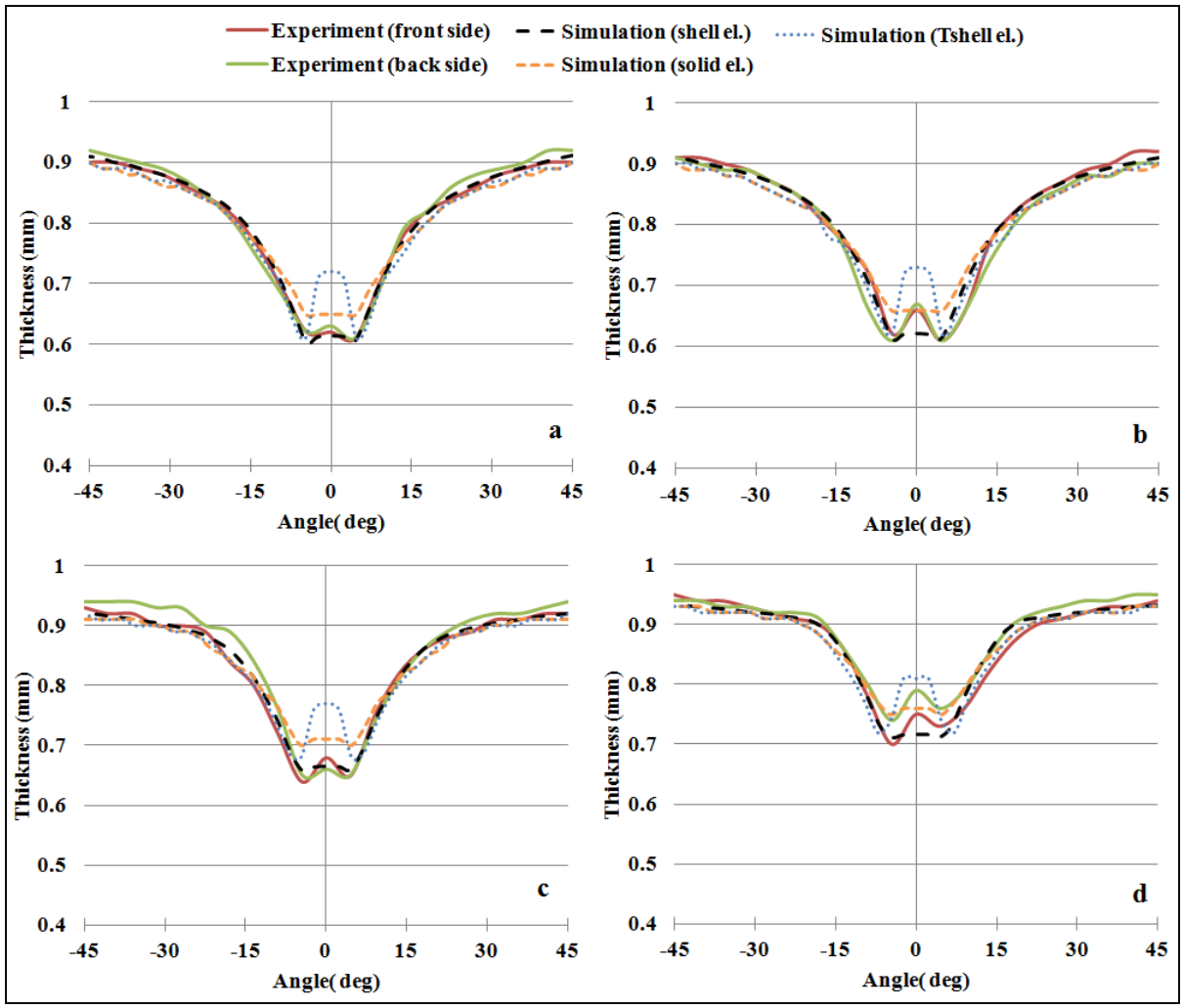

Figure 3.10: Thickness variation in tubes with 0.9 mm thickness
(a) free end (b) loading path 1 (c) loading path 2 and (d) loading path 3

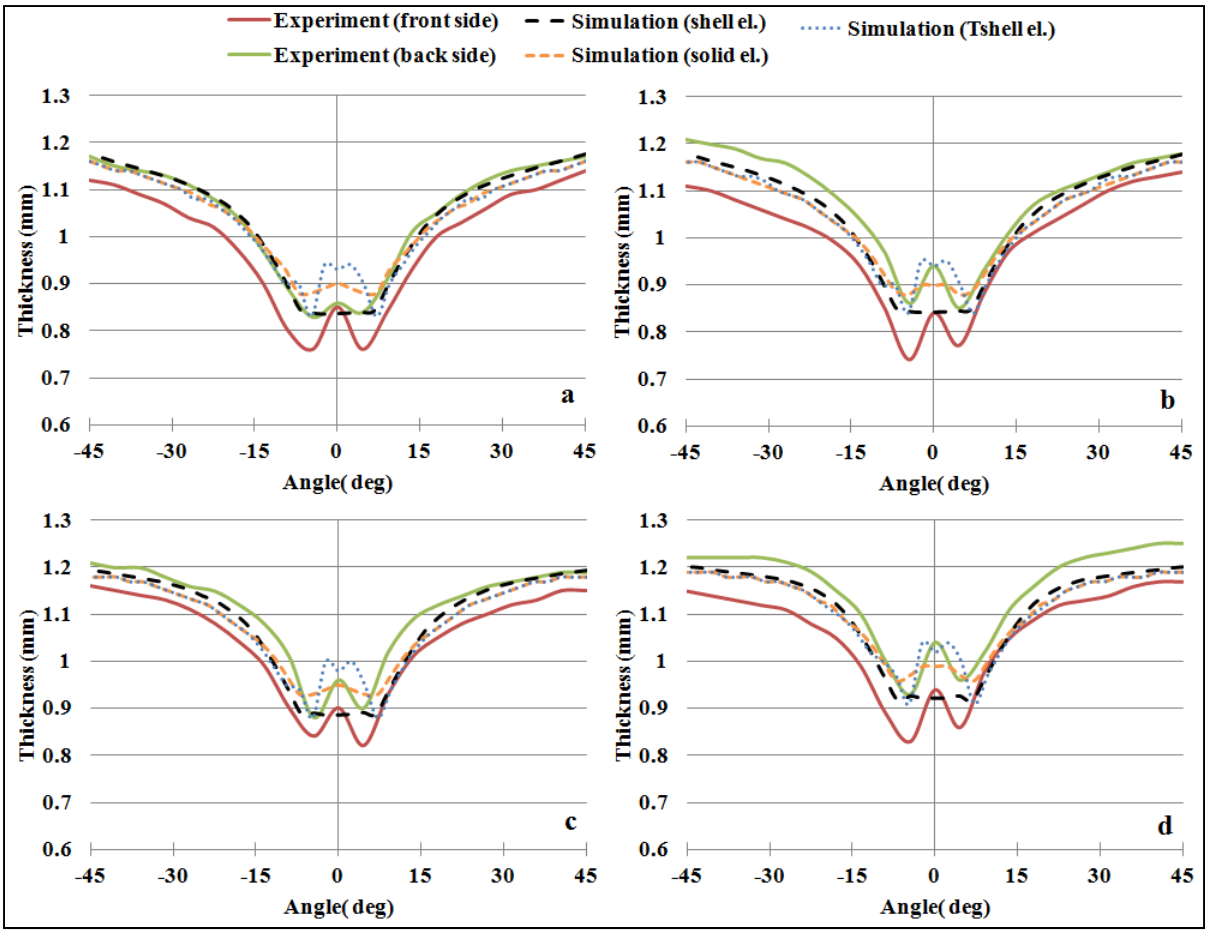

Figure 3.11: Thickness variation in tubes with 1.2 mm thickness
(a) free end (b) loading path 1 (c) loading path 2 and (d) loading path 3

The third parameter that was taken into account for selecting the best element type was calculation time. For the same simulation, the calculation time was 35 hours and 25 minutes for the Tshell, 4 hours and 30 minutes for the solid and 40 minutes for the shell element. In other words, the shell element is almost seven times faster than the solid element and 53 times faster than the Tshell element.

From the above results, it was concluded that using FEM constructed with shell elements is the best choice among the other options as it is faster and has a good computational accuracy.

3.2.3 Strain distribution

ARGUS® measurement system was used to measure the in-plane strain distribution at the outer surface of the tubes to verify the accuracy of the FEMs. From Figure 3.12 to Figure 3.15 the measured strains are compared with the simulation results.

Figure 3.12 and Figure 3.13 show the major and minor strains of the tube with 0.9 mm thickness that was hydroformed using the minimum end feeding (load path 1). The major strain is in the hoop or circumferential direction and the minor strain is in the axial or longitudinal direction of the tubes. The experimental and simulation results show that the maximum major strain occurs at the tube corner. During the calibration stage, most of the tube surface is in contact with the die and the deformation continues at the tube corners where there is no restriction for metal to flow. The maximum major strain that is measured by ARGUS® is equal to 50% while this value is equal to 53% from the simulation results. This shows 6% error between the experimental and simulation results.

The maximum value of the minor strain for loading path 1 occurred at the end of transition zone and at the beginning of the expansion zone, as shown in Figure 3.13. This is due to the low end feeding in load path 1 that makes the tube to stretch mostly in the longitudinal direction during the process.

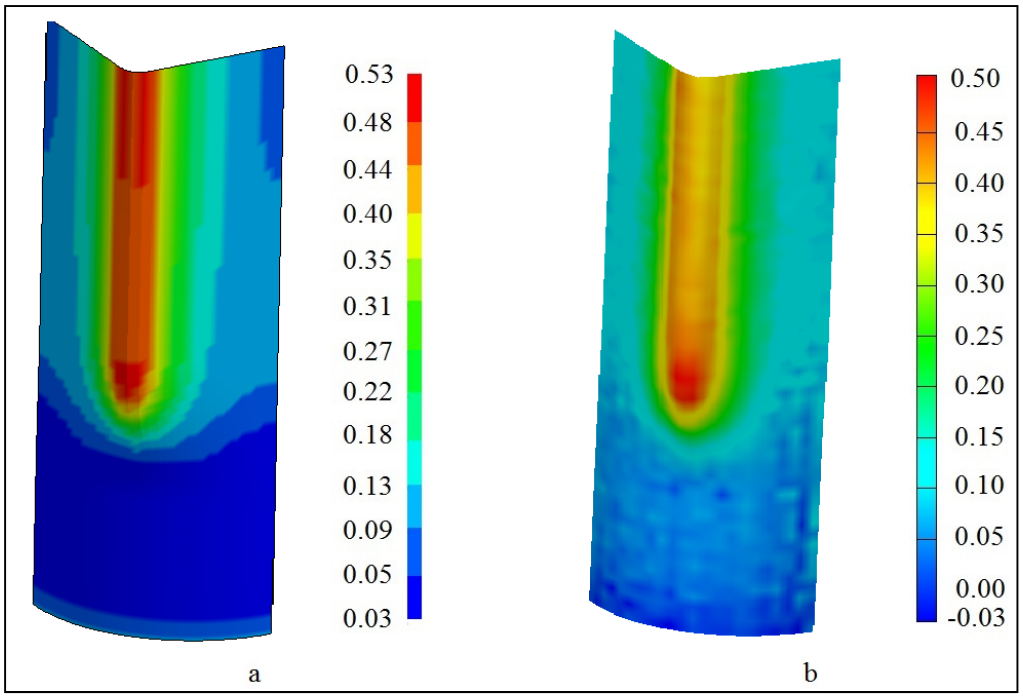

Figure 3.12: Major strain distribution on the surface of the tube for loading path 1 (0.9 mm) (a) simulation (b) experiment

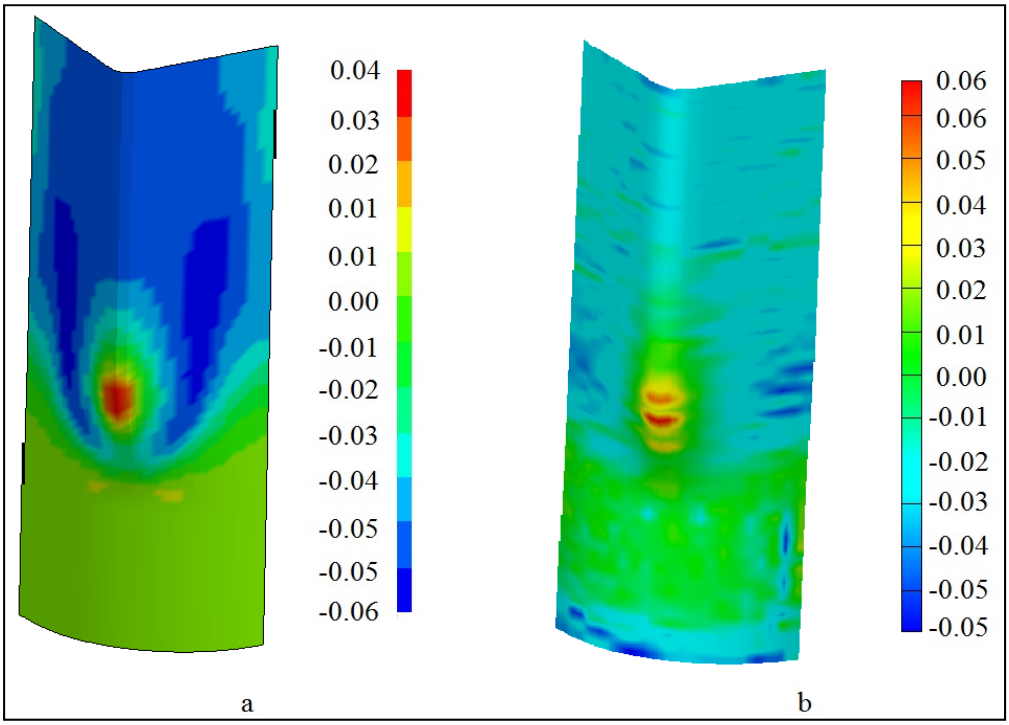

Figure 3.13: Minor strain distribution on the surface of the tube for loading path 1 (0.9 mm) (a) simulation (b) experiment

Figure 3.14 and Figure 3.15 illustrates the major and minor strains of the tube with 0.9 mm thickness that was hydroformed using the maximum end feeding (load path 3). In this case, the maximum major strain that is obtained from ARGUS® measurement system and FEA is equal to 45% and 43%, respectively; which indicates 4% error. By comparing the results of loading path 1 and loading path 3, it can be seen that both ARGUS® and FEA results show a reduction in major strain value. Also, by comparing the minor strains in the loading paths it can be seen that the minor strain in loading path 3 has changed to compression state while in loading path 1 the strain state is a combination of compression and tension, which is due to less end feeding in loading path 1.

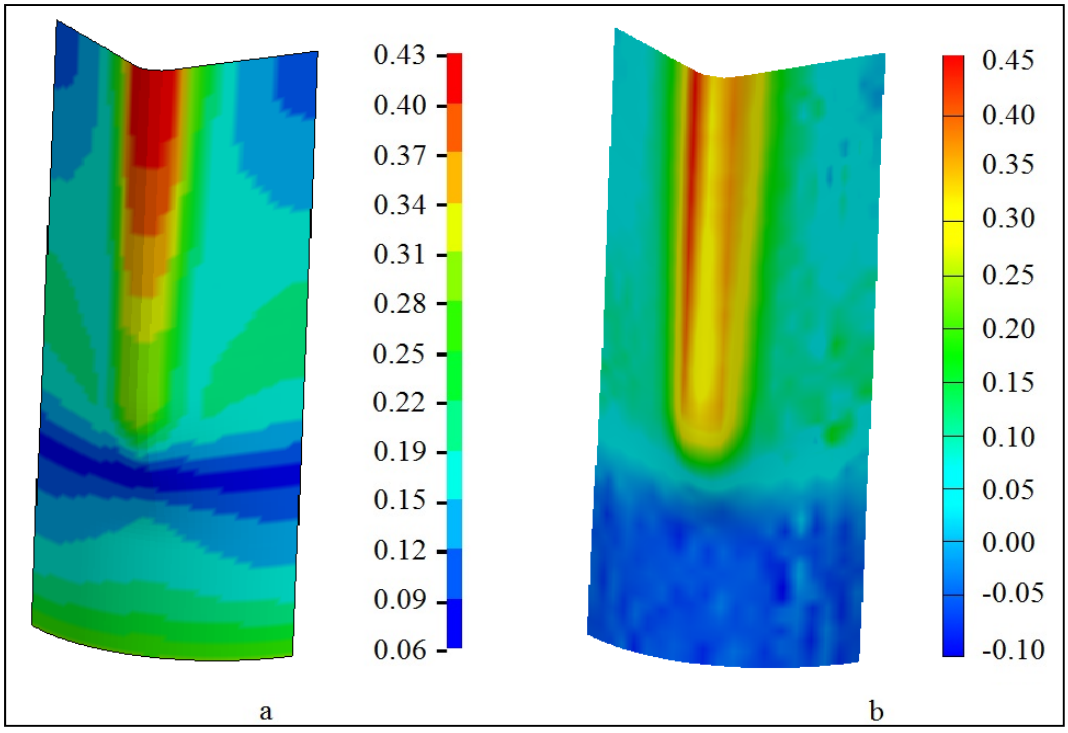

Figure 3.14: Major strain distribution on the surface of the tube
for loading path 3 (0.9 mm) (a) simulation (b) experiment

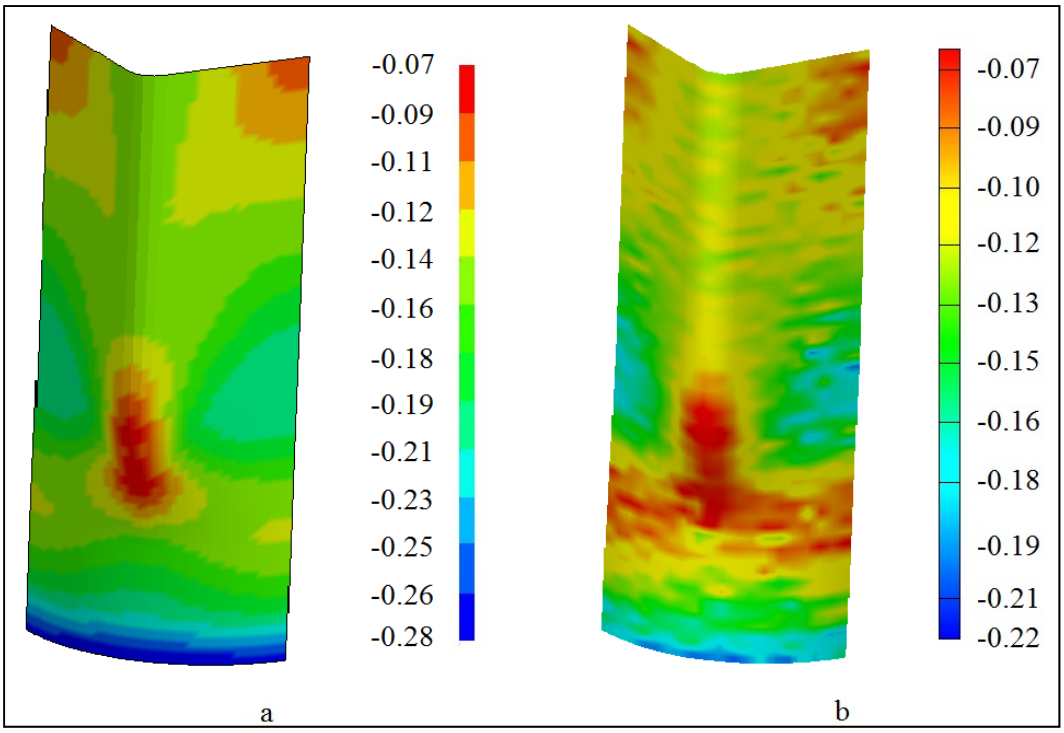

Figure 3.15: Minor strain distribution on the surface of the tube
for loading path 3 (0.9 mm) (a) simulation (b) experiment

To have a better understanding of the strain distribution in hydroformed tubes, the major, minor and through thickness strain distributions at mid length of the tubes are plotted in Figure 3.16. As it can be seen, the results from both ARGUS® and FEA follow the same trend. Both experimental and FEA results of the strain distribution in hydroformed tubes show that end feeding changes the strain distribution in hydroformed tubes in a way that higher expansion is possible. However, there are some differences between the ARGUS® and FEA results for minor and through thickness strains in loading path 3 (Figure 3.16b). The differences between the experimental and FEM results could be due to utilization of shell element in the FEM. As mentioned before, the shell elements cannot capture the through thickness stresses and this deficiency could affect the results. The other source of error in the FEM is the COF was considered constant during the simulation, while in reality it is not constant during the whole THF process.

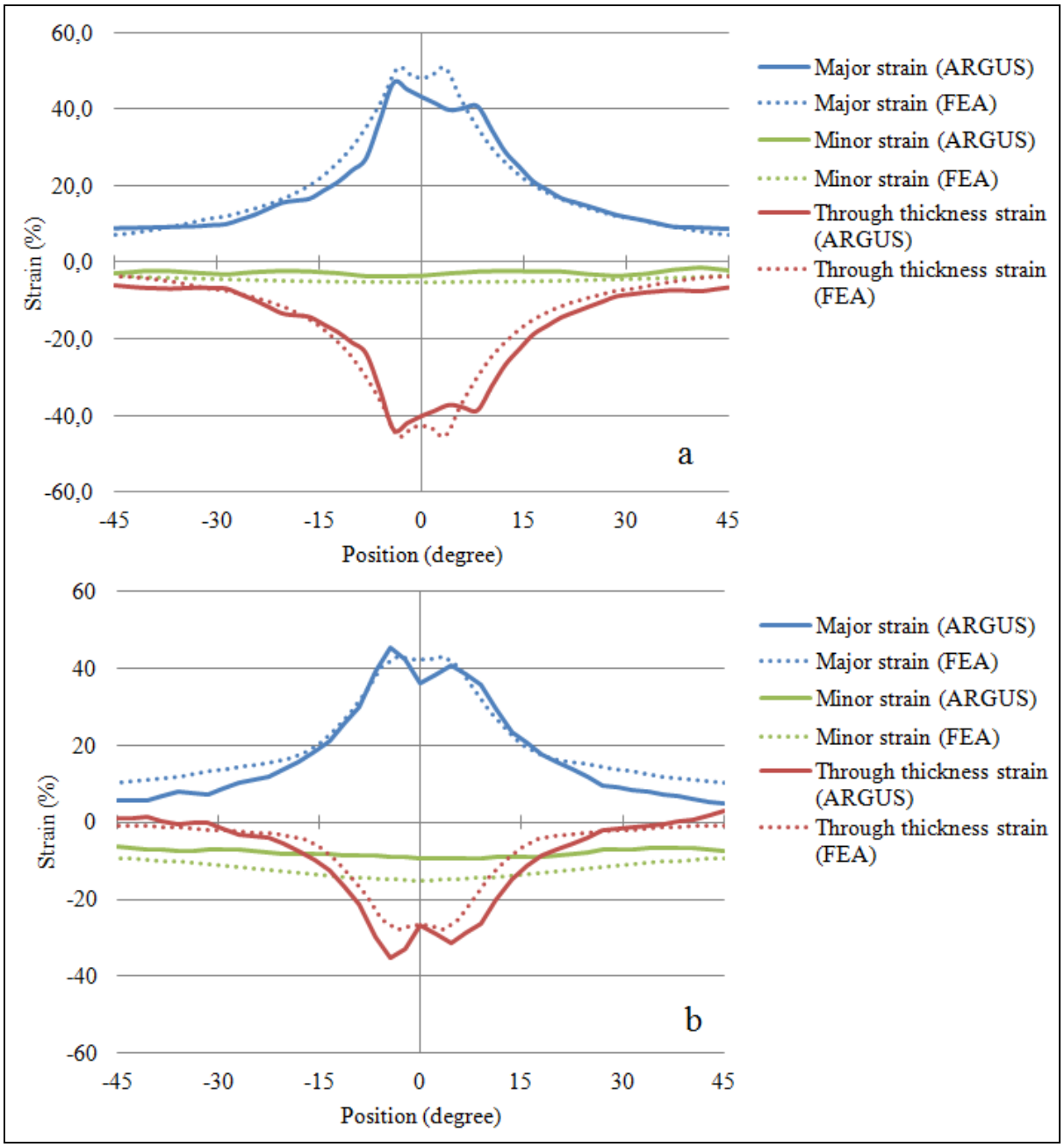

Figure 3.16: Strain distribution for mid length cross section of 0.9 mm tubes hydroformed with (a) loading path 1 (b) loading path 3

3.3 Effect of lubrication

To investigate the effect of lubrication and friction force on the tube expansion and tube thickness variation, two different lubricants were used in this study. The load path 2 was

considered as the loading path for hydroforming the lubricated tubes. Then, the hydroforming process with 0.9 mm and 1.2 mm thick tubes and different COFs were modeled. The tube expansion and the tube thickness were compared from experiments and FEMs to find the proper COF that can be used in the FEM for lubricants used in this study.

Figure 3.17 shows the experimental results of the tube expansion versus the internal pressure for 0.9 mm and 1.2 mm thick tubes with different COF values. The results show no big difference between the two lubricants that were tested in this study. By comparing the expansion values from lubricated and unlubricated tubes, it can be seen that there is an increase in the tube expansion for lubricated tubes after the forming stage ($P > 40$ MPa). At the beginning of the process, the tube does not have that much of contact with the die in the expansion zone. Therefore, friction does not play an important role in the tube expansion at the beginning of the forming stage. So, the tube expansion is the same for different lubrication conditions. At the end of forming stage, most of the tube surface is in contact with the die cavity and the contact between the tube and the die increases, so the friction effect becomes more noticeable. As it is illustrated in Figure 3.17, the tubes with lubrication start to expand more compared to the tubes without lubrication at $P > 40$ MPa. The reason is that the lower friction in lubricated tubes assists the material flow in circumferential direction, so the lubricated tubes can deform and expand easier compared to the unlubricated tube; where higher friction restricts the material flow. For both tube thicknesses, at higher internal pressures ($P > 150$ MPa), the tube expansion for lubricated and unlubricated tubes converge to the same value. At this point the die is almost filled and there is no more room for the tube to expand. At the end of the process, the maximum tube expansion is almost the same for both lubricated and unlubricated tubes. Figure 3.18 illustrates the tube thickness variation in circumferential direction for both lubricated and unlubricated tubes. As it is seen, the thickness of the tubes with lubrication is much more uniform compared to the unlubricated tube, which shows severe thickness variation. These variations are more severe at the regions close to the corners which deform the most compared to the other regions. These results suggest that the tube expansion at the end of the calibration stage in unlubricated tubes is

obtained due to the thickness reduction. The tube expansion and thickness variation results for both lubricants are presented in Appendix F and G, respectively.

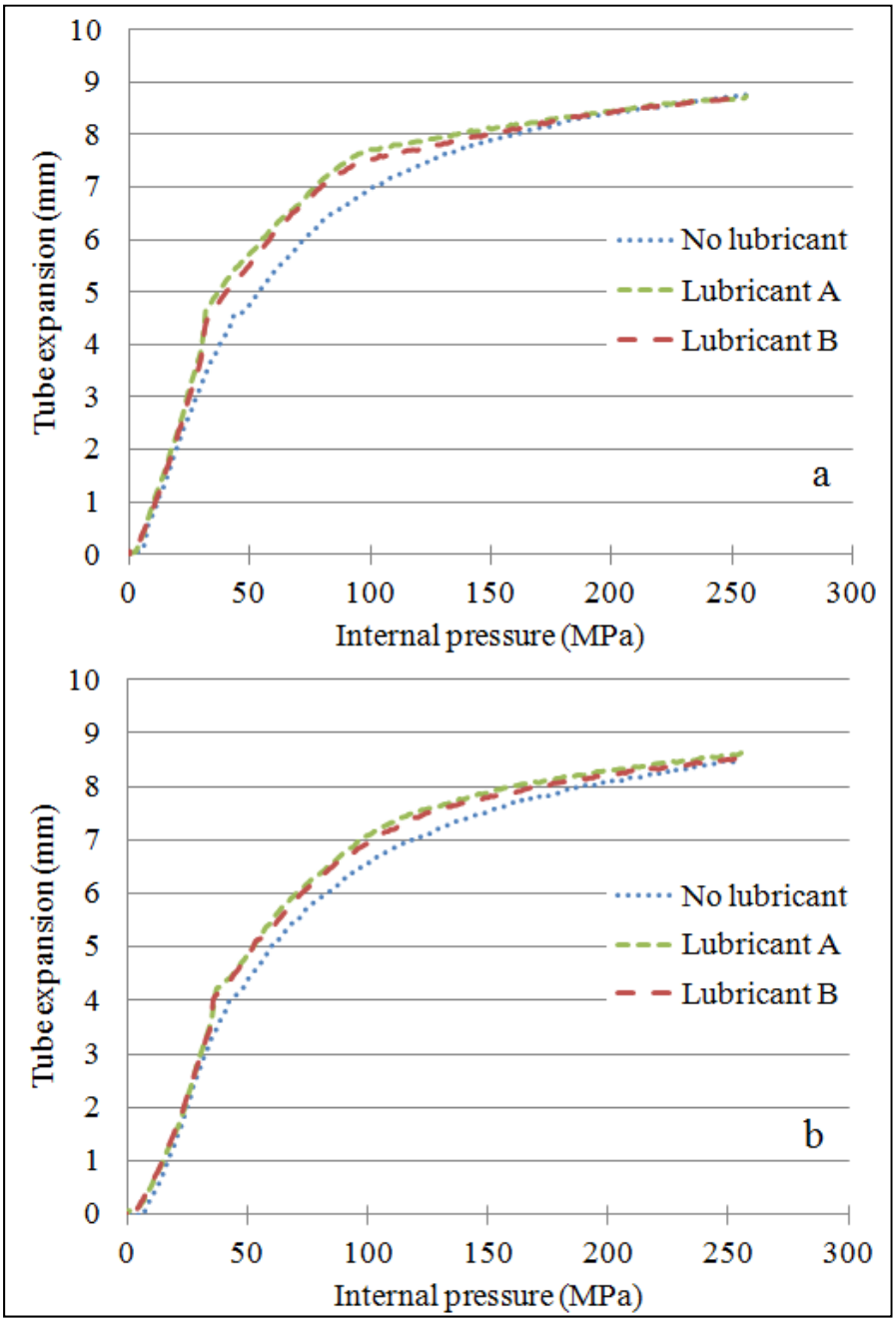

Figure 3.17: Expansion for tubes with different lubricants
(a) 0.9 mm and (b) 1.2 mm thick tubes

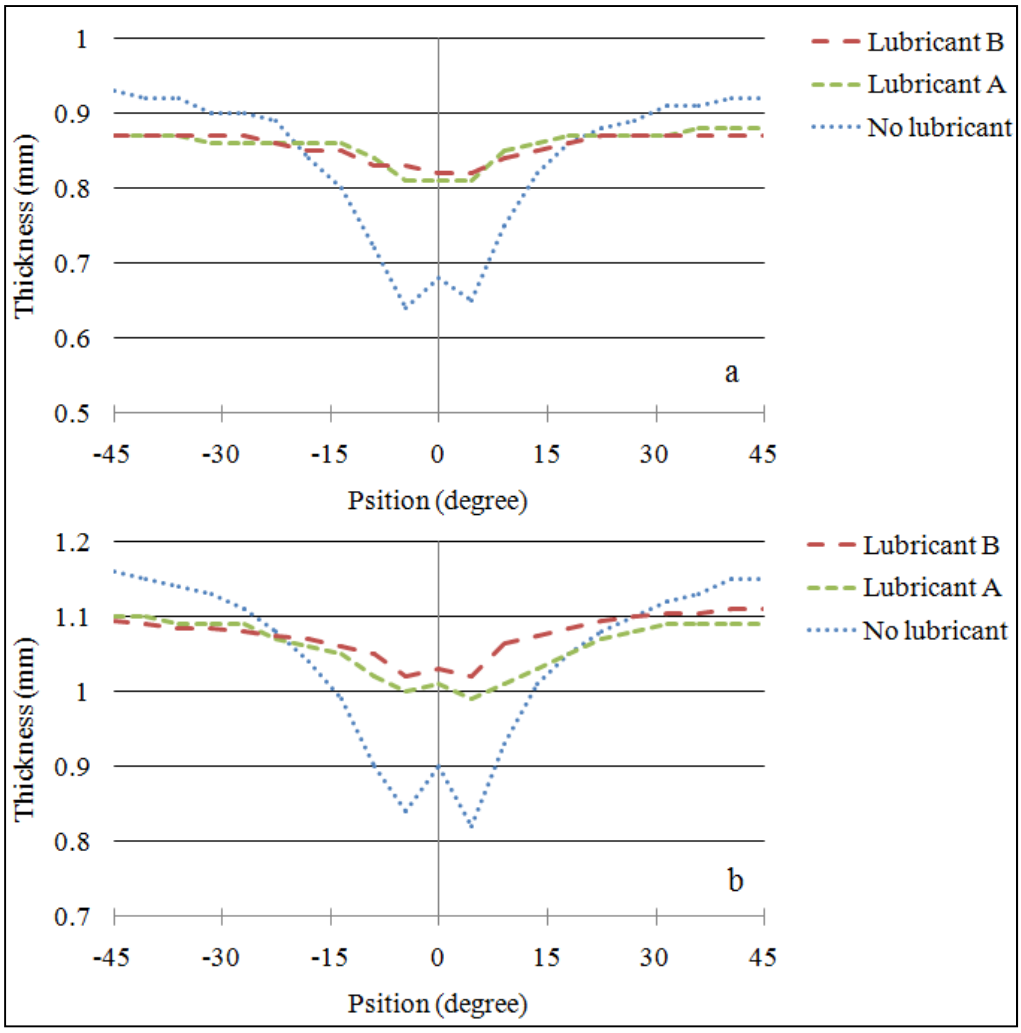

Figure 3.18: Thickness variation of tubes with different lubricants
(a) 0.9 mm and (b) 1.2 mm thick tubes

To investigate the effect of friction on the final part, different COF values were used in the FEM to simulate the process. Figure 3.19 shows the effect of COF on the tube expansion for both tube thicknesses. It can be seen that up to 40 MPa, the tube expansion is almost the same for all the COF values. From this point up to about 120 MPa internal pressure, the tube expansion increases by decreasing the COF. After that up to the end of the process, the tube expansion value converges to the same value for all COFs; indicating the die is fully filled at this point. Based on the Figure 3.19, the tube expansion curve obtained from FEA with COF equal to 0.01 is the closest to the experimental curve.

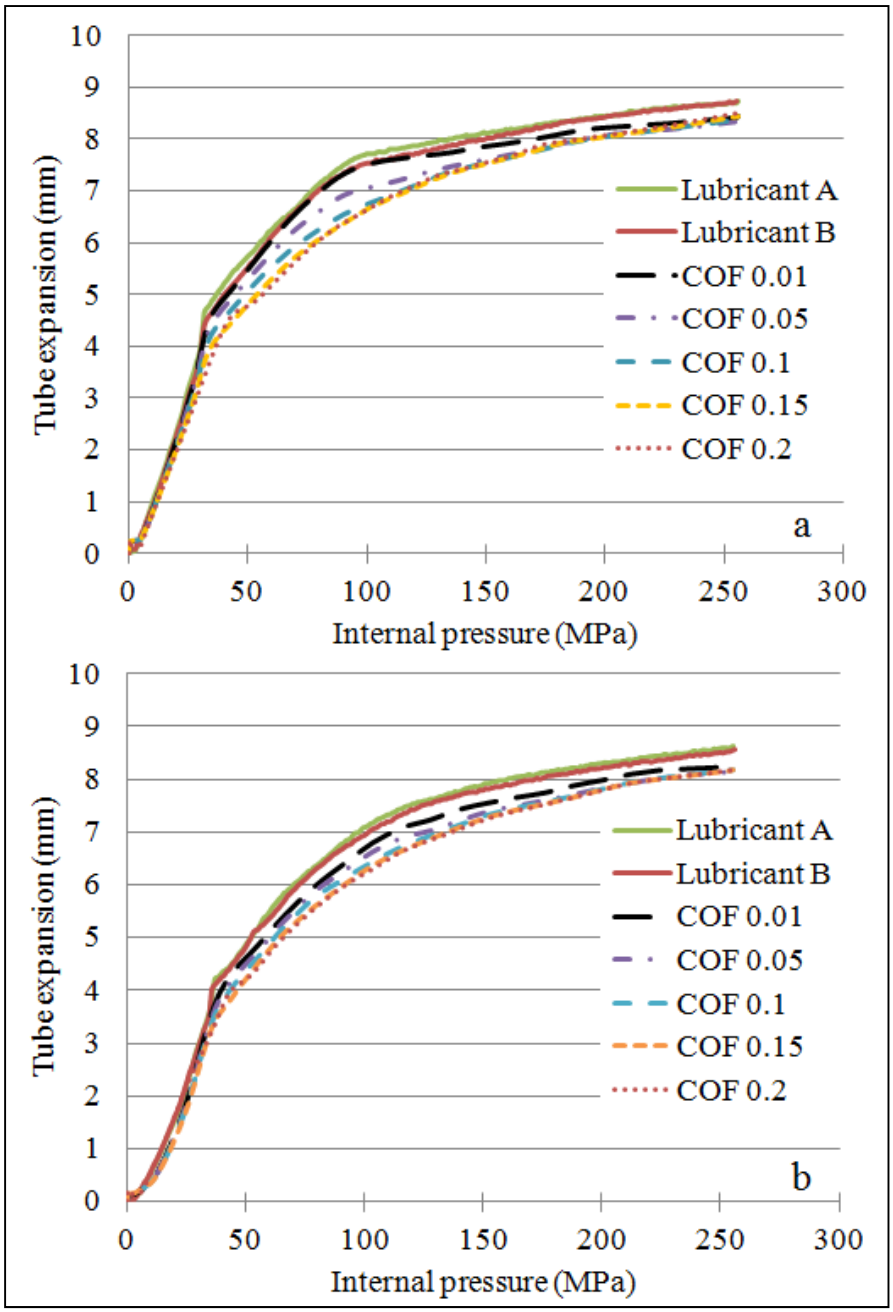

Figure 3.19: Tube expansion curves for different COFs
(a) 0.9 mm (b) 1.2 mm thick tubes

In Figure 3.20 the predicted tube thickness variation for different COF values are presented. Based on this figure, by increasing the COF value, the thickness variation increases as well. So the most uniform thickness distribution is obtained using COF equal to 0.01. For 0.9 mm thick tubes, the minimum thickness that was obtained from the maximum COF (0.2) is equal

to 0.66 mm while this value for the minimum COF (0.01) is equal to 0.86 mm. This indicates 30% increase in the minimum thickness in the section. The minimum thickness for 1.2 mm thick tubes is equal to 1.05 mm and 0.89 mm for 0.01 and 0.2 COFs, respectively. This shows 18% increase in the minimum thickness by decreasing the COF from 0.2 to 0.01. Also, the experimental results that are obtained from lubricated tubes are in good agreement with the FEA results from COFs equal to 0.05 indicating the performance of the lubricants used in this study.

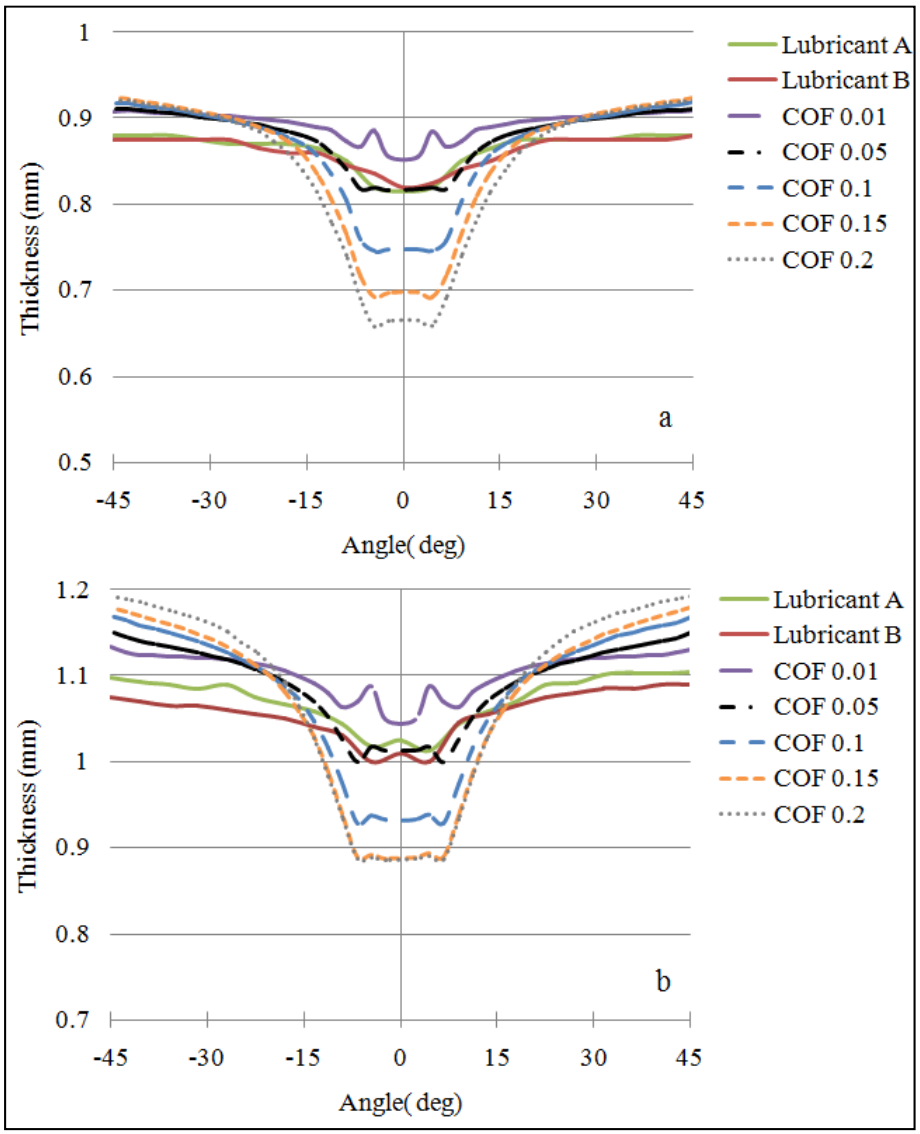

Figure 3.20: Tube thickness variation for different COFs
(a) 0.9 mm (b) 1.2 mm thick tubes

3.4 Optimization

LS-OPT software was used for loading path optimization of the THF process. The goal was to find a loading path that could hydroform a tube with the most uniform thickness distribution. The no lubrication condition was used for the optimization process to eliminate the effects of lubrication. The optimization process was conducted using the settings described in chapter 2. Hundred load paths (10 iterations of 10 runs each) for tubes with 0.9 mm thickness and sixty load paths (6 iterations of 10 runs each) for tubes with 1.2 mm thickness were simulated to find the optimum loading path. Figure 3.21 compares the optimum loading paths that are obtained from optimization process with the applied loading pathes and Table 3.1 and Table 3.2 summarises the results from all the loading paths for both tube thicknesses.

Table 3.1 and Table 3.2 indicate that the maximum and minimum tube thicknesses that are obtained from optimum load paths are closer to the initial tube thicknesses. Compared to the load path 1, the optimum load paths increased the minimum tube thickness by 26% and 21% in 0.9 mm and 1.2 mm thick tubes, respectively. The difference between the minimum and the maximum thickness for load path 1 is equal to 0.53 mm and 0.59 mm for 0.9 mm and 1.2 mm thick tubes, respectively. This difference for the optimum load path is equal to 0.45 mm and 0.43 mm for 0.9 mm and 1.2 mm thick tubes, respectively. The results suggest that using the optimum load path for hydroforming leads to more uniform tube thickness, which was the objective of the optimization process.

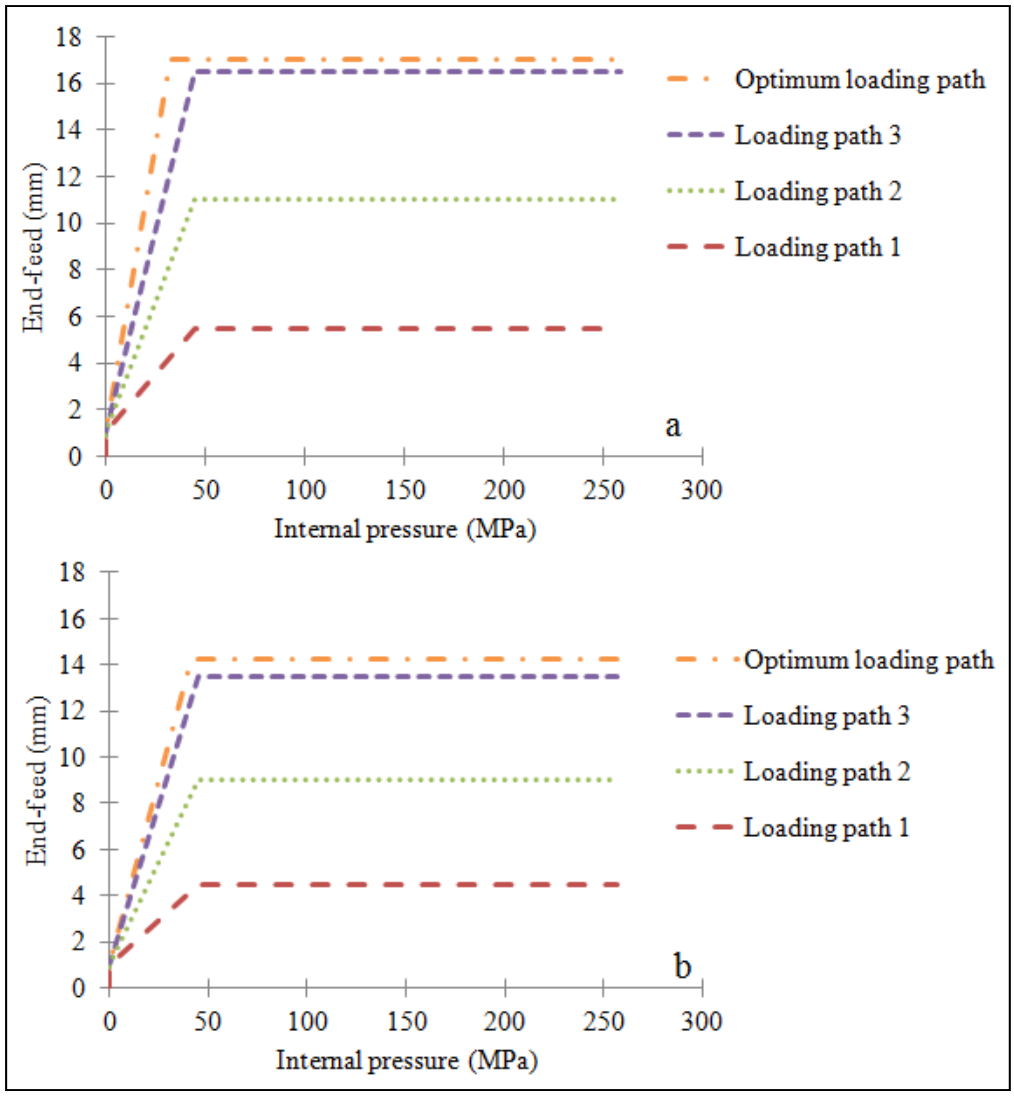

Figure 3.21: Loading paths for tubes with
(a) 0.9 mm (b) 1.2 mm thicknesses

Table 3.1: Optimization results for 0.9 mm tube thickness

	Pressure (MPa)	End feed (mm)	Minimum thickness (mm)	Maximum thickness (mm)
Loading path 1	45	5.5	0.57	1.1
Loading path 2	45	11	0.66	1.16
Loading path 3	45	16.5	0.71	1.25
Optimum loading path	32.2	17	0.72	1.17

Table 3.2: Optimization results for 1.2 mm tube thickness

	Pressure (MPa)	End feed (mm)	Minimum thickness (mm)	Maximum thickness (mm)
Loading path 1	45	4.5	0.79	1.38
Loading path 2	45	9	0.86	1.43
Loading path 3	45	13.5	0.92	2.19
Optimum loading path	41	14.2	0.96	1.39

The optimized loading paths that were obtained for 0.9 mm and 1.2 mm thick tubes were used for hydroforming of the tubes. Figure 3.22 and Figure 3.23 compare the experimental and numerical results for tube expansion and tube thickness, respectively. Some minor differences can be seen between the results that can be due to utilization of shell element and friction condition during the experiments. The simulation results correspond well with the experimental results, indicating that the approach can be used for optimization of more complex shapes. The tube expansion and the tube thickness results for optimum load paths are presented in Appendix H and I, respectively.

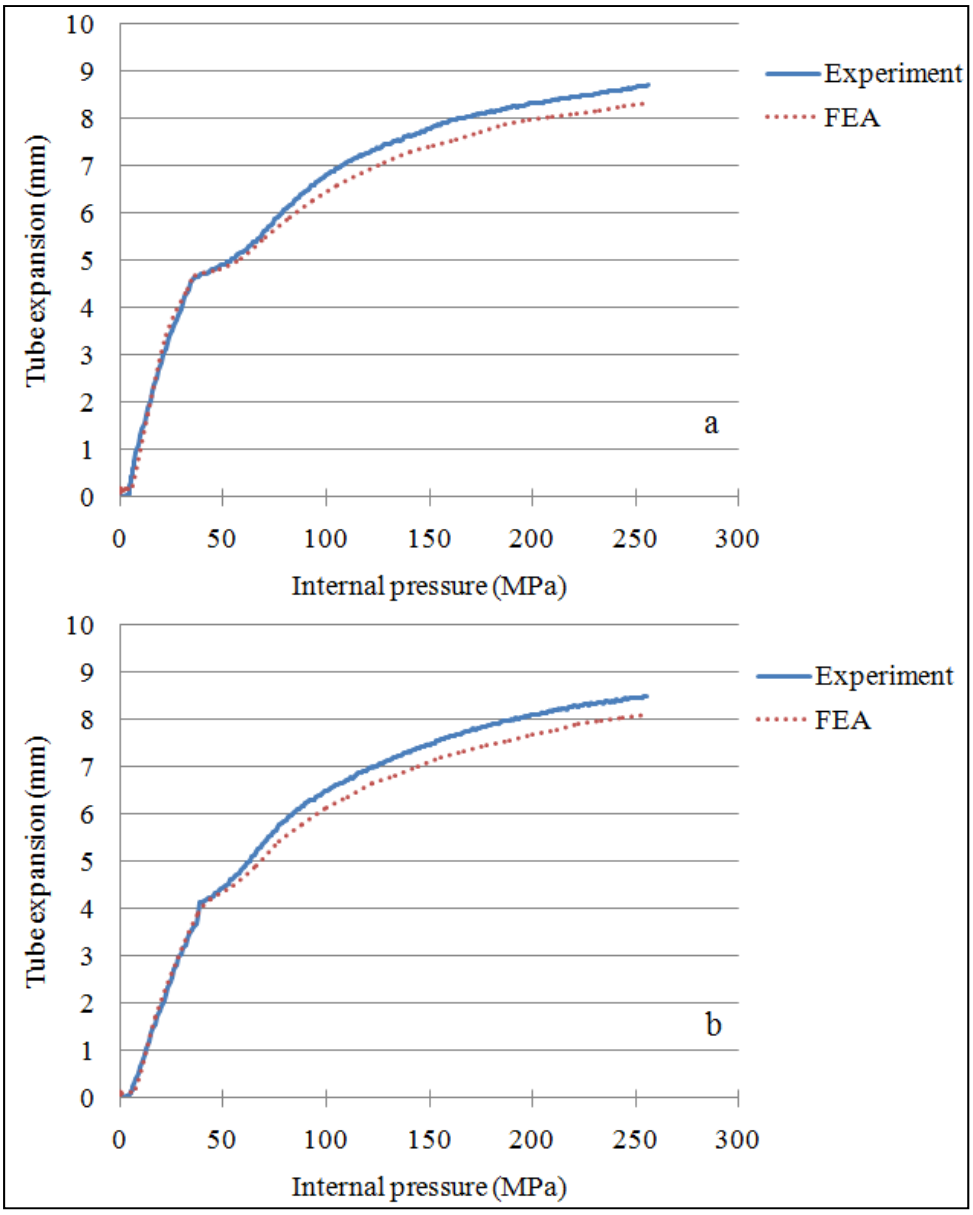

Figure 3.22: Tube expansion curves for optimum loading paths
(a) 0.9 mm and (b) 1.2 mm thicknesses

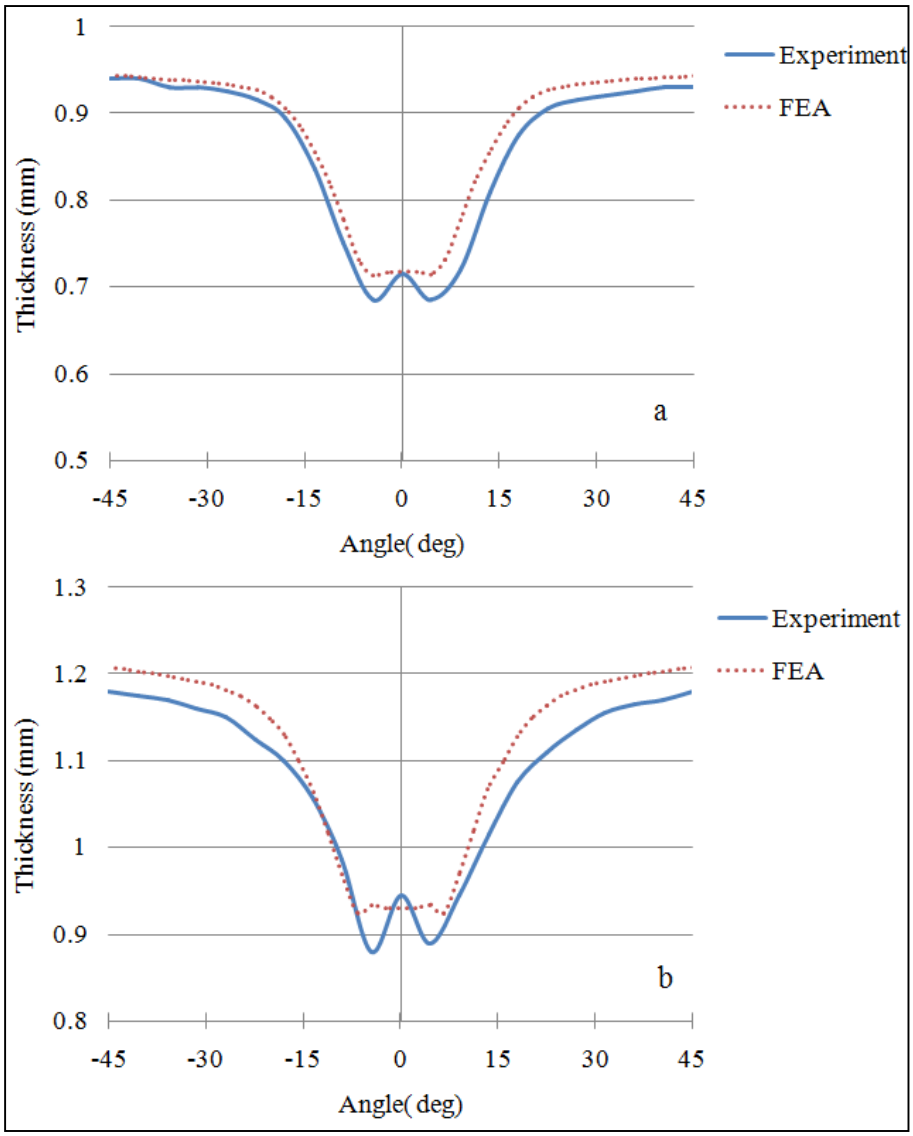

Figure 3.23: Tube thickness variations for optimum loading paths
(a) 0.9 mm and (b) 1.2 mm thicknesses

CONCLUSION

Experimental and numerical analyses were conducted to study the close die THF process. The effects of end feeding and lubrication on THF of SS321 tubes with 0.9 mm and 1.2 mm thicknesses were investigated. Different FEMs were developed using two different material properties and three element types. Then, the results from experimental and FEA were compared to verify the developed FEMs. For comparison, the tube expansion and thickness variation were measured experimentally and numerically. The shell model was used to investigate the effect of lubrication as well as finding the optimum loading path in the THF process.

Different loading paths were used to hydroform the tubes. The thickness at the mid section of the blank tubes was measured, which was varying in the circumferential direction. For this reason, an average thickness was considered based on averaging the thickness in the front and back quarters of the tube at mid section.

It was shown that by tripling the end feeding, the minimum thickness of the tubes increased by 18% and 10% for 0.9 mm and 1.2 mm thick tubes, respectively. The expansion at the calibration stage was limited to the die corners. Because the tubes fully filled the die cavity, the effect of end feeding was less evident on the total tube expansion.

Two different material properties were obtained from the free expansion and tensile tests and were used for the FEAs. The comparison between the FEM results and the experimental data showed that the material properties obtained from the free expansion test leads to more accurate results.

Three different elements were used in modelling of the THF process; shell, solid and Tshell. Compared to the Tshell element, the results of the shell and solid elements were relatively closer to the experiments. For reducing the computational cost the shell element was used in this study as it was seven times faster than solid element.

Measured principal strains were compared with the ones that were obtained from the FEAs. For 0.9 mm thick tube, the FEA predicted the maximum major strain with maximum 6% errors. Although there was a slight discrepancy between the FEA and experimental results, the trend and magnitudes of the results were in good agreements, indicating that the FEM developed in this study can be used with good confidence for predicting the THF process of components with similar complexities.

Different COFs were used to model the process and predict the tube expansion along with the tube thickness in THF process. The results showed that during the forming stage, decreasing the COF increased the tube expansion for both tube thicknesses. Also, decreasing the COF led to more uniform thickness in the tubes. The simulation results with COF equal to 0.01 predicted better the experimental data for the lubricated tubes.

LS-OPT software was used to find the optimum load path in hydroforming process. The goal was to find a load path that could hydroform the tube with the most uniform thickness distribution. Compared to minimum end feed condition (load path 1), it was shown that the optimum load path increased the minimum tube thickness by 26% and 21% in 0.9 mm and 1.2 mm thick tubes, respectively.

RECOMMENDATIONS

The following recommendations are proposed to further improve numerical and experimental investigation of THF process.

In the present study, a square shape hydroforming process was investigated. This work can be extended further by investigating hydroforming of more complex geometries with different performing stages.

For generalizing the approach adopted in this study, further studies can be performed using different aerospace materials.

The FEM used in this study is not predicting the necking and bursting in the THF process. Therefore, developing a FEM with the ability to predict failure in the process would be of interest.

For optimization procedure, other objectives and constraints could be defined and various aspect of the THF process can be investigated. Also developing an optimization code for comparing the obtained results would be a good approach.

APPENDIX A

SHELL ELEMENT MODEL FOR ROUND TO SQUARE HYDROFORMING

```
$ User supplied input:
$---+----1----+----2----+----3----+----4----+----5----+----6----+----7----+----8
$
$ Title:        Shell Element Model of Round to Square Hydroforming
$ Date:         Feb 12, 2013
$ Base units of: mm, msec, grams gives other units of N, MPa
$ Author:       Saeed Mojarad Farimani
$
$---+----1----+----2----+----3----+----4----+----5----+----6----+----7----+----8
$
*KEYWORD
$
*TITLE
Round to Square
$
*CONTROL_TERMINATION
$ Time (in millisec) that the simulation stops after.
$   ENDTIM    ENDCYC     DTMIN    ENDNEG    ENDMAS
          8.0                 0
$
*CONTROL_HOURGLASS
$ Change the default hourglass control to a Flanagan-Belytschko with exact volum
$ integration... recommended for large deformations
$      IHQ        QH
         3         0.1
$
*CONTROL_SHELL
$ BWC (warping stiffness) changed from 2 to 1.  Recommended for B-T elements
$ ISTUPD (shell thickness change option) changed to 1 to allow membrane strains
$ to affect the shell thickness.
$   WRPANG    ITRIST     IRNXX    ISTUPD    THEORY       BWC     MITER
         20.0              2           -1              1              2           2              1
$
$--------------------------Only for solid model-----------------------------------
*CONTROL_SOLID
$    ESORT    FMATRX   NIPTETS    SWLOCL
              1              1              4              2
$-------------------------------------------------------------------------------
$
*CONTROL_CONTACT
$ Allow the Shell thickness to be considered in surface to surface and node to
$ surface type contacts.
$THE LAST TWO LINES ARE FOR INTFOR AND FRICTIONAL ENERGY
$
$   SLSFAC    RWPNAL    ISLCHK    SHLTHK    PENOPT    THKCHG     ORIEN
          0.1                 0              2              1              1              0              1
```

```
$  USRSTR   USRFAC    NSBCS   INTERM   XPENEN
           0          0         10         0        4.0
$   SFRIC    DFRIC     EDC      VFC       TH    TH_SF   PEN_SF

$  IGNORE   FRCENG  SKIPRWG   OUTSEG  SPOTSTP  SPOTDEL
           1
$
*CONTROL_ENERGY
$ Used to allow hourglass energy to be calculated and stored in the
$ GLSTAT and MATSUM ASCII files
$    HGEN     RWEN   SLNTEN    RYLEN
          2          2          2          1
$
$---+----1----+----2----+----3----+----4----+----5----+----6----+----7----+----8
$
$ ASCII and LS TAURUS output
$
$---+----1----+----2----+----3----+----4----+----5----+----6----+----7----+----8
$
*DATABASE_BINARY_INTFOR
$      DT
       0.2
$
*DATABASE_RCFORC
$      DT
       0.2
$
*DATABASE_RBDOUT
$      DT
       0.2
$
*DATABASE_BINARY_D3PLOT
$  DT/CYCL     LCDT    NOBEAM
       0.2
$
*DATABASE_EXTENT_BINARY
$   NEIPH    NEIPS   MAXINT   STRFLG   SIGFLG   EPSFLG   RLTFLG   ENGFLG
          2        0        5        1        1        1        1        1
$  CMPFLG   IEVERP   BEAMIP    DCOMP     SHGE    STSSZ
           0        0        0        2        0        0
$
$---+----1----+----2----+----3----+----4----+----5----+----6----+----7----+----8
$
$ Parts
$
$---+----1----+----2----+----3----+----4----+----5----+----6----+----7----+----8
$
*PART
Tube
$     PID    SECID      MID    EOSID     HGID     GRAV   ADPOPT
        1        2        1        0        0        0        0
$
*PART
Die
```

```
$     PID    SECID      MID    EOSID     HGID     GRAV   ADPOPT
        2        1        2        0        0        0        0
$
$---+----1----+----2----+----3----+----4----+----5----+----6----+----7----+----8
$
$ Section data
$
$---+----1----+----2----+----3----+----4----+----5----+----6----+----7----+----8
$                                                   $
*SECTION_SHELL
$     SID   ELFORM     SHRF      NIP    PROPT   QR/IRID    ICOMP
        1        2      1.0      3.0      0.0      0.0        0
$      T1       T2       T3       T4     NLOC
       1.0      1.0      1.0      1.0        0
$
$--------------------------Only for shell model-----------------------------------
*SECTION_SHELL
$     SID   ELFORM     SHRF      NIP    PROPT   QR/IRID    ICOMP
        2        2      1.0      5.0      0.0      0.0        0
$      T1       T2       T3       T4     NLOC
     1.22     1.22     1.22     1.22        0
$-------------------------------------------------------------------------------
$
$--------------------------Only for solid model-----------------------------------
*SECTION_SOLID
$#   secid    elform      aet
        2        1        0
$-------------------------------------------------------------------------------
$
$--------------------------Only for Tshell model----------------------------------
*SECTION_TSHELL
$     SID   ELFORM     SHRF      NIP    PROPT   QR/IRID    ICOMP
        2        3     0.83        3      3.0      0.0        0
$-------------------------------------------------------------------------------
$
$---+----1----+----2----+----3----+----4----+----5----+----6----+----7----+----8
$
$ Contact Definitions
$
$---+----1----+----2----+----3----+----4----+----5----+----6----+----7----+----8
$
*CONTACT_SURFACE_TO_SURFACE_ID
$#     cid                                             title
       Die to Tube
$#    ssid     msid    sstyp    mstyp   sboxid   mboxid      spr      mpr
         1        2        3        3        0        0        1        1
$#      fs       fd       dc       vc      vdc   penchk       bt       dt
       0.2      0.2      1.0   118.65     20.0        0        0        0
$#     sfs      sfm      sst      mst     sfst     sfmt      fsf      vsf

$
$--------------------------Only for shell model-----------------------------------
*CONTACT_AUTOMATIC_GENERAL
```

```
$    SSID     MSID    SSTYP    MSTYP    SBOXID    MBOXID      SPR      MPR
         1        0        3
$      FS       FD       DC       VC      VDC    PENCHK       BT       DT
       0.2      0.2      1.0   118.65       20         0        0
$     SFS      SFM      SST      MST     SFST     SFMT      FSF      VSF

$--------------------------------------------------------------------------------
$
$---+----1----+----2----+----3----+----4----+----5----+----6----+----7----+----8
$
$ Internal Pressure Load
$
$---+----1----+----2----+----3----+----4----+----5----+----6----+----7----+----8
$
*LOAD_SEGMENT_SET_ID
$#      id
         1
$#    ssid     lcid       sf       at       dt
          1        2      1.0      0.0      0.0
$
$---+----1----+----2----+----3----+----4----+----5----+----6----+----7----+----8
$
$ End-Feeding
$
$---+----1----+----2----+----3----+----4----+----5----+----6----+----7----+----8
$
*BOUNDARY_PRESCRIBED_MOTION_SET
$    NSID      DOF      VAD     LCID       SF      VID    DEATH    BIRTH
          5        3        2       12      1.0        0      8.0        0.0
$
*INCLUDE
Material.insert
$
*INCLUDE
Load-Path.insert
$
*INCLUDE
Tube.insert
$
*INCLUDE
Die.insert
$
*END
```

APPENDIX B

CODE FOR SPRING BACK SIMULATION

```
*KEYWORD 210000000
$
*TITLE
 Springback 0.4ff
$
$ User supplied input:
$
$ This is the deck for springback of the 3" tube bending operation
$
$ User supplied input:
$
$---+----1----+----2----+----3----+----4----+----5----+----6----+----7----+----8
$
$ Title:
$ Date:
$ Base units of: mm, msec, grams gives other units of N, MPa
$ Author:
$
$ Optional Control Cards that have been modified.
$
$---+----1----+----2----+----3----+----4----+----5----+----6----+----7----+----8
$
*CONTROL_TERMINATION
$ Time (in millisec) that the simulation stops after.
$   ENDTIM    ENDCYC     DTMIN    ENDNEG    ENDMAS
         0.004                 0
$
$
*CONTROL_SHELL
$ BWC (warping stiffness) changed from 2 to 1.  Recommended for B-T elements
$ ISTUPD (shell thickness change option) changed to 1 to allow membrane strains
$ to affect the shell thickness.
$   WRPANG    ITRIST     IRNXX    ISTUPD    THEORY       BWC     MITER
        20.000             2            -1             1                2            2              1
$
$
*CONTROL_ENERGY
$ Used to allow hourglass energy to be calculated and stored in the
$ GLSTAT and MATSUM ASCII files
$     HGEN      RWEN    SLNTEN     RYLEN
             2              2               2              1
$
$
$---+----1----+----2----+----3----+----4----+----5----+----6----+----7----+----8
$
$ ASCII and LS TAURUS output
$
```

```
$---+----1----+----2----+----3----+----4----+----5----+----6----+----7----+----8
$
$
$$*DATABASE_GLSTAT
$       DT
$$  0.025
$
$$*DATABASE_MATSUM
$       DT
$$  0.025
$
$$*DATABASE_RBDOUT
$       DT
$$  0.025
$
*DATABASE_BINARY_D3PLOT
$  DT/CYCL      LCDT    NOBEAM
         0.001
$
*DATABASE_EXTENT_BINARY
$    NEIPH     NEIPS    MAXINT    STRFLG    SIGFLG    EPSFLG    RLTFLG    ENGFLG
             0             0              5              1              1              1              1              1
$   CMPFLG    IEVERP    BEAMIP     DCOMP      SHGE     STSSZ
               0              0              0              2              0              0
$
$
$---+----1----+----2----+----3----+----4----+----5----+----6----+----7----+----8
$
$ Part definitions
$
$---+----1----+----2----+----3----+----4----+----5----+----6----+----7----+----8
$
*PART
 Tube
$      PID     SECID       MID     EOSID      HGID      GRAV    ADPOPT
           1             1             1              0
$
*SECTION_SHELL
$      SID    ELFORM      SHRF       NIP     PROPT   QR/IRID     ICOMP
           1              2         1.0         5.0           0.0           0.0               0
$       T1        T2        T3        T4      NLOC
     0.94      0.94      0.94      0.94               0
$
*INCLUDE
dynain.insert
$
$
$---+----1----+----2----+----3----+----4----+----5----+----6----+----7----+----8
$
$ Material and section definitions
$
$---+----1----+----2----+----3----+----4----+----5----+----6----+----7----+----8
$
*INCLUDE
```

```
mat-S0.9-Spline.insert
$
$
$---+----1----+----2----+----3----+----4----+----5----+----6----+----7----+----8
$
$ Implicit Springback information
$
$---+----1----+----2----+----3----+----4----+----5----+----6----+----7----+----8
$
*CONTROL_IMPLICIT_GENERAL
$   IMFLAG      DT0    IMFORM      NSBS       IGS
             1     0.001                1             4           2
$
$
*CONTROL_IMPLICIT_STABILIZATION
$      IAS     SCALE    TSTART      TEND
          1         0.100
$
$
*CONTROL_IMPLICIT_LINEAR
$  LSOLVER    LPRINT    NEGEIG
               0              0              2
$
$
*CONTROL_IMPLICIT_NONLINEAR
$   NSOLVR    ILIMIT    MAXREF     DCTOL    ECTOIL     RCTOL     LSTOL      RSSF
             0            1            150           0.0           0.0                    99999
$    DNORM   DIVFLAG   INISTIF   NLPRINT
                                                  1
$
*CONTROL_IMPLICIT_AUTO
$    IAUTO    ITEOPT    ITEWIN     DTMIN     DTMAX
           1          200             0       0.0001         0.001
$
*END
```

APPENDIX C

CODE FOR OPTIMIZATION OF THF PROCESS USING LS-OPT 4.2

```
"Round-to-Square-THF"
$
Author "Saeed Mojarad Farimani"
$ Created on Tue Sep 10 15:40:30 2013
$
$ DESIGN VARIABLES
$
variables 2
 Variable 'F' 10.
  Lower bound variable 'F' 0.
  Upper bound variable 'F' 20.
 Variable 'P' -40.
  Lower bound variable 'P' -60.
  Upper bound variable 'P' -20.

$$$$$$$$$$$$$$$$$$$$$$$$$$$$$$$$
$      OPTIMIZATION METHOD
$$$$$$$$$$$$$$$$$$$$$$$$$$$$$$$$
$
Optimization Method SRSM

$$$$$$$$$$$$$$$$$$$$$$$$$$$$$$$$
$      SOLVER "THF-Process"
$$$$$$$$$$$$$$$$$$$$$$$$$$$$$$$$
$
$ DEFINITION OF SOLVER "THF-Process"
$
 solver dyna960 'THF-Process'
  solver command "C:\LSDYNA\program\ls-dyna_smp_d_R700_winx64_ifort101.exe"
  solver input file "1.k"
  solver check output on
  solver compress d3plot off
$ ------ Pre-processor --------
$   NO PREPROCESSOR SPECIFIED
$ ------ Post-processor --------
$   NO POSTPROCESSOR SPECIFIED
$ ------ Metamodeling ---------
  solver order quadratic
  solver experiment design dopt
$ ------ Job information ------
  solver concurrent jobs 5
$
$ RESPONSES FOR SOLVER "THF-Process"
$
 response 'MaxThickness' 1 0 "D3PlotResponse -pids 1  -res_type misc  -cmp shell_thickness -select MAX -
start_time 0.0000"
```

```
 response 'FLD' 1 0 "D3PlotResponse -pids 1  -res_type fld  -cmp upper_eps1/fldc -fld_curve 4  -select MAX -
start_time 0.0000"
 response 'MinThickness' 1 0 "D3PlotResponse -pids 1  -res_type misc  -cmp shell_thickness -select MIN -
start_time 0.0000"

composites 2
$
$ COMPOSITE EXPRESSIONS
$
 composite 'Obj1' {((MinThickness-1.22)/1.22)*((MinThickness-1.22)/1.22)}
 composite 'Obj2' {((MaxThickness-1.22)/1.22)*((MaxThickness-1.22)/1.22)}
$
$ OBJECTIVE FUNCTIONS
$
 objectives 2
 objective 'Obj1' 1
 objective 'Obj2' 1
$
$ CONSTRAINT DEFINITIONS
$
 constraints 1
 constraint 'FLD'
  strict
  upper bound constraint 'FLD' 1
$
$ PARAMETERS FOR METAMODEL OPTIMIZATION
$
 Metamodel Optimization Strategy DOMAINREDUCTION
$
  iterate param design 0.01
  iterate param objective 0.01
  iterate param stoppingtype and
  iterate param response 1
$
$ OPTIMIZATION ALGORITHM
$
 Optimization Algorithm hybrid ga
  Use GSA
$
$ JOB INFO
$
 iterate 10
STOP
```

APPENDIX D

TUBE EXPANSION

Pressure (MPa)	Tubes with 0.9 mm initial thickness																										
	Free end						Loading path 1						Loading path 2						Loading path 3								
	Front side			Back side			Front side			Back side			Front side			Back side			Front side			Back side					
	1	2	3	1	2	3	1	2	3	1	2	3	1	2	3	1	2	3	1	2	3	1	2	3			
0	0.00	0.00	0.00	0.00	0.00	0.00	0.00	0.00	0.00	0.00	0.00	0.00	0.00	0.00	0.00	0.00	0.00	0.00	0.00	0.00	0.00	0.00	0.00	0.00			
10	0.24	0.27	0.22	0.44	0.51	0.35	0.27	0.27	0.19	0.40	0.46	0.30	0.74	0.77	0.72	0.85	0.92	0.76	0.91	0.97	0.91	1.14	1.23	1.09			
20	1.68	1.73	1.65	1.66	1.69	1.56	1.56	1.63	1.50	1.59	1.59	1.51	2.09	2.14	2.06	2.03	2.06	1.93	2.17	2.21	2.08	2.50	2.56	2.48			
30	3.00	3.07	2.90	2.98	3.06	2.96	3.12	3.19	3.05	3.20	3.23	3.13	3.28	3.35	3.18	3.24	3.32	3.22	3.36	3.46	3.36	3.58	3.59	3.50			
40	4.11	4.18	4.07	4.27	4.32	4.25	4.21	4.31	4.12	4.36	4.45	4.29	4.24	4.31	4.20	4.15	4.20	4.13	4.28	4.38	4.19	4.55	4.63	4.55			
50	4.94	4.99	4.94	5.03	5.09	5.00	4.97	4.98	4.93	5.02	5.07	4.97	4.84	4.89	4.84	4.69	4.75	4.66	4.79	4.89	4.73	5.09	5.15	5.01			
60	5.61	5.62	5.54	5.66	5.68	5.59	5.60	5.63	5.50	5.72	5.73	5.69	5.50	5.51	5.43	5.27	5.29	5.20	5.15	5.19	5.07	5.34	5.41	5.24			
70	6.04	6.11	5.96	6.11	6.14	6.06	6.14	6.19	6.05	6.24	6.26	6.18	6.00	6.07	5.92	5.77	5.80	5.72	5.67	5.69	5.64	5.67	5.75	5.65			
80	6.34	6.40	6.28	6.49	6.49	6.43	6.43	6.45	6.38	6.56	6.61	6.50	6.45	6.51	6.39	6.25	6.25	6.19	6.07	6.09	6.06	6.07	6.07	6.03			
90	6.71	6.79	6.62	6.74	6.77	6.72	6.72	6.75	6.72	6.82	6.83	6.77	6.79	6.87	6.70	6.55	6.58	6.53	6.49	6.51	6.39	6.43	6.51	6.41			
100	7.07	7.17	7.04	6.99	7.05	6.89	6.98	7.05	6.98	7.07	7.08	7.04	7.07	7.17	7.04	6.84	6.90	6.74	6.74	6.84	6.73	6.75	6.85	6.65			
110	7.27	7.28	7.17	7.19	7.21	7.18	7.23	7.26	7.19	7.30	7.39	7.24	7.36	7.37	7.26	7.07	7.09	7.06	6.96	7.04	6.96	7.00	7.07	7.00			

260	250	240	230	220	210	200	190	180	170	160	150	140	130	120
8.79	8.75	8.71	8.67	8.61	8.53	8.49	8.37	8.32	8.23	8.12	7.95	7.80	7.64	7.47
8.82	8.79	8.81	8.76	8.70	8.62	8.55	8.40	8.36	8.29	8.15	7.98	7.84	7.64	7.56
8.72	8.67	8.61	8.67	8.59	8.47	8.40	8.34	8.28	8.13	8.10	7.85	7.73	7.64	7.47
8.83	8.82	8.79	8.77	8.68	8.64	8.54	8.47	8.44	8.39	8.27	8.14	7.92	7.67	7.44
8.91	8.91	8.88	8.86	8.77	8.73	8.57	8.56	8.44	8.48	8.34	8.18	8.02	7.76	7.48
8.79	8.72	8.72	8.68	8.67	8.54	8.46	8.45	8.35	8.34	8.26	8.14	7.86	7.58	7.37
8.75	8.74	8.69	8.67	8.61	8.56	8.47	8.44	8.36	8.26	8.12	7.99	7.81	7.62	7.46
8.81	8.75	8.71	8.74	8.67	8.60	8.51	8.48	8.39	8.31	8.13	8.04	7.85	7.69	7.46
8.69	8.74	8.60	8.62	8.58	8.50	8.47	8.41	8.32	8.22	8.08	7.89	7.78	7.61	7.37
8.88	8.88	8.82	8.75	8.67	8.59	8.53	8.44	8.37	8.26	8.09	8.00	7.88	7.77	7.53
8.93	8.93	8.88	8.76	8.70	8.61	8.54	8.49	8.45	8.29	8.12	8.08	7.91	7.81	7.60
8.79	8.79	8.73	8.66	8.63	8.49	8.52	8.34	8.33	8.26	8.04	7.99	7.84	7.70	7.52
8.87	8.85	8.78	8.74	8.65	8.60	8.54	8.47	8.36	8.24	8.12	8.04	7.90	7.77	7.58
8.91	8.89	8.88	8.83	8.74	8.69	8.60	8.50	8.40	8.30	8.15	8.07	7.94	7.77	7.67
8.79	8.77	8.68	8.74	8.63	8.54	8.45	8.44	8.32	8.14	8.10	7.94	7.83	7.77	7.58
8.67	8.62	8.56	8.47	8.42	8.36	8.29	8.23	8.14	8.02	7.88	7.75	7.59	7.43	7.25
8.75	8.71	8.65	8.56	8.51	8.45	8.32	8.32	8.14	8.11	7.95	7.79	7.69	7.52	7.29
8.62	8.52	8.49	8.38	8.41	8.26	8.21	8.21	8.05	7.97	7.87	7.75	7.53	7.34	7.18
8.62	8.59	8.52	8.47	8.41	8.32	8.27	8.16	8.06	7.97	7.79	7.70	7.56	7.39	7.19
8.68	8.64	8.61	8.51	8.50	8.36	8.28	8.26	8.16	7.99	7.80	7.76	7.62	7.41	7.27
8.59	8.49	8.52	8.46	8.33	8.26	8.26	8.14	8.02	7.94	7.71	7.60	7.49	7.29	7.14
8.66	8.69	8.60	8.53	8.44	8.40	8.27	8.22	8.13	8.03	7.92	7.78	7.60	7.45	7.25
8.70	8.73	8.60	8.59	8.54	8.45	8.37	8.24	8.19	8.13	8.00	7.86	7.63	7.52	7.31
8.63	8.68	8.55	8.49	8.39	8.34	8.21	8.14	8.06	7.94	7.84	7.71	7.51	7.39	7.23

Pressure (MPa)	Tubes with 1.2 mm initial thickness																										
	Free end						Loading path 1						Loading path 2						Loading path 3								
	Front side			Back side			Front side			Back side			Front side			Back side			Front side			Back side					
	1	2	3	1	2	3	1	2	3	1	2	3	1	2	3	1	2	3	1	2	3	1	2	3			
0	0.00	0.00	0.00	0.00	0.00	0.00	0.00	0.00	0.00	0.00	0.00	0.00	0.00	0.00	0.00	0.00	0.00	0.00	0.00	0.00	0.00	0.00	0.00	0.00			
10	0.00	0.00	0.08	0.00	0.06	0.10	0.10	0.12	0.00	0.10	0.10	0.05	0.30	0.33	0.28	0.30	0.37	0.21	0.57	0.63	0.57	0.57	0.66	0.52			
20	1.12	1.19	1.06	1.13	1.13	1.05	1.02	1.06	0.96	1.02	1.12	0.99	1.38	1.43	1.35	1.38	1.41	1.28	1.66	1.70	1.57	1.78	1.84	1.76			
30	2.51	2.58	2.44	2.48	2.51	2.41	2.44	2.52	2.35	2.44	2.47	2.35	2.72	2.79	2.62	2.72	2.80	2.70	2.83	2.93	2.83	2.78	2.79	2.70			
40	3.57	3.67	3.48	3.57	3.66	3.50	3.60	3.60	3.57	3.60	3.67	3.50	3.74	3.81	3.70	3.74	3.79	3.72	3.77	3.87	3.68	3.60	3.68	3.60			
50	4.42	4.43	4.38	4.37	4.42	4.32	4.41	4.50	4.38	4.41	4.43	4.36	4.39	4.44	4.39	4.39	4.45	4.36	4.34	4.44	4.28	4.18	4.24	4.10			
60	5.09	5.12	4.99	5.01	5.02	4.98	5.05	5.05	5.04	5.05	5.15	4.99	5.03	5.04	4.96	5.03	5.05	4.96	4.77	4.81	4.69	4.57	4.64	4.47			
70	5.55	5.60	5.46	5.50	5.52	5.44	5.55	5.60	5.51	5.55	5.64	5.50	5.52	5.59	5.44	5.52	5.55	5.47	5.23	5.25	5.20	4.96	5.04	4.94			
80	5.96	5.98	5.91	5.93	5.98	5.87	5.98	6.01	5.94	5.98	6.03	5.93	5.91	5.97	5.85	5.91	5.91	5.85	5.66	5.68	5.65	5.38	5.38	5.34			
90	6.31	6.34	6.31	6.26	6.27	6.21	6.33	6.40	6.23	6.33	6.35	6.33	6.26	6.34	6.17	6.26	6.29	6.24	6.02	6.04	5.92	5.72	5.80	5.70			
100	6.60	6.67	6.60	6.57	6.58	6.54	6.63	6.67	6.58	6.63	6.69	6.60	6.57	6.67	6.54	6.57	6.63	6.47	6.33	6.43	6.32	6.06	6.16	5.96			
110	6.82	6.85	6.78	6.81	6.90	6.75	6.85	6.87	6.76	6.85	6.87	6.77	6.83	6.84	6.73	6.83	6.85	6.82	6.59	6.67	6.59	6.34	6.41	6.34			
120	6.99	6.99	6.90	7.03	7.10	7.02	7.02	7.09	6.92	7.02	7.04	6.97	7.05	7.14	7.05	7.05	7.09	6.98	6.82	6.90	6.77	6.54	6.60	6.52			
130	7.17	7.24	7.16	7.18	7.22	7.11	7.21	7.26	7.13	7.21	7.31	7.15	7.22	7.22	7.22	7.22	7.31	7.13	7.01	7.03	6.91	6.73	6.80	6.67			

260	250	240	230	220	210	200	190	180	170	160	150	140
8.42	8.36	8.31	8.26	8.22	8.13	8.02	7.91	7.84	7.74	7.60	7.47	7.32
8.48	8.37	8.33	8.33	8.28	8.17	8.06	7.95	7.87	7.79	7.61	7.52	7.36
8.42	8.36	8.22	8.21	8.19	8.07	8.02	7.88	7.80	7.70	7.56	7.37	7.29
8.52	8.50	8.43	8.34	8.26	8.16	8.08	7.99	7.89	7.80	7.70	7.54	7.36
8.52	8.55	8.49	8.35	8.29	8.18	8.09	8.04	7.97	7.83	7.73	7.62	7.39
8.50	8.41	8.34	8.25	8.22	8.06	8.07	7.89	7.85	7.80	7.65	7.53	7.32
8.43	8.39	8.34	8.26	8.22	8.16	8.09	8.05	7.94	7.84	7.67	7.55	7.35
8.49	8.43	8.39	8.31	8.27	8.24	8.16	8.13	7.96	7.91	7.76	7.57	7.37
8.33	8.33	8.32	8.24	8.12	8.09	8.05	7.95	7.94	7.74	7.59	7.52	7.31
8.43	8.39	8.34	8.26	8.22	8.16	8.09	8.05	7.94	7.84	7.67	7.55	7.35
8.43	8.45	8.35	8.28	8.26	8.16	8.11	8.10	7.95	7.92	7.75	7.56	7.36
8.42	8.29	8.33	8.18	8.21	8.16	8.04	7.95	7.90	7.74	7.59	7.46	7.27
8.49	8.45	8.39	8.30	8.24	8.17	8.07	8.01	7.87	7.78	7.69	7.52	7.38
8.53	8.49	8.49	8.39	8.33	8.26	8.13	8.04	7.91	7.84	7.72	7.55	7.42
8.41	8.37	8.29	8.30	8.22	8.11	7.98	7.98	7.83	7.68	7.67	7.42	7.31
8.49	8.45	8.39	8.30	8.24	8.17	8.07	8.01	7.87	7.78	7.69	7.52	7.38
8.57	8.54	8.48	8.39	8.33	8.26	8.10	8.10	7.87	7.87	7.76	7.56	7.48
8.44	8.35	8.32	8.21	8.23	8.07	7.99	7.99	7.78	7.73	7.68	7.52	7.32
8.22	8.19	8.12	8.06	7.99	7.90	7.81	7.72	7.62	7.49	7.34	7.26	7.11
8.28	8.24	8.21	8.10	8.08	7.94	7.82	7.82	7.72	7.51	7.35	7.32	7.17
8.19	8.09	8.12	8.05	7.91	7.84	7.80	7.70	7.58	7.46	7.26	7.16	7.04
8.22	8.19	8.14	8.06	7.97	7.90	7.77	7.67	7.55	7.37	7.22	7.07	6.92
8.26	8.23	8.14	8.12	8.07	7.95	7.87	7.69	7.61	7.47	7.30	7.15	6.95
8.19	8.18	8.09	8.02	7.92	7.84	7.71	7.59	7.48	7.28	7.14	7.00	6.83

APPENDIX E

THICKNESSES AT TUBE CROSS SECTION

Position (degree)	Tubes with 0.9 mm initial thickness																							
	Free end						Loading path 1						Loading path 2						Loading path 3					
	Front side			Back side			Front side			Back side			Front side			Back side			Front side			Back side		
	1	2	3	1	2	3	1	2	3	1	2	3	1	2	3	1	2	3	1	2	3	1	2	3
45.0	0.9	0.91	0.90	0.92	0.93	0.91	0.92	0.93	0.92	0.9	0.91	0.89	0.92	0.93	0.91	0.94	0.95	0.93	0.94	0.94	0.94	0.95	0.96	0.95
40.5	0.9	0.92	0.89	0.92	0.93	0.91	0.92	0.93	0.91	0.9	0.91	0.90	0.92	0.93	0.91	0.93	0.93	0.92	0.93	0.93	0.93	0.95	0.95	0.95
36.0	0.89	0.90	0.88	0.9	0.90	0.89	0.9	0.91	0.89	0.88	0.88	0.86	0.91	0.92	0.91	0.92	0.92	0.92	0.93	0.94	0.93	0.94	0.94	0.94
31.5	0.88	0.88	0.86	0.89	0.91	0.88	0.89	0.91	0.89	0.88	0.89	0.87	0.91	0.92	0.91	0.92	0.93	0.90	0.92	0.93	0.92	0.94	0.95	0.94
27.0	0.86	0.86	0.85	0.88	0.89	0.86	0.87	0.88	0.85	0.86	0.87	0.85	0.89	0.91	0.88	0.91	0.93	0.90	0.91	0.93	0.91	0.93	0.95	0.93
22.5	0.84	0.86	0.83	0.86	0.87	0.85	0.85	0.86	0.84	0.84	0.86	0.82	0.88	0.89	0.86	0.89	0.90	0.88	0.9	0.91	0.9	0.92	0.93	0.91
18.0	0.82	0.83	0.82	0.82	0.83	0.82	0.82	0.83	0.81	0.8	0.82	0.79	0.86	0.88	0.85	0.86	0.86	0.86	0.87	0.87	0.87	0.9	0.90	0.89
13.5	0.78	0.78	0.77	0.79	0.80	0.79	0.77	0.78	0.77	0.74	0.75	0.73	0.82	0.83	0.80	0.81	0.82	0.79	0.82	0.83	0.82	0.85	0.85	0.83
9.0	0.7	0.72	0.69	0.69	0.70	0.67	0.66	0.68	0.64	0.66	0.66	0.65	0.75	0.77	0.74	0.74	0.75	0.73	0.76	0.77	0.76	0.79	0.81	0.72
4.5	0.61	0.61	0.59	0.61	0.63	0.60	0.61	0.61	0.61	0.64	0.64	0.63	0.65	0.66	0.65	0.65	0.66	0.64	0.73	0.75	0.66	0.76	0.76	0.68
0	0.62	0.63	0.60	0.63	0.64	0.63	0.66	0.68	0.64	0.67	0.69	0.66	0.68	0.68	0.67	0.66	0.67	0.64	0.75	0.76	0.69	0.79	0.79	0.69

-45	-40.5	-36.0	-31.5	-27.0	-22.5	-18.0	-13.5	-9.0	-4.5
0.9	0.9	0.89	0.88	0.86	0.84	0.81	0.76	0.69	0.62
0.90	0.91	0.90	0.88	0.86	0.85	0.82	0.78	0.70	0.63
0.89	0.89	0.89	0.87	0.86	0.84	0.80	0.75	0.67	0.62
0.92	0.91	0.9	0.89	0.87	0.84	0.8	0.74	0.68	0.62
0.94	0.92	0.90	0.89	0.87	0.85	0.82	0.75	0.64	0.62
0.91	0.91	0.88	0.88	0.85	0.82	0.80	0.72	0.63	0.61
0.91	0.91	0.9	0.89	0.87	0.85	0.81	0.77	0.72	0.62
0.92	0.92	0.91	0.91	0.89	0.86	0.82	0.77	0.74	0.62
0.90	0.90	0.88	0.87	0.86	0.83	0.81	0.76	0.71	0.61
0.91	0.9	0.89	0.89	0.87	0.85	0.82	0.76	0.66	0.61
0.91	0.91	0.89	0.90	0.88	0.87	0.83	0.76	0.66	0.61
0.91	0.90	0.88	0.88	0.87	0.85	0.82	0.75	0.65	0.60
0.93	0.92	0.92	0.9	0.9	0.89	0.84	0.8	0.72	0.64
0.94	0.92	0.92	0.91	0.91	0.90	0.85	0.81	0.72	0.65
0.92	0.92	0.91	0.90	0.89	0.88	0.82	0.80	0.71	0.63
0.94	0.94	0.94	0.93	0.93	0.9	0.89	0.84	0.76	0.65
0.95	0.95	0.94	0.93	0.93	0.91	0.91	0.85	0.77	0.66
0.93	0.93	0.94	0.92	0.92	0.89	0.89	0.84	0.76	0.64
0.95	0.94	0.94	0.93	0.92	0.91	0.9	0.86	0.78	0.7
0.97	0.96	0.96	0.93	0.93	0.92	0.90	0.87	0.80	0.71
0.95	0.94	0.94	0.93	0.92	0.91	0.9	0.86	0.78	0.68
0.94	0.94	0.93	0.93	0.92	0.92	0.91	0.86	0.8	0.74
0.96	0.94	0.94	0.95	0.94	0.93	0.93	0.86	0.81	0.75
0.94	0.94	0.93	0.93	0.92	0.92	0.91	0.86	0.8	0.68

Position (degree)	Tubes with 1.2 mm initial thickness																										
	Free end						Loading path 1						Loading path 2						Loading path 3								
	Front side			Back side			Front side			Back side			Front side			Back side			Front side			Back side					
	1	2	3	1	2	3	1	2	3	1	2	3	1	2	3	1	2	3	1	2	3	1	2	3	1	2	3
45.0	1.14	1.15	1.13	1.17	1.18	1.16	1.14	1.14	1.14	1.18	1.20	1.18	1.15	1.16	1.15	1.19	1.20	1.18	1.17	1.17	1.16	1.25	1.26	1.24			
40.5	1.12	1.12	1.10	1.16	1.16	1.16	1.13	1.13	1.11	1.17	1.19	1.16	1.15	1.15	1.14	1.19	1.19	1.18	1.17	1.18	1.16	1.25	1.26	1.24			
36.0	1.1	1.10	1.09	1.15	1.16	1.14	1.12	1.14	1.11	1.16	1.16	1.15	1.13	1.14	1.12	1.18	1.18	1.17	1.16	1.17	1.15	1.24	1.24	1.23			
31.5	1.09	1.11	1.09	1.14	1.15	1.13	1.1	1.11	1.10	1.14	1.15	1.12	1.12	1.12	1.12	1.17	1.18	1.15	1.14	1.14	1.13	1.23	1.23	1.23			
27.0	1.06	1.08	1.05	1.12	1.12	1.10	1.07	1.07	1.06	1.12	1.12	1.11	1.1	1.11	1.08	1.16	1.16	1.15	1.13	1.14	1.11	1.22	1.23	1.22			
22.5	1.03	1.04	1.02	1.09	1.10	1.08	1.04	1.04	1.03	1.1	1.10	1.10	1.08	1.09	1.06	1.14	1.16	1.14	1.12	1.14	1.10	1.2	1.20	1.18			
18.0	1	1.01	1.00	1.05	1.07	1.03	1.01	1.02	1.00	1.07	1.08	1.07	1.05	1.07	1.03	1.12	1.12	1.12	1.09	1.09	1.08	1.16	1.17	1.14			
13.5	0.93	0.94	0.93	1.01	1.02	1.01	0.97	0.97	0.96	1.01	1.02	0.99	1.01	1.02	1.00	1.09	1.10	1.08	1.05	1.06	1.03	1.11	1.12	1.09			
9.0	0.84	0.85	0.83	0.91	0.91	0.91	0.88	0.89	0.87	0.93	0.94	0.91	0.93	0.93	0.92	1.02	1.04	1.00	0.98	1.00	0.98	1.02	1.03	1.02			
4.5	0.76	0.78	0.76	0.84	0.85	0.84	0.77	0.78	0.76	0.85	0.86	0.84	0.82	0.82	0.80	0.9	0.91	0.90	0.86	0.86	0.86	0.96	0.98	0.95			
0	0.85	0.85	0.84	0.86	0.88	0.85	0.84	0.85	0.83	0.94	0.96	0.94	0.9	0.91	0.89	0.96	0.98	0.96	0.94	0.94	0.93	1.04	1.04	1.03			
-4.5	0.76	0.78	0.74	0.83	0.84	0.82	0.74	0.75	0.73	0.86	0.86	0.85	0.84	0.85	0.84	0.88	0.89	0.87	0.83	0.84	0.83	0.93	0.93	0.93			
-9.0	0.8	0.81	0.80	0.89	0.90	0.89	0.85	0.85	0.85	0.97	0.98	0.97	0.9	0.91	0.89	1.01	1.03	1.00	0.89	0.91	0.88	1	1.00	0.99			

-45	-40.5	-36.0	-31.5	-27.0	-22.5	-18.0	-13.5
1.12	1.11	1.09	1.07	1.04	1.02	0.97	0.9
1.12	1.11	1.10	1.07	1.04	1.02	0.98	0.91
1.11	1.10	1.08	1.06	1.04	1.00	0.97	0.89
1.17	1.15	1.14	0.97	0.89	0.83	0.86	0.97
1.18	1.16	1.15	1.15	1.11	1.09	1.05	0.98
1.17	1.15	1.13	1.12	1.10	1.07	1.03	0.96
1.11	1.1	1.08	1.06	1.04	1.02	0.99	0.94
1.11	1.11	1.10	1.07	1.05	1.03	1.01	0.95
1.09	1.10	1.06	1.05	1.02	1.00	0.98	0.92
1.21	1.2	1.19	1.17	1.16	1.13	1.09	1.04
1.22	1.20	1.20	1.17	1.17	1.15	1.09	1.05
1.19	1.19	1.17	1.15	1.15	1.12	1.09	1.03
1.16	1.15	1.14	1.13	1.11	1.08	1.04	0.99
1.17	1.16	1.14	1.14	1.12	1.08	1.06	1.00
1.14	1.14	1.12	1.13	1.10	1.06	1.04	0.99
1.21	1.2	1.2	1.18	1.16	1.15	1.12	1.08
1.23	1.21	1.22	1.18	1.16	1.15	1.13	1.10
1.19	1.19	1.18	1.16	1.16	1.15	1.11	1.07
1.15	1.14	1.13	1.12	1.11	1.08	1.05	0.99
1.15	1.15	1.14	1.13	1.13	1.08	1.05	1.00
1.15	1.13	1.12	1.11	1.09	1.07	1.03	0.98
1.22	1.22	1.22	1.22	1.21	1.19	1.15	1.1
1.22	1.24	1.23	1.24	1.23	1.19	1.16	1.12
1.21	1.20	1.21	1.21	1.20	1.18	1.14	1.09

APPENDIX F

TUBE EXPANSION FOR DIFFERENT LUBRICANTS

Pressure (MPa)	Tubes with 0.9 mm initial thickness												Tubes with 1.2 mm initial thickness											
	Lubricant A						Lubricant B						Lubricant A						Lubricant B					
	Front side			Back side			Front side			Back side			Front side			Back side			Front side			Back side		
	1	2	3	1	2	3	1	2	3	1	2	3	1	2	3	1	2	3	1	2	3	1	2	3
0	0.00	0.00	0.00	0.00	0.00	0.00	0.00	0.00	0.00	0.00	0.00	0.00	0.00	0.00	0.00	0.00	0.00	0.00	0.00	0.00	0.00	0.00	0.00	0.00
10	1.00	1.03	0.98	1.02	1.09	0.93	0.89	0.89	0.81	0.92	0.98	0.82	0.63	0.65	0.53	0.43	0.43	0.38	1.97	1.97	1.89	0.59	0.65	0.49
20	2.31	2.36	2.28	2.40	2.43	2.30	2.30	2.37	2.24	2.25	2.25	2.17	1.66	1.70	1.60	1.40	1.50	1.37	3.27	3.34	3.21	1.61	1.61	1.53
30	4.01	4.08	3.91	3.98	4.06	3.96	3.86	3.93	3.79	3.79	3.82	3.72	3.14	3.22	3.05	2.75	2.78	2.66	4.51	4.58	4.44	3.00	3.03	2.93
40	5.26	5.33	5.22	5.18	5.23	5.16	5.09	5.19	5.00	4.88	4.97	4.81	4.51	4.51	4.48	4.14	4.21	4.04	5.96	6.06	5.87	4.22	4.31	4.15
50	5.75	5.80	5.75	5.75	5.81	5.72	5.56	5.57	5.52	5.47	5.52	5.42	5.09	5.18	5.06	4.62	4.64	4.57	6.22	6.23	6.18	4.86	4.91	4.81
60	6.28	6.29	6.21	6.23	6.25	6.16	6.17	6.20	6.07	6.07	6.08	6.04	5.68	5.68	5.67	5.28	5.38	5.22	6.49	6.52	6.39	5.41	5.42	5.38
70	6.66	6.73	6.58	6.67	6.70	6.62	6.68	6.73	6.59	6.49	6.51	6.43	6.21	6.26	6.17	5.77	5.86	5.72	6.74	6.79	6.65	6.00	6.02	5.94
80	7.14	7.20	7.08	7.16	7.16	7.10	7.12	7.14	7.07	6.92	6.97	6.86	6.54	6.57	6.50	6.18	6.23	6.13	6.99	7.01	6.94	6.41	6.46	6.35
90	7.45	7.53	7.36	7.55	7.58	7.53	7.43	7.46	7.43	7.21	7.22	7.16	6.97	7.04	6.87	6.55	6.57	6.55	7.24	7.27	7.24	6.76	6.77	6.71
100	7.67	7.77	7.64	7.79	7.85	7.69	7.62	7.69	7.62	7.42	7.43	7.39	7.30	7.34	7.25	6.86	6.92	6.83	7.49	7.56	7.49	7.02	7.03	6.99
110	7.75	7.76	7.65	7.89	7.91	7.88	7.71	7.74	7.67	7.54	7.63	7.48	7.49	7.51	7.40	7.15	7.17	7.07	7.74	7.77	7.70	7.27	7.36	7.21

260	250	240	230	220	210	200	190	180	170	160	150	140	130	120
8.74	8.67	8.66	8.64	8.57	8.52	8.42	8.40	8.32	8.22	8.16	8.07	8.00	7.93	7.82
8.78	8.71	8.76	8.73	8.66	8.61	8.48	8.43	8.36	8.28	8.19	8.10	8.04	7.93	7.91
8.66	8.59	8.56	8.64	8.55	8.46	8.33	8.37	8.28	8.12	8.14	7.97	7.93	7.93	7.82
8.74	8.69	8.68	8.65	8.62	8.56	8.47	8.41	8.35	8.29	8.23	8.18	8.12	8.03	7.94
8.82	8.78	8.77	8.74	8.71	8.65	8.50	8.50	8.35	8.38	8.30	8.22	8.22	8.12	7.98
8.69	8.59	8.61	8.56	8.61	8.46	8.39	8.39	8.26	8.24	8.22	8.18	8.06	7.94	7.87
8.76	8.73	8.67	8.61	8.59	8.52	8.46	8.39	8.33	8.21	8.13	8.05	7.97	7.89	7.78
8.82	8.74	8.69	8.68	8.65	8.56	8.50	8.43	8.36	8.26	8.14	8.10	8.01	7.96	7.78
8.70	8.73	8.58	8.56	8.56	8.46	8.46	8.36	8.29	8.17	8.09	7.95	7.94	7.88	7.69
8.66	8.62	8.61	8.55	8.50	8.42	8.36	8.32	8.22	8.15	8.05	7.94	7.85	7.73	7.62
8.71	8.67	8.67	8.56	8.53	8.44	8.37	8.37	8.30	8.18	8.08	8.02	7.88	7.77	7.69
8.57	8.53	8.52	8.46	8.46	8.32	8.35	8.22	8.18	8.15	8.00	7.93	7.81	7.66	7.61
8.81	8.79	8.72	8.68	8.62	8.54	8.50	8.39	8.31	8.23	8.14	8.05	7.92	7.82	7.70
8.87	8.83	8.77	8.73	8.67	8.62	8.57	8.47	8.33	8.30	8.23	8.07	7.94	7.87	7.77
8.71	8.73	8.70	8.66	8.52	8.47	8.46	8.29	8.31	8.13	8.06	8.02	7.88	7.74	7.60
8.41	8.37	8.30	8.25	8.22	8.15	8.09	8.02	7.99	7.92	7.82	7.74	7.60	7.43	7.34
8.41	8.43	8.31	8.27	8.26	8.15	8.11	8.07	8.00	8.00	7.90	7.75	7.61	7.53	7.36
8.40	8.27	8.29	8.17	8.21	8.15	8.04	7.92	7.95	7.82	7.74	7.65	7.52	7.37	7.29
8.62	8.76	8.70	8.62	8.56	8.50	8.43	8.37	8.29	8.23	8.17	8.09	8.03	7.97	7.91
8.68	8.77	8.72	8.69	8.62	8.54	8.47	8.41	8.32	8.28	8.18	8.14	8.07	8.04	7.91
8.62	8.76	8.61	8.57	8.53	8.44	8.43	8.34	8.25	8.19	8.13	7.99	8.00	7.96	7.82
8.49	8.54	8.50	8.40	8.37	8.34	8.25	8.17	8.10	8.01	7.92	7.82	7.71	7.62	7.45
8.49	8.59	8.56	8.41	8.40	8.36	8.26	8.22	8.18	8.04	7.95	7.90	7.74	7.66	7.52
8.47	8.45	8.41	8.31	8.33	8.24	8.24	8.07	8.06	8.01	7.87	7.81	7.67	7.55	7.44

APPENDIX G

TUBE THICKNESS FOR DIFFERENT LUBRICANTS

Position (degree)	Tubes with 0.9 mm initial thickness												Tubes with 1.2 mm initial thickness											
	Lubricant A						Lubricant B						Lubricant A						Lubricant B					
	Front side			Back side			Front side			Back side			Front side			Back side			Front side			Back side		
	1	2	3	1	2	3	1	2	3	1	2	3	1	2	3	1	2	3	1	2	3	1	2	3
45.0	0.88	0.89	0.87	0.88	0.89	0.87	0.87	0.88	0.87	0.89	0.89	0.89	1.07	1.09	1.06	1.14	1.15	1.14	1.06	1.08	1.05	1.12	1.14	1.12
40.5	0.88	0.88	0.87	0.88	0.89	0.86	0.87	0.87	0.86	0.88	0.89	0.88	1.07	1.07	1.06	1.13	1.14	1.12	1.06	1.07	1.05	1.12	1.12	1.12
36.0	0.88	0.89	0.87	0.88	0.89	0.86	0.87	0.88	0.86	0.88	0.90	0.86	1.07	1.09	1.05	1.14	1.15	1.13	1.05	1.06	1.04	1.12	1.14	1.12
31.5	0.87	0.87	0.86	0.88	0.89	0.87	0.87	0.88	0.86	0.88	0.89	0.87	1.07	1.08	1.07	1.13	1.15	1.11	1.05	1.06	1.05	1.12	1.12	1.11
27.0	0.87	0.87	0.87	0.88	0.90	0.88	0.87	0.89	0.86	0.88	0.88	0.88	1.06	1.07	1.04	1.12	1.14	1.11	1.05	1.05	1.05	1.11	1.12	1.09
22.5	0.87	0.89	0.87	0.88	0.88	0.88	0.87	0.88	0.86	0.88	0.88	0.86	1.05	1.05	1.03	1.13	1.14	1.13	1.04	1.06	1.04	1.11	1.12	1.10
18.0	0.87	0.88	0.85	0.88	0.89	0.88	0.86	0.88	0.85	0.87	0.89	0.85	1.03	1.03	1.02	1.11	1.11	1.10	1.03	1.04	1.02	1.10	1.12	1.09
13.5	0.86	0.86	0.84	0.87	0.88	0.85	0.85	0.86	0.84	0.85	0.86	0.84	1.01	1.02	0.99	1.11	1.11	1.10	1.02	1.04	1.01	1.09	1.11	1.09
9.0	0.85	0.87	0.84	0.85	0.85	0.84	0.84	0.85	0.82	0.84	0.85	0.82	0.99	0.99	0.99	1.10	1.11	1.09	1.01	1.03	1.01	1.08	1.09	1.07
4.5	0.81	0.82	0.79	0.83	0.84	0.81	0.82	0.83	0.81	0.83	0.84	0.83	0.97	0.98	0.96	1.06	1.07	1.04	0.96	0.97	0.96	1.04	1.05	1.04
0	0.81	0.83	0.80	0.82	0.83	0.81	0.82	0.82	0.81	0.82	0.82	0.81	0.99	1.00	0.98	1.06	1.06	1.05	0.97	0.98	0.96	1.05	1.06	1.04

-45	-40.5	-36.0	-31.5	-27.0	-22.5	-18.0	-13.5	-9.0	-4.5
0.87	0.87	0.87	0.86	0.86	0.86	0.86	0.86	0.84	0.81
0.87	0.89	0.88	0.86	0.88	0.87	0.86	0.87	0.85	0.81
0.87	0.85	0.86	0.85	0.85	0.86	0.85	0.86	0.84	0.80
0.89	0.89	0.89	0.89	0.88	0.88	0.88	0.87	0.86	0.83
0.91	0.90	0.90	0.91	0.90	0.90	0.88	0.88	0.87	0.83
0.89	0.89	0.87	0.88	0.88	0.88	0.87	0.85	0.85	0.82
0.87	0.87	0.87	0.87	0.87	0.86	0.85	0.85	0.83	0.83
0.87	0.89	0.87	0.88	0.89	0.86	0.85	0.86	0.85	0.84
0.86	0.85	0.86	0.86	0.86	0.85	0.84	0.83	0.83	0.82
0.88	0.88	0.88	0.88	0.88	0.87	0.87	0.87	0.86	0.84
0.88	0.88	0.90	0.89	0.90	0.89	0.88	0.88	0.87	0.85
0.87	0.87	0.88	0.86	0.86	0.85	0.87	0.87	0.85	0.83
1.08	1.08	1.07	1.07	1.07	1.05	1.04	1.03	1.00	0.98
1.08	1.10	1.08	1.08	1.08	1.06	1.06	1.04	1.01	0.99
1.06	1.08	1.07	1.06	1.05	1.03	1.03	1.02	1.00	0.97
1.11	1.10	1.11	1.10	1.11	1.10	1.09	1.09	1.09	1.05
1.13	1.11	1.12	1.10	1.12	1.11	1.11	1.10	1.10	1.06
1.11	1.09	1.09	1.09	1.11	1.09	1.08	1.08	1.08	1.05
1.05	1.05	1.04	1.04	1.03	1.03	1.02	1.01	0.99	0.96
1.06	1.07	1.05	1.06	1.04	1.05	1.03	1.02	1.00	0.97
1.04	1.04	1.03	1.03	1.03	1.02	1.00	1.00	0.99	0.96
1.10	1.09	1.09	1.09	1.09	1.08	1.08	1.07	1.07	1.04
1.10	1.11	1.09	1.10	1.10	1.10	1.08	1.08	1.08	1.04
1.09	1.08	1.08	1.08	1.08	1.06	1.07	1.06	1.05	1.04

APPENDIX H

TUBE EXPANSION FOR OPTIMUM LOADING PATHS

Pressure (MPa)	Tubes with 0.9 mm initial thickness						Tubes with 1.2 mm initial thickness					
	Front side			Back side			Front side			Back side		
	1	2	3	1	2	3	1	2	3	1	2	3
0	0.00	0.00	0.00	0.00	0.00	0.00	0.00	0.00	0.00	0.00	0.00	0.00
10	1.22	1.28	1.22	1.41	1.50	1.36	0.62	0.65	0.60	0.67	0.74	0.58
20	2.62	2.66	2.53	3.07	3.13	3.05	1.83	1.88	1.80	1.98	2.01	1.88
30	3.80	3.90	3.80	4.28	4.29	4.20	3.12	3.19	3.02	3.08	3.16	3.06
40	4.53	4.63	4.44	4.91	4.99	4.91	4.12	4.19	4.08	4.18	4.23	4.16
50	4.74	4.84	4.68	5.10	5.16	5.02	4.44	4.49	4.44	4.44	4.50	4.41
60	5.10	5.14	5.02	5.28	5.35	5.18	4.93	4.94	4.86	4.84	4.86	4.77
70	5.57	5.59	5.54	5.64	5.72	5.62	5.46	5.53	5.38	5.36	5.39	5.31
80	6.02	6.04	6.01	6.15	6.15	6.11	5.92	5.98	5.86	5.82	5.82	5.76
90	6.42	6.44	6.32	6.53	6.61	6.51	6.25	6.33	6.16	6.20	6.23	6.18
100	6.74	6.84	6.73	6.85	6.95	6.75	6.54	6.64	6.51	6.46	6.52	6.36
110	7.07	7.15	7.07	7.10	7.17	7.10	6.77	6.78	6.67	6.67	6.69	6.66
120	7.29	7.37	7.24	7.27	7.33	7.25	7.00	7.09	7.00	6.89	6.93	6.82
130	7.48	7.50	7.38	7.46	7.53	7.40	7.16	7.16	7.16	7.11	7.20	7.02
140	7.64	7.70	7.57	7.65	7.68	7.56	7.35	7.39	7.28	7.30	7.40	7.24
150	7.79	7.85	7.69	7.77	7.85	7.70	7.50	7.53	7.40	7.45	7.49	7.45
160	7.95	7.96	7.87	7.96	8.04	7.88	7.67	7.70	7.65	7.62	7.69	7.61
170	8.04	8.06	8.01	8.05	8.15	7.96	7.81	7.87	7.71	7.74	7.83	7.69
180	8.16	8.26	8.12	8.14	8.20	8.07	7.89	7.93	7.85	7.88	7.88	7.79
190	8.27	8.37	8.25	8.24	8.26	8.16	8.00	8.03	7.97	8.00	8.09	7.98
200	8.32	8.33	8.31	8.32	8.42	8.26	8.09	8.15	8.00	8.12	8.15	8.04
210	8.41	8.45	8.35	8.37	8.42	8.31	8.18	8.27	8.12	8.21	8.30	8.11
220	8.46	8.55	8.38	8.45	8.55	8.40	8.27	8.36	8.25	8.30	8.39	8.29
230	8.54	8.58	8.53	8.52	8.58	8.48	8.31	8.40	8.31	8.35	8.44	8.26
240	8.58	8.67	8.58	8.60	8.60	8.55	8.36	8.46	8.26	8.43	8.52	8.36
250	8.69	8.74	8.59	8.65	8.69	8.64	8.40	8.44	8.32	8.50	8.59	8.40
260	8.71	8.78	8.63	8.72	8.82	8.65	8.45	8.49	8.42	8.52	8.60	8.45

APPENDIX I

TUBE THICKNESS FOR OPTIMUM LOADING PATHS

Position (degree)	Tubes with 0.9 mm initial thickness						Tubes with 1.2 mm initial thickness					
	Front side			Back side			Front side			Back side		
	1	2	3	1	2	3	1	2	3	1	2	3
45.0	0.91	0.92	0.91	0.91	0.91	0.91	1.11	1.12	1.10	1.21	1.21	1.21
40.5	0.91	0.93	0.90	0.91	0.92	0.90	1.10	1.10	1.09	1.20	1.20	1.19
36.0	0.90	0.92	0.88	0.91	0.92	0.89	1.10	1.12	1.09	1.19	1.21	1.19
31.5	0.90	0.92	0.88	0.90	0.90	0.88	1.09	1.11	1.08	1.18	1.19	1.16
27.0	0.90	0.90	0.88	0.89	0.89	0.89	1.08	1.08	1.07	1.15	1.15	1.13
22.5	0.88	0.88	0.88	0.87	0.89	0.87	1.06	1.07	1.05	1.12	1.14	1.12
18.0	0.85	0.85	0.83	0.84	0.84	0.83	1.03	1.04	1.02	1.08	1.08	1.07
13.5	0.80	0.82	0.80	0.76	0.76	0.74	0.99	0.99	0.97	1.00	1.00	0.99
9.0	0.70	0.71	0.69	0.68	0.68	0.68	0.90	0.91	0.88	0.95	0.96	0.93
4.5	0.66	0.66	0.66	0.65	0.66	0.64	0.82	0.82	0.81	0.92	0.92	0.91
0	0.68	0.68	0.67	0.69	0.70	0.69	0.87	0.87	0.86	0.98	0.99	0.98
-4.5	0.65	0.66	0.63	0.66	0.68	0.65	0.79	0.81	0.78	0.93	0.94	0.93
-9.0	0.75	0.75	0.75	0.69	0.70	0.69	0.87	0.88	0.86	1.06	1.06	1.04
-13.5	0.82	0.83	0.81	0.79	0.81	0.78	0.96	0.96	0.95	1.11	1.12	1.10
-18.0	0.88	0.89	0.86	0.85	0.86	0.83	1.02	1.04	1.02	1.14	1.15	1.13
-22.5	0.90	0.91	0.88	0.89	0.89	0.88	1.05	1.07	1.05	1.16	1.18	1.15
-27.0	0.91	0.92	0.89	0.90	0.90	0.88	1.09	1.11	1.07	1.17	1.18	1.16
-31.5	0.91	0.93	0.90	0.91	0.92	0.90	1.10	1.11	1.09	1.18	1.19	1.18
-36.0	0.91	0.92	0.90	0.91	0.92	0.91	1.11	1.11	1.11	1.19	1.19	1.19
-40.5	0.92	0.93	0.91	0.92	0.93	0.92	1.12	1.14	1.11	1.19	1.21	1.17
-45	0.92	0.92	0.90	0.92	0.92	0.91	1.13	1.15	1.13	1.19	1.20	1.18

LIST OF BIBLIOGRAPHICAL REFERENCES

Abedrabbo, Nader, Naeem Zafar, Ron Averill, Farhang Pourboghrat et Ranny Sidhu. 2011. « Optimization of a tube hydroforming process ». In *SME Technical Papers - 3rd and 4th Quarter 2011*. (One SME Drive - P.O. Box 930, Dearborn, 48121-0930, United States) Vol. TP11PUB20, p. 1-6. Coll. « Technical Paper - Society of Manufacturing Engineers »: Society of Manufacturing Engineers.

Abrantes, J. P., A. Szabo-Ponce et G. F. Batalha. 2005. « Experimental and numerical simulation of tube hydroforming (THF) ». *Journal of Materials Processing Technology,* vol. 164–165, n^{o} 0, p. 1140-1147.

Ahmed, M., et M. S. J. Hashmi. 1998. « Three dimensional finite element simulation of axisymmetric tube bulging ». In *Proceedings of the Pacific Conference on Manufacturing & Management*. (Brisbane, Australia), p. 515-21.

Ahmed, M., et M. S. J. Hashmi. 2001. « Three-dimensional finite-element simulation of bulge forming ». *Journal of Materials Processing Technology,* vol. 119, n^{o} 1–3, p. 387-392.

Ahmetoglu, M., et T. Altan. 2000. « Tube hydroforming: state-of-the-art and future trends ». *Journal of Materials Processing Technology,* vol. 98, n^{o} 1, p. 25-33.

Ahmetoglu, M., K. Sutter, X. J. Li et T. Altan. 2000. « Tube hydroforming: current research, applications and need for training ». *Journal of Materials Processing Technology,* vol. 98, n^{o} 2, p. 224-231.

Alaswad, A., K. Y. Benyounis et A. G. Olabi. 2012. « Tube hydroforming process: A reference guide ». *Materials & Design,* vol. 33, n^{o} 0, p. 328-339.

Alaswad, A., A. G. Olabi et K. Y. Benyounis. 2010. « A comparison between RSM and classical iterative optimization algorithms for bi-layered tube hydroforming ». In *Proceedings IMC27 Conference*. (Galway Mayo Institute of Technology, Ireland, 1st-3rd September), p. 185-192.

Alaswad, A., A. G. Olabi et K. Y. Benyounis. 2011. « Multi-response Optimization of Geometrical Factors in Bi-layered Tube Hydroforming ». In *International Conference on Advances in Materials and Processing Technologies (AMPT 2010), 24-27 Oct. 2010*. (USA) Vol. 1315, p. 481-6. Coll. « AIP Conf. Proc. (USA) »: American Institute of Physics.

An, Honggang. 2010. « Multi-objective optimization of tube hydroforming using hybrid global and local search ». Ph.D. Ann Arbor, University of Windsor (Canada), 218 p.

ARGUS User's Manual, Version , GOM Optical Measuring Techniques. 2012.

Aydemir, A., J. H. P. de Vree, W. A. M. Brekelmans, M. G. D. Geers, W. H. Sillekens et R. J. Werkhoven. 2005. « An adaptive simulation approach designed for tube hydroforming processes ». *Journal of Materials Processing Technology,* vol. 159, n° 3, p. 303-310.

Bortot, P., E. Ceretti et C. Giardini. 2008. « The determination of flow stress of tubular material for hydroforming applications ». *Journal of Materials Processing Technology,* vol. 203, n° 1–3, p. 381-388.

Carleer, B., G. van der Kevie, L. de Winter et B. van Veldhuizen. 2000. « Analysis of the effect of material properties on the hydroforming process of tubes ». *Journal of Materials Processing Technology,* vol. 104, n° 1–2, p. 158-166.

Chu, E., et Yu Xu. 2004. « Hydroforming of aluminum extrusion tubes for automotive applications. Part I: buckling, wrinkling and bursting analyses of aluminum tubes ». *International Journal of Mechanical Sciences,* vol. 46, n° 2, p. 263-283.

Dohmann, F., et Ch Hartl. 1996. « Hydroforming - a method to manufacture light-weight parts ». *Journal of Materials Processing Technology,* vol. 60, n° 1–4, p. 669-676.

Dohmann, F., et Ch Hartl. 1997. « Tube hydroforming—research and practical application ». *Journal of Materials Processing Technology,* vol. 71, n° 1, p. 174-186.

Endelt, B., et K. Nielsen. 2001. « Least-square formulation of the object function, applied on hydro mechanical tube forming ». In *Proceedings of SheMet*.

Fann, Kuang-Jau, et Pou-Yuan Hsiao. 2003. « Optimization of loading conditions for tube hydroforming ». *Journal of Materials Processing Technology,* vol. 140, n° 1–3, p. 520-524.

Fuchizawa, S. 1984. « Influence of strain hardening exponent on the deformation of thin-walled tube of finite length subjected to hydrostatic external pressure ». *Adv Technol Plasticity*, p. 297-302.

Fuchizawa, S. 1987. « Influence of plastic anisotropy on deformation of thin walled tubes in bulge forming ». *Adv Technol Plasticity*, p. 727-732.

Fuchizawa, S., et M. Narazaki. 1993. « Bulge test for determining stress–strain characteristics of thin tubes ». In *Proceedings of the 4th International Conference on Technology of Plasticity*. (Beijing, China, 5–9 September), p. 488–493.

Fuchs, Jr F. J. 1966. « Hydrostatic pressure -- Its role in metal forming ». *Mechanical Engineering,* vol. 88, n° 4, p. 34-40.

Guan, Y., F. Pourboghrat et W. R. Yu. 2006. « Fourier series based finite element analysis of tube hydroforming: An axisymmetric model ». Engineering Computations (Swansea, Wales), vol. 23, no 7, p. 697-728.

Hama, T., T. Ohkubo, K. Kurisu, H. Fujimoto et H. Takuda. 2006. « Formability of tube hydroforming under various loading paths ». *Journal of Materials Processing Technology,* vol. 177, n° 1–3, p. 676-679.

Holmberg, Stefan, Bertil Enquist et Per Thilderkvist. 2004. « Evaluation of sheet metal formability by tensile tests ». *Journal of Materials Processing Technology,* vol. 145, n° 1, p. 72-83.

Hwang, Yeong-Maw, et Yi-Kai Lin. 2002. « Analysis and finite element simulation of the tube bulge hydroforming process ». *Journal of Materials Processing Technology,* vol. 125–126, n° 0, p. 821-825.

Hwang, Yeong-Maw, Yi-Kai Lin et Taylan Altan. 2007. « Evaluation of tubular materials by a hydraulic bulge test ». *International Journal of Machine Tools and Manufacture,* vol. 47, n° 2, p. 343-351.

Imaninejad, M., G. Subhash et A. Loukus. 2005. « Loading path optimization of tube hydroforming process ». *International Journal of Machine Tools and Manufacture,* vol. 45, n° 12–13, p. 1504-1514.

Imaninejad, Mehdi, Ghatu Subhash et Adam Loukus. 2004. « Influence of end-conditions during tube hydroforming of aluminum extrusions ». *International Journal of Mechanical Sciences,* vol. 46, n° 8, p. 1195-1212.

Jansson, Mikael, Larsgunnar Nilsson et Kjell Simonsson. 2005. « On constitutive modeling of aluminum alloys for tube hydroforming applications ». *International Journal of Plasticity,* vol. 21, n° 5, p. 1041-1058.

Jansson, Mikael, Larsgunnar Nilsson et Kjell Simonsson. 2007. « On process parameter estimation for the tube hydroforming process ». *Journal of Materials Processing Technology,* vol. 190, n° 1–3, p. 1-11.

Jeong, Kim, Kang Sung-Jong et Kang Beom-Soo. 2003. « A comparative study of implicit and explicit FEM for the wrinkling prediction in the hydroforming process ». *International Journal of Advanced Manufacturing Technology,* vol. 22, n° 7-8, p. 547-52.

Jirathearanat, S., et T. Altan. 2004. « Optimization of loading paths for tube hydroforming ». In *Materials Processing and Design. Modeling, Simulation and Applications. NUMIFORM 2004. Proceedings of the 8th International Conference on Numerical*

Methods in Industrial Forming Processes, 13-17 June 2004. (USA), 712, p. 1148-53. Coll. « AIP Conf. Proc. (USA) »: AIP.

Johnson, K. I., B. N. Nguyen, R. W. Davies, G. J. Grant et M. A. Khaleel. 2004. « A numerical process control method for circular-tube hydroforming prediction ». *International Journal of Plasticity,* vol. 20, n° 6, p. 1111-1137.

Kandil, S. E. A. E. 1976. « HYDROSTATIC METAL TUBE BULGING AS A BASIC PROCESS ». *Metallurgia,* vol. 43, n° 5, p. 152-155.

Kang, Boo Hyun, Moon Yong Lee, Sung Man Shon et Young Hoon Moon. 2007. « Forming various shapes of tubular bellows using a single-step hydroforming process ». *Journal of Materials Processing Technology,* vol. 194, n° 1–3, p. 1-6.

Kang, Sung-Jong, Hyoung-Kwang Kim et Beom-Soo Kang. 2005. « Tube size effect on hydroforming formability ». *Journal of Materials Processing Technology,* vol. 160, n° 1, p. 24-33.

Kim, Jeong, Sang-Woo Kim, Hoon-Jae Park et Beom-Soo Kang. 2006. « A prediction of bursting failure in tube hydroforming process based on plastic instability ». *The International Journal of Advanced Manufacturing Technology,* vol. 27, n° 5-6, p. 518-524.

Kim, Jeong, Yong-Wook Kim, Beom-Soo Kang et Sang-Moon Hwang. 2004. « Finite element analysis for bursting failure prediction in bulge forming of a seamed tube ». *Finite Elements in Analysis and Design,* vol. 40, n° 9–10, p. 953-966.

Kim, Sungtae, et Youngsuk Kim. 2002. « Analytical study for tube hydroforming ». *Journal of Materials Processing Technology,* vol. 128, n° 1–3, p. 232-239.

Koç, Muammer. 2003. « Investigation of the effect of loading path and variation in material properties on robustness of the tube hydroforming process ». *Journal of Materials Processing Technology,* vol. 133, n° 3, p. 276-281.

Koç, Muammer. 2008. *Hydroforming for advanced manufacturing*. Coll. « Woodhead publishing in materials ». Cambridge : Boca Raton: Woodhead publishing CRC Press.

Koç, Muammer, Ted Allen, Suwat Jiratheranat et Taylan Altan. 2000. « The use of FEA and design of experiments to establish design guidelines for simple hydroformed parts ». *International Journal of Machine Tools and Manufacture,* vol. 40, n° 15, p. 2249-2266.

Koç, Muammer, et Taylan Altan. 2001. « An overall review of the tube hydroforming (THF) technology ». *Journal of Materials Processing Technology,* vol. 108, n° 3, p. 384-393.

Koç, Muammer, et Taylan Altan. 2002. « Prediction of forming limits and parameters in the tube hydroforming process ». *International Journal of Machine Tools and Manufacture,* vol. 42, n° 1, p. 123-138.

Koç, Muammer, Yingyot Aue-u-lan et Taylan Altan. 2001. « On the characteristics of tubular materials for hydroforming—experimentation and analysis ». *International Journal of Machine Tools and Manufacture,* vol. 41, n° 5, p. 761-772.

Kömmelt, P. 2004. « Optimisation of the initial tube geometry for tube hydroforming ». Netherlands, University of Twente.

Kridli, G. T., L. Bao, P. K. Mallick et Y. Tian. 2003. « Investigation of thickness variation and corner filling in tube hydroforming ». *Journal of Materials Processing Technology,* vol. 133, n° 3, p. 287-296.

Labergere, C., et J. C. Gelin. 2004. « New strategies for optimal control of command laws for tube hydroforming processes ». In *Materials Processing and Design. Modeling, Simulation and Applications. NUMIFORM 2004. Proceedings of the 8th International Conference on Numerical Methods in Industrial Forming Processes, 13-17 June 2004*. (USA), 712, p. 1136-41. Coll. « AIP Conf. Proc. (USA) »: AIP.

Lange, K., M. Herrmann, P. Keck et M. Wilhelm. 1991. « Application of an elasto-plastic finite-element code to the simulation of metal forming processes ». *Journal of Materials Processing Technology,* vol. 27, n° 1–3, p. 239-261.

Lee, B. H., Y. T. Keum et R. H. Wagoner. 2002. « Modeling of the friction caused by lubrication and surface roughness in sheet metal forming ». *Journal of Materials Processing Technology,* vol. 130–131, n° 0, p. 60-63.

Lianfa, Yang, et Guo Cheng. 2008. « Determination of stress–strain relationship of tubular material with hydraulic bulge test ». *Thin-Walled Structures,* vol. 46, n° 2, p. 147-154.

Limb, M. E. , J. Chakrabarty, S. Garber et P. B. Mellor. 1973. « The forming of axisymmetric and asymmetric components from tube ». In *14th International MTDR Conference*. p. 799-805.

LS-Dyna Keyword User's Manual, Version 971, Livermore Software Technology Corporation (LSTC), USA, February (2013). 2013. I.

Mac Donald, B. J., et M. S. J. Hashmi. 2000. « Finite element simulation of bulge forming of a cross-joint from a tubular blank ». *Journal of Materials Processing Technology,* vol. 103, n° 3, p. 333-342.

Manabe, K., S. Mori, K. Suzuki et H. Nishimura. 1984. « Bulge forming of thin-walled tubes by micro-computer controlled hydraulic press ». *Adv. Technol. Plasticity*, p. 279-284.

Manabe, Ken-ichi, et Masaaki Amino. 2002. « Effects of process parameters and material properties on deformation process in tube hydroforming ». *Journal of Materials Processing Technology,* vol. 123, n° 2, p. 285-291.

Manabe, Ken-ichi, et Hisashi Nishimura. 1983. « INFLUENCE OF MATERIAL PROPERTIES IN FORMING OF TUBES ». *Baender Bleche Rohre,* vol. 24, n° 9, p. 266-269.

Meinders, T., I. A. Burchitz, M. H. A. Bonte et R. A. Lingbeek. 2008. « Numerical product design: Springback prediction, compensation and optimization ». *International Journal of Machine Tools and Manufacture,* vol. 48, n° 5, p. 499-514.

Ngaile, Gracious, Stefan Jaeger et Taylan Altan. 2004a. « Lubrication in tube hydroforming (THF): Part I. Lubrication mechanisms and development of model tests to evaluate lubricants and die coatings in the transition and expansion zones ». *Journal of Materials Processing Technology,* vol. 146, n° 1, p. 108-115.

Ngaile, Gracious, Stefan Jaeger et Taylan Altan. 2004b. « Lubrication in tube hydroforming (THF): Part II. Performance evaluation of lubricants using LDH test and pear-shaped tube expansion test ». *Journal of Materials Processing Technology,* vol. 146, n° 1, p. 116-123.

Nikhare, C., M. Weiss et P. D. Hodgson. 2009. « FEA comparison of high and low pressure tube hydroforming of TRIP steel ». *Computational Materials Science,* vol. 47, n° 1, p. 146-152.

Ogura, T., et T. Ueda. 1968. « Liquid bulge forming ». *Metalworking Production,* vol. 112, n° 17, p. 73-81.

Orban, Hatem, et S. Jack Hu. 2007. « Analytical modeling of wall thinning during corner filling in structural tube hydroforming ». *Journal of Materials Processing Technology,* vol. 194, n° 1–3, p. 7-14.

Plancak, M., F. Vollertsen et J. Woitschig. 2005. « Analysis, finite element simulation and experimental investigation of friction in tube hydroforming ». *Journal of Materials Processing Technology,* vol. 170, n° 1–2, p. 220-228.

Ray, P., et B. J. Mac Donald. 2004. « Determination of the optimal load path for tube hydroforming processes using a fuzzy load control algorithm and finite element analysis ». *Finite Elements in Analysis and Design,* vol. 41, n° 2, p. 173-192.

Ray, P., et B. J. Mac Donald. 2005. « Experimental study and finite element analysis of simple X- and T-branch tube hydroforming processes ». *International Journal of Mechanical Sciences,* vol. 47, n° 10, p. 1498-1518.

Ray, Pinaki. 2005. « Computer aided optimization of tube hydroforming processes ». Dublin City University.

Rebelo, N., J. C. Nagtegaal, L. M. Taylor et R. Passmann. 1992. « Industrial application of implicit and explicit finite element methods to forming processes ». In. Vol. 5, p. 67-76.

Schmoeckel, D., C. Hielscher, R. Huber et M. Prier. 1997. *Internal high pressure forming at PtU*. Germany: PtU der Technischen Hochschule Darmstadt.

Siegert, Klaus, Markus Häussermann, Bruno Lösch et Ralf Rieger. 2000. « Recent developments in hydroforming technology ». *Journal of Materials Processing Technology,* vol. 98, n° 2, p. 251-258.

Sillekens, W., et R. Werkhoven. 2001a. « Hydroforming processes for tubular parts: optimisation by means of adaptive and iterative FEM simulation ». *International Journal of Forming Processes,* vol. 4(3-4), p. 377-393.

Sillekens, W., et R. Werkhoven. 2001b. « Hydroforming processes for tubular parts: optimisation by means of adaptive and iterative FEM simulation ». *International Journal of Forming Processes,* vol. 4 (3–4), p. 377-393.

Strano, Matteo, Suwat Jirathearanat, Shiuan-Guang Shr et Taylan Altan. 2004. « Virtual process development in tube hydroforming ». *Journal of Materials Processing Technology,* vol. 146, n° 1, p. 130-136.

Varma, N. Siva Prasad, et R. Narasimhan. 2008. « A numerical study of the effect of loading conditions on tubular hydroforming ». *Journal of Materials Processing Technology,* vol. 196, n° 1–3, p. 174-183.

Velasco, R., N. Boudeau et G. Michel. 2008. « Determination of tube material hardening law using bulging tests ». *Int J Mater Form (Suppl 1)*, p. 331-334.

Vollertsen, F., et M. Plancak. 2002. « On possibilities for the determination of the coefficient of friction in hydroforming of tubes ». *Journal of Materials Processing Technology,* vol. 125–126, n° 0, p. 412-420.

Woo, D. M. 1973. « TUBE-BULGING UNDER INTERNAL PRESSURE AND AXIAL FORCE ». *American Society of Mechanical Engineers (Paper)*, n° 73 -Mat-V.

Xia, Z. C. 2001. « Failure analysis of tubular hydroforming ». *Transactions of the ASME. Journal of Engineering Materials and Technology,* vol. 123, n° 4, p. 423-9.

Yang, Jae-Bong, Byung-Hee Jeon et Soo-Ik Oh. 2001. « Design sensitivity analysis and optimization of the hydroforming process ». *Journal of Materials Processing Technology,* vol. 113, n° 1–3, p. 666-672.

Yeong-Maw, Hwang, et Huang Li-Shan. 2005. « Friction tests in tube hydroforming ». *Proceedings of the Institution of Mechanical Engineers, Part B (Journal of Engineering Manufacture),* vol. 219, n° B8, p. 587-93.

Yi, Hyae Kyung, Hong Sup Yim, Gun Yeop Lee, Sung Mun Lee, Gi Suk Chung et Young-Hoon Moon. 2011. « Experimental investigation of friction coefficient in tube hydroforming ». *Transactions of Nonferrous Metals Society of China,* vol. 21, Supplement 1, n° 0, p. s194-s198.

Yuan, Shijian, Xiaosong Wang, Gang Liu et Z. R. Wang. 2007. « Control and use of wrinkles in tube hydroforming ». *Journal of Materials Processing Technology,* vol. 182, n° 1–3, p. 6-11.

Yuan, Shijian, Wenjian Yuan et Xiaosong Wang. 2006. « Effect of wrinkling behavior on formability and thickness distribution in tube hydroforming ». *Journal of Materials Processing Technology,* vol. 177, n° 1–3, p. 668-671.

Zhang, S. H. 1999. « Developments in hydroforming ». *Journal of Materials Processing Technology,* vol. 91, n° 1–3, p. 236-244.

Zribi, Temim, Ali Khalfallah et Hedi BelHadjSalah. 2013. « Experimental characterization and inverse constitutive parameters identification of tubular materials for tube hydroforming process ». *Materials & Design,* vol. 49, n° 0, p. 866-877.